THE UNIVERSITY OF CHICAGO

DENDRITIC MECHANISMS UNDERLYING RETINAL DIRECTION SELECTIVITY

A DISSERTATION SUBMITTED TO

THE FACULTY OF THE DIVISION OF THE BIOLOGICAL SCIENCES

AND THE PRITZKER SCHOOL OF MEDICINE

IN CANDIDACY FOR THE DEGREE OF

DOCTOR OF PHILOSOPHY

INTERDISCIPLINARY SCIENTIST TRAINING PROGRAM: NEUROBIOLOGY

BY

DAVID KOREN

CHICAGO, ILLINOIS

AUGUST 2017

Table of Contents

List of Figures

List of abbreviations and definitions

AMPA receptor:	aminomethylphosphonic acid receptor, a synaptic glutamate receptor coupled to influx of sodium and calcium ions into a cell
Centrifugal (CF):	radially outward from the center
Centripetal (CP):	radially inward from the center
Contrast:	used here to denote the relative luminance of a visual stimulus compared to background visual stimulation; see Chapter 2.
Dendritic contact:	used here to denote close apposition between dendritic processes which may or may not contain functional presynaptic and/or postsynaptic components
DSGC:	direction-selective ganglion cell
DSI:	direction selectivity index. A relative measure of the response (in terms of firing rate, spike count, amplitude of current or fluorescence, or time-integral of current or fluorescence) to a null-direction stimulus and a preferred-direction stimulus.
GABA:	gamma-aminobutyric acid, the principal inhibitory neurotransmitter in the nervous system
mGluR2:	metabotropic glutamate receptor 2, a group II metabotropic glutamate receptor, a transmembrane protein that couples glutamate binding to the activation of a secondary messenger cascade that is mediated by the inhibitory G protein Gi/Go.
NMDA receptor:	N-methyl-D-aspartate receptor, a voltage-gated synaptic glutamate

	receptor coupled to influx of sodium and calcium ions into the cell
SAC:	starburst amacrine cell
Tiling factor:	the product of the dendritic field area and the spatial density of a distinct cell type in the retina
Volume transmission:	interneuronal communication that is characterized by extensive neurotransmitter diffusion to distant post-synaptic receptors and not restricted to discrete synaptic sites
Wired transmission:	interneuronal communication that is restricted to discrete synaptic sites, defined by concentrated presynaptic vesicles and postsynaptic receptors on opposite sides of a narrow synaptic cleft

Acknowledgments

I would like to thank my advisor, Wei Wei, for her painstaking training, support, and enthusiasm, and for being open to taking the project in unexpected directions. James Grove, formerly of the Wei laboratory, performed some of the paired recordings and provided inspiration for the mGluR2 study. Chen Zhang, a technician in the Wei laboratory, performed some of the intravitreal injections and managed the mouse colony and mouse genotyping. I would also like to thank Alon Poleg-Polsky at the University of Colorado for contributing important insights into our data and discussing their potential relevance for theoretical mechanisms of motion computation.

I am grateful for the support and friendship of all members of the Wei laboratory. Zhe (Jenny) Pei trained me in retinal dissection, animal care, and intravitreal injections, often during late nights in the lab; Qiang (Chris) Chen and Hector Acarón Ledesma provided much-needed critical feedback on my project, as well as support, advice, and perspective on countless occasions; other lab members, including Lindsay Huang and Benno Giammarinaro, enriched the lab with interesting conversations and contributed to a fun and diverse working environment.

My thesis committee, which included Ruth Anne Eatock, Murray Sherman, and Christian Hansel, guided me throughout multiple stages in the project and provided invaluable advice as experts in neurophysiology. I would also like to thank Ruth Anne for chairing the thesis committee, co-sponsoring my fellowship application, and for being so generous with her time.

The administration of the Medical Scientist Training Program, especially Director Marcus Clark and Deans of Students Elise Covic and Alison Anastasio, were fully supportive

during challenging times in the last few years and I am grateful for their encouragement and advice.

I am deeply appreciative of the wisdom, kindness, and expertise of members of my classmates in the Medical Scientist Training Program. They have been a tremendous source of ideas and encouragement over the past several years and have kept me grounded, motivated, and on track.

Finally, I am grateful to my parents and my brother for encouraging me to pursue scientific research. Their unwavering love and support has made my path easier at every turn.

Abstract

The ability to sense motion, both self-motion and motion in the environment, is crucial for animal behavior. In the mammalian visual system, motion selectivity begins in the retina, where nonselective light-evoked signals are converted to the direction-selective responses of a class of ganglion cells. These direction-selective ganglion cells (DSGCs) enable higher-order computations in the brain that are important for behavior in response to motion in the environment. DSGCs, each of which fires action potentials preferentially in response to motion in one of the four cardinal directions, owe their selectivity to direction-selective inhibition from non-spiking interneurons called starburst amacrine cells (SACs). SACs exhibit radial direction selectivity: segments of the dendritic tree depolarize preferentially during motion outward from the cell body to their distal tips. Recent experiments have clarified how radial direction selectivity in SACs is translated to linear direction selectivity in DSGCs. However, the mechanisms that underlie and modulate radial direction selectivity in SACs are unclear.

One property that is thought to be crucial for SAC direction selectivity is electrotonic isolation between distinct sectors of the SAC dendritic tree. Here we use calcium imaging from SAC dendrites to show that SAC sectors are not completely isolated during moving visual stimulation of the retina, and that a degree of signal integration between SAC sectors improves the response to outward motion. We further show that reducing electrotonic isolation, by preventing signaling via metabotropic glutamate receptor 2 (mGluR2), reduces direction selectivity of SACs and DSGCs by enabling aberrant propagation of depolarization between SAC sectors. Thus, mGluR2 signaling controls direction selectivity by modulating the degree of trans-sector propagation of depolarization. Using pharmacology and patch-clamp recording, we show that mGluR2 signaling

occurs through modulation of P/Q- and N-type voltage-gated calcium channels, with no detected effect on voltage-gated potassium channels.

Furthermore, using current-clamp recordings from the somata of SACs along with pharmacological and genetic manipulations, we test the effect of mGluR2 signaling, voltage-gated potassium channels, and synaptic inhibition of SACs through $GABA_A$ receptors on electrotonic isolation. We find that blockade of mGluR2 signaling improves the propagation of depolarization from distal dendrites to the soma, while blockade of K_v channels prolongs the somatic depolarization in response to motion restricted to a single dendritic sector. Because the somatic depolarization in response to these spatially restricted visual stimuli is indicative of the fidelity of trans-sector propagation, these experiments suggest distinct roles for mGluR2 signaling and K_v channels in controlling the spread of depolarization across a SAC. By contrast, conditional knockout of $GABA_A$ receptors on SACs did not affect direction selectivity measured at the soma, suggesting that inhibition by other amacrine cells does not affect direction selectivity of SACs as measured at the soma.

Together, our data illustrate mechanisms by which propagation of depolarization along dendrites may be modulated by cell-intrinsic, as well as activity-dependent, cell-extrinsic factors. Because restricted propagation along dendrites is crucial for the function of SACs in direction selectivity, our results directly link molecular mechanisms to the function of motion detection in the mammalian visual system.

Chapter 1: Introduction

1.1 Summary

The nervous system performs complex computations in order to enable animals to function in their environment. However, the complexity of the nervous system is a major roadblock to understanding the computations that occur at the cellular and circuit level. The retina is a part of the brain whose input (light) can be measured and controlled and whose output (action potentials in the optic nerve) can be identified and recorded. As a result, the function of several neural circuits in the retina has been relatively well defined, enabling mechanistic analysis of the role of intrinsic properties of its cell types and synapses in generating its output. This work investigates mechanisms underlying the ability of some retinal neurons, Starburst Amacrine Cells (SACs) and Direction-Selective Ganglion Cells (DSGCs), to detect particular directions of motion. This property, known as direction selectivity, is thought to arise from the combination of the morphology, intrinsic physiological properties, and specificity of synaptic connectivity of the dendrites of these neurons. Chapter 1 will summarize previous work on synaptic and dendritic physiology in the retina and elsewhere in the nervous system. First, Section 1.2 will review the function of dendrites. Next, Section 1.3 will discuss neurotransmitter co-release, a critical feature of the direction selectivity circuit. Finally, Sections 1.4 through 1.9 will provide an overview of the current understanding of the retina and mechanisms of direction selectivity, and outline the questions asked in this work.

1.2 Function of dendrites

Dendritic trees have long been considered the structures that receive inputs from other neurons for the purpose of conduction to the soma and the axon (Cajal, 1893). The passive cable properties of dendrites, including their membrane resistance, axial resistance, and membrane capacitance, determine the degree of spatiotemporal decay of any given synaptic input traveling toward the site of action potential initiation (Rall, 1964). Early modeling using Rall's theory of dendritic propagation indicated that distal inputs decay in amplitude before reaching the soma, yet are significantly prolonged, allowing them to contribute to integration and action potential generation (Rall, 1964). Furthermore, synaptic nonlinearities, such as the effect of the temporal order of activation of synaptic inputs, dramatically affect the resultant somatic potential (Segev et al., 1995; Rall, 1964; Abbas et al., 2013). Passive dendritic models predict that centrifugal (proximal to distal) activation of excitatory inputs results in a prolonged but diminished response at the soma, while centripetal (distal to proximal) activation results in a transient but larger response (Segev et al., 1995; Rall, 1964). The relative localization of excitatory and inhibitory inputs also has an important role: an excitatory input is most likely to be prevented from reaching the soma by a concurrent inhibitory input at a more proximal point along the dendrite, indicating that proximal inhibition exerts a more global effect on somatic depolarization (Koch et al., 1982; Rall, 1964; Williams and Stuart, 2003; Jadi et al., 2012).

In many neurons, active (voltage-gated) conductances can modify the contribution of dendritic inputs and therefore expand the computational power of the dendrites (Rall and Shepherd, 1968; Miller et al., 1985; Perkel and Perkel, 1985; Shepherd et al., 1985). In either nonspiking or

spiking dendrites, the interplay of voltage-gated calcium and potassium channels can adjust the gain of dendrites and modulate their responsiveness to synaptic input (Laurent, 1993; Mehaffey et al., 2005). In spiking dendrites, the density of voltage-gated channels as well as the dendritic morphology can determine the probability of spike propagation in the centrifugal and centripetal direction (Rall, 1959; Llinas, 1969; Gasparini et al., 2004; Kim et al., 2012; Schachter et al., 2010), which may allow weak distal inputs to be faithfully transmitted to the soma (Jarsky et al., 2005; Endo et al., 2008; Sun et al., 2014).

Dendritic spikes are an intriguing feature of dendritic computation because of their often-restricted spatial propagation, which can confer input specificity, and because of their capacity for modulation. Aside from allowing distant synaptic inputs to contribute to firing probability, active dendritic conductances may have complex short-term effects on local dendritic excitability that are important for circuit function (Manita et al., 2017). For instance, in CA1 pyramidal neurons, dendritic spikes evoked by an input reduce the probability of immediately subsequent dendritic spikes along the same branch, and also dramatically reduce the dendritic spike probability throughout the dendritic tree on a different time scale (Remy et al., 2009). Even individual dendritic branches can exhibit differential synaptic integration along their length (Branco and Häusser, 2011; Branco and Häusser, 2010). Recent work suggests that input-selective dendritic spiking is a hallmark, not an exception, of neuronal computation in mammals (Branco et al., 2010) and is important for circuit computations such as cortical orientation selectivity (Smith et al., 2013), spatial navigation using grid cells (Schmidt-Hieber et al., 2017),

and retinal ganglion cell direction selectivity (Oesch et al., 2005; Sivyer and Williams, 2013; Brombas et al., 2017).

Compartmentalization of dendritic excitation is vital to the function of dendrites from the perspective of neural circuitry. In purkinje cells, calcium spikes evoked by climbing fiber stimulation can potentiate parallel fiber synapses, but these spikes typically decay rapidly before reaching the distal dendrites under basal conditions. However, activity-dependent mechanisms including mGluR1 activation enhance the spread of the calcium spike to distal dendrites and increase the likelihood of plasticity (Otsu et al., 2014). Similarly, muscarinic and $GABA_B$ receptors modulate the spread of backpropagating spikes in the dendrites of CA1 pyramidal neurons (Tsubokawa and Ross, 1997; Leung and Peloquin, 2006). Various other cell-intrinsic and extrinsic mechanisms have been shown to gate dendritic spike propagation, including adrenergic modulation of HCN channels (Barth et al., 2008; Endo et al., 2008), NMDA receptor activation (Losonczy et al., 2006), and A-type potassium channels (Otsu et al., 2014; Ascoli et al., 2010). The importance of compartmentalization and control of compartmentalization is particularly apparent for dendrites that release neurotransmitter. In the olfactory bulb, mitral cells locally excite granule cell dendrites, causing local GABAergic feedback; in comparison, when granule cells spike, a backpropagating action potential causes global GABA release from all synapses contacting mitral cells (Lledo and Lagier, 2006; Schoppa and Urban, 2003; Rall and Shepherd, 1968; Jahr and Nicoll, 1982). The excitability of granule cells is regulated by corticofugal fibers, indicating a mechanism by which network activity can modulate the compartmentalization of dendritic impulses (Lledo and Lagier, 2006).

1.3 Neurotransmitter co-release

Co-release of classical neurotransmitters (i.e. those synthesized at the axon terminal, including GABA, glycine, glutamate, acetylcholine, and monoamines) has been observed in many central synapses and is likely to have important functional implications for neural circuits (Seal and Edwards, 2006). Interestingly, the mechanisms of co-release of classical neurotransmitters are diverse, ranging from total subcellular segregation to vesicular co-release. Imaging and electrophysiological methods may be used to determine the scale of co-release. The most convincing evidence for vesicular co-release is the identification of biphasic miniature PSPs and pharmacological studies to distinguish the two components. A common example in the spinal cord and brainstem is vesicular co-release of GABA and glycine (Jonas et al., 1998; O'Brien and Berger, 1999; Russier et al., 2002; Wu et al., 2002; Rahman et al., 2013), which readily occurs because the two molecules compete for the same vesicular transporter (Apostolides and Trussell, 2013). The distinct kinetic properties of GABA and glycine receptors allows postsynaptic cells to respond differently depending on their receptor distribution (Russier et al., 2002). The expression of the transmitter may change during development as the temporal requirements of a synapse change (Nabekura et al., 2004), illustrating the functional consequence of neurotransmitter expression.

Mammalian neurons have also been observed to release glutamate and acetylcholine or monoamines (Li et al., 2004; Trudeau, 2004; Herzog et al., 2004; Nishimaru et al., 2005; Ren et al., 2011), either in individual vesicles (El Mastikawi et al., 2011), in the same terminals but different vesicle pools (Adrover et al., 2014; Zhang et al., 2015), or in distinct cellular domains

(Nishimaru et al., 2005). When two transmitters other than GABA and glycine are co-released, the interactions between their transporters may govern whether they can be co-released at the level of individual vesicles. Although all vesicular transporters rely on the activity of a vesicular ATPase that pumps protons into the vesicle, differences in the mechanism of transport suggest the potential for their independent regulation: VAChT activity relies on intravesicular pH and is charge-neutral, while VGluT activity relies mainly on the chloride concentration and relative positive charge in the vesicle lumen and does not directly affect vesicle pH (Munster-Wandowski et al., 2016). Import of glutamate and acetylcholine or other monoamines may even occur synergistically, as import of chloride and glutamate by VGluT stimulates vesicle acidification by the vesicular ATPase (El Mestikawi et al., 2011) and thus increases the driving force for import of acetylcholine. Consistent with this, conditional VGluT3-knockout mice show a reduction in loading of acetylcholine in the striatum (Gras et al., 2008). Co-released glutamate and acetylcholine may act on the same post-synaptic cells with different kinetics (Ren et al., 2011), illustrating the flexibility that co-release imparts to circuit computation.

A particularly interesting form of co-release is the release of both an excitatory and an inhibitory neurotransmitter from the same cell. Aside from target specificity, which could enable a presynaptic cell to have opposing effects on two postsynaptic cells, this feature dramatically increases the operating range of individual cell-cell connections. Co-release of an excitatory and an inhibitory neurotransmitter that exhibit different sensitivity to calcium or other signals could allow a presynaptic cell to regulate the membrane potential of a postsynaptic cell bidirectionally, depending on the extrinsic inputs and network state. The mechanism of vesicular transport of

GABA is still controversial (Ahnert-Hilger and Jahn, 2011), but suggests possibilities for selective modulation of GABA vesicle loading. VGAT activity is dependent on vesicle pH, suggesting that it acts similarly to VAChT, by exchanging protons for GABA and therefore increasing vesicle pH (Riazanski et al., 2011). Nevertheless, VGAT can also load GABA in a charge-dependent, pH-independent manner by acting as a chloride/GABA co-importer (Juge et al., 2009). Thus, the potential exists for VGAT to act synergistically or competitively with the transporters for glutamate or other neurotransmitters, suggesting that relative amount of release of GABA and other neurotransmitters may be subject to modulation even when both transmitters are found in the same vesicles or synaptic terminals.

Co-release of glutamate and GABA or glycine in adult mammals has been shown in individual synaptic terminals of immature brainstem neurons in the ventral tegmental area (Yoo et al., 2016), mossy fiber terminals in CA3 (Beltran and Gutierrez, 2012), and in the lateral habenula (Shabel et al., 2014; Meye et al., 2016), as well as in spatially segregated sites in a subtype of retinal amacrine cells (Lee et al., 2016). Co-release of GABA and acetylcholine was first discovered in SACs (O'Malley and Masland, 1989) but is also common among VIP-expressing interneurons in the cortex (Tasic et al., 2016; Granger et al., 2017). The role of acetylcholine in cortical interneurons is unknown, but one study suggested that acetylcholine and GABA released by these neurons reach different post-synaptic targets (Karnani et al., 2016).

In most cases of co-release of inhibitory and excitatory neurotransmitters from the same terminals, it is unclear if there is co-release at the vesicular level. Two exceptions involving

vesicular co-release of glutamate and GABA are in some cortical neurons, where the relative release of the two transmitters compensates homeostatically for changes in circuit activity (Fattorini et al., 2015), and in the lateral habenula, where the ratio of the two transmitters is altered in mouse models of depression and withdrawal and is rescued by antidepressants (Shebel et al., 2014; Meye et al., 2016). These studies illustrate that modulation of the balance of co-release, even at the level of single vesicles, can be crucial for circuit function and behavior.

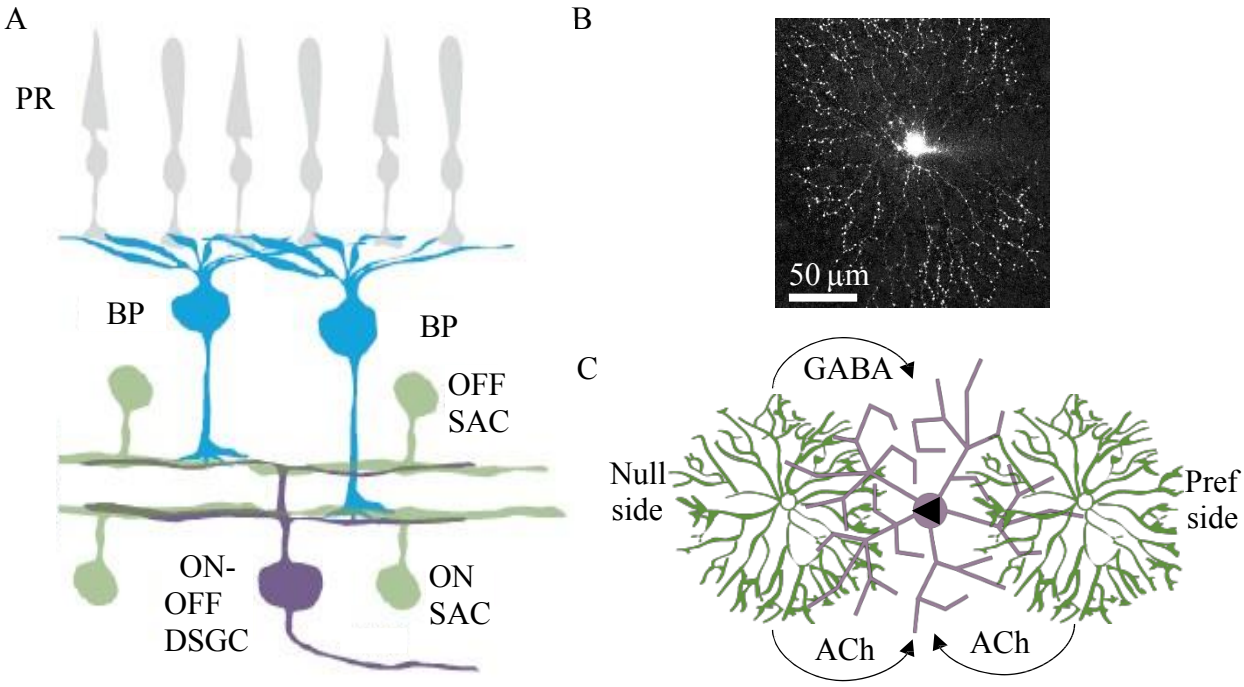

Figure 1.1: The retinal direction selectivity circuit
A: Schematic adapted from Wei et al., 2011 illustrating the components of the circuit as seen from a cross-section of the retina. Photoreceptors (PR) detect light and release glutamate onto the dendrites of bipolar cells (BP), which terminate in either the Off or the On synaptic layers of the retina and excite either Off or On starburst amacrine cells (SACs), respectively, as well as OnOff direction-selective ganglion cells (DSGCs). SACs also form synapses onto DSGCs.
B: Z-projection of an On SAC filled with dye and imaged from the ganglion cell layer using twophoton microscopy. Note the thin proximal branches and distal varicosities.
C: Schematic of the interactions between SACs (green) and DSGCs (purple) in the synaptic layers where their dendrites overlap. DSGC prefers motion in the direction labeled by the black arrowhead. SACs on the preferred side of the DSGC (the side from which preferred stimuli originate) release only acetylcholine onto DSGCs. By contrast, SACs on the null side of a DSGC release both acetylcholine and GABA onto DSGCs.

1.4 The retina as a model system

For over a century, the retina has been viewed as a uniquely accessible and tractable portion of the forebrain. Its layered structure has been appreciated since Cajal first catalogued the main cell types (1893). The logic of retinal organization is readily apparent (Figure 1.1), its layered structure suggestive of information flow from photoreceptors in the outer nuclear layer to ganglion cell axons in the optic nerve. The earliest identified function of the retina is to detect light from throughout visual space and transduce it to electrochemical signals while maintaining its inherent spatiotemporal information. This function is accomplished by the first retinal synapse by photoreceptors (Korenbrot, 2012). Rods and cones detect photons and hyperpolarize in response to light increment (On response) and depolarize in response to light decrement (Off response), modifying their release of glutamate. Bipolar cells, which collect information across cone or rod photoreceptors, already form a functionally diverse group of at least 14 types that respond differentially to stimulus contrast, size, and luminance (Demb and Singer, 2015). This diversity arises in part from the photoreceptors contacting these cells, in part from the intrinsic cellular properties such as receptor expression, and in part from modulation by horizontal cells and amacrine cells (Demb and Singer, 2015).

The "inner" retina, i.e. containing the cells postsynaptic to bipolar cells (amacrine and ganglion cells), is devoted to complex computations which extract visual features from patterns of bipolar cell activation to drive retinal ganglion cells. Unique types of ganglion cells and bipolar cells generally co-stratify narrowly within one of ten substrata within the synaptic layer called the inner plexiform layer (IPL) (Demb and Singer, 2015). Bipolar cells of distinct types stratify at

different depths within the IPL: On bipolar cell terminals are located in the inner half of the IPL, while Off bipolar terminals are located in the outer half of the IPL. Thus, the location and extent of ganglion cell and amacrine cell dendritic stratification largely determines the properties of glutamatergic drive they receive.

Even considering the differences in receptive field properties among bipolar cell types, the diversity and selectivity of ganglion cell responses is surprising. At least 30 types of ganglion cells are identified based on their physiological responses to properties of visual stimuli, including direction selectivity, orientation selectivity, edge detection, luminance increment, and luminance decrement (Demb and Singer, 2015; Gollisch and Meister, 2010; Dhande et al., 2015). These cell types form dedicated pathways that enable downstream visual areas, including the thalamus, cortex, superior colliculus, suprachiasmatic nucleus, and others to perform specific computations (Dhande et al., 2015). Therefore, the ultimate function of the retina is not to present an accurate representation of the visual world as does a camera, but to extract salient visual features for segregated processing (Gollisch and Meister, 2010).

The layered organization of the retina presents several advantages for physiological experiments. Visual stimuli can be focused on the photoreceptor layer while recordings are performed from amacrine and ganglion cells (Wei et al., 2010). Because there is little lateral divergence of excitatory inputs, the receptive field of a retinal cell largely corresponds to its dendritic field (Yang and Masland, 1994). As a result, stimulation of the retina can be tightly controlled in a physiological manner.

Retinal neurons belonging to any physiologically-defined cell type form a mosaic, typically covering the retina with regular spacing relative to one another. Additionally, for terminals of all types of bipolar cells and dendrites of most types of ganglion cells, homotypic repulsion ensures that any point in visual space is represented by only one cell encoding a particular feature. Therefore, there is little functional redundancy in the excitatory pathway of the retina. By contrast, amacrine cell dendrites are generally not territorial, exhibiting mosaic spacing with significant overlap in their inputs and outputs. Amacrine cells are the least understood and most diverse class of cells in the retina, though they are crucial for the specific responses of ganglion cells. One roadblock in studying the contribution of amacrine cells to the circuitry of various ganglion cells has been the lack of cellular markers of individual cell types. Where amacrine cells have been genetically identified, electrophysiological studies have confirmed their important role in determining the response properties of ganglion cells (Park et al., 2015). The best studied example of a retinal circuit, aided by the discovery of genetic markers (Huberman et al., 2009; Rivlin-Etzion et al., 2011), is the direction-selective circuit made up of SACs and DSGCs.

1.5 Direction selectivity

Visual motion is a fundamental sensory feature that is important for predator avoidance, prey capture, perception of self-motion, and many other behaviors across animals. Although direction-selective cells were first discovered in the cortex and assumed to be an emergent property of cortical computations (Hubel and Wiesel, 1959), Barlow and Hill, along with others, soon

discovered that a subset of retinal ganglion cells in many mammals were also highly direction selective (Barlow and Hill, 1963 (rabbit); Maturana and Frenk, 1963 (pidgeon); Norton et al., 1970 (frog); Cleland and Levick, 1974 (cat); Bowling, 1980 (turtle)). A thorough characterization of these DSGCs in rabbit showed that most are On-Off and prefer one of four cardinal directions (superior, inferior, anterior, or posterior), corresponding to the orientations of the force exerted by the rectus muscles of the eye (Oyster and Barlow, 1967). A smaller group are On and prefer either superior, inferior, or anterior (Oyster and Barlow, 1967). A recent study showed that On DSGCs preferring the posterior direction also exist, but were previously missed because of their weaker selectivity (Sabbah et al., 2017). On-Off DSGCs are known to project to the superior colliculus and the lateral geniculate nucleus (LGN) (Dhande et al., 2015), and there is evidence that they underlie direction- and orientation-selective responses in both structures, at least in mice (Marshel et al., 2012; Piscopo et al., 2013; Cruz-Martin et al., 2014; Suresh et al., 2016; Shi et al., 2017). The direction-selective retinogeniculate projection drives direction-selective thalamic input to layer 1 (Cruz-Martin et al., 2014) and layer 2/3 (Hillier et al., 2017), suggesting that a portion of cortical direction selectivity is driven by input from On-Off DSGCs. On the other hand, On DSGCs project to the accessory optic system (AOS) across mammals (Oyster et al., 1980; Hoffmann and Stone, 1985; Sun et al., 2015) and are important for generating the optokinetic reflex (Yoshida et al., 2001; Sugita et al., 2013; Sun et al., 2015).

The main difference in the physiological responses between On and On-Off DSGCs is their speed tuning: On DSGCs respond to stimuli moving at 0.01-2 degrees per second, whereas On-Off DSGCs respond to speeds of 0.5-10 degrees per second (Oyster, 1968). In fact, two rare slow

types of On-Off DSGCs, with preference for the anterior and inferior directions, also project to the AOS, suggesting that speed tuning, rather than stratification, is the defining characteristic of this group (Kay et al., 2011; Dhande et al., 2013; Dhande et al., 2015). Whole-cell recordings indicate that this difference is due to the speed tuning of excitatory inputs, since the inhibitory input to both cell types exhibits broad speed tuning (Sivyer et al., 2010). This is consistent with a common mechanism for inhibition of On and On-Off DSGCs.

Early experiments on these DSGCs indicated that two separate mechanisms were involved in computing direction selectivity: null-direction inhibition and preferred-direction facilitation (Barlow and Levick, 1965). Experiments using simulated motion showed that the receptive field of DSGCs comprised many overlapping direction-selective subunits, each of which covered at least 1 degree of visual space but could compute direction selectivity for stimuli moving as little as 0.25 degrees (Barlow and Levick, 1965; Vaney et al., 2012). This subunit was later shown to be SAC dendrites, which are required for direction selectivity in DSGCs and the optokinetic reflex (Yoshida et al., 2001; Yonehara et al., 2016).

Motion in the null direction but not the preferred direction reduces the response of a DSGC to a subsequent stationary spot (Barlow and Levick, 1965), indicating the presence of null-direction inhibition. Picrotoxin or gabazine, but not strychnine, uncovers null-direction firing in DSGCs (Caldwell et al., 1978; Kittila and Massey, 1995), showing that this direction-selective inhibition is GABAergic. Whole-cell recordings from DSGCs at the reversal potential for excitatory currents have consistently found direction-selective inhibition (Sivyer et al., 2010; Wei et al.,

2011; Pei et al., 2015; Chen et al. 2016) evoked by motion in the null direction. SAC activity and GABA release are required for this direction-selective GABAergic transmission (Pei et al., 2015; Yonehara et al., 2016). A landmark study that combined calcium imaging of DSGC responses to motion and volumetric reconstruction of electron microscopy images from a patch of retina showed that SAC dendrites make spatially asymmetrical connections with DSGCs that match this anisotropy in IPSCs: the SAC dendrites that synapse onto a particular DSGC prefer motion in the DSGC's null direction (Brigmann et al., 2011). These studies unambiguously showed that the direction-selective inhibition responsible for direction selectivity arises from the activity of SACs and the distribution of their synapses onto DSGCs.

In comparison, the excitatory input to DSGCs has been a subject of controversy. Much of DSGC firing is abolished in the absence of cholinergic input (Kittila and Massey, 1997; Brombas et al., 2017). Most studies using extracellular recordings indicate that acetylcholine provides motion facilitation in all directions (Cohen and Miller, 1995; Kittila and Massey, 1997; Grzywacz et al., 1998b), though the isotropy may be stimulus-dependent (Grzywacz et al., 1998). In particular, acetylcholine is necessary for the early phase of the DSGC response to motion in the preferred direction (Sethuramanujam et al., 2016; Brombas et al., 2017) which begins while the stimulus is still outside the dendritic field of the cell (Amthor et al., 1996; Sethuramanujam et al., 2016; Brombas et al., 2017). This timing of this response is consistent with that of acetylcholine release from centrifugally-stimulated SAC branches that overlap with the DSGC dendrites.

Most studies using whole-cell recordings in DSGCs have found that EPSCs are direction selective, with directional tuning that matches that of spiking and opposes that of IPSCs (Sivyer et al., 2010; Pei et al., 2015). The nature of direction-selective EPSCs has been highly controversial, because complicated circuit wiring is required to account for anisotropic excitation. Most studies have found that pharmacological blockade of either NMDA receptors (Cohen and Miller, 1995; Kittila and Massey, 1997; Poleg-Polsky and Diamond, 2016a; Grzywacz et al., 1998a) or nicotinic acetylcholine receptors (Kittila and Massey, 1997; but see Grzywacz et al, 1998b) maintains directional preference in DSGCs. However, these manipulations cause a dramatic reduction in DSGC firing and are not selective to DSGCs, complicating the interpretation of direction selectivity measures. Anisotropic glutamatergic transmission would require the existence of direction-selective bipolar cells and/or asymmetric connectivity between bipolar cells and DSGCs, for which there is no evidence. One theoretical mechanism (Lee and Zhou., 2006) involves selective inhibition of bipolar cells by SACs or other amacrine cells at the sites where selective SAC-DSGC synapses occur. However, recordings from the bipolar cell types that co-stratify with On SAC dendrites failed to show inhibition by SACs (Chen et al., 2014). Wide-field amacrine cells inhibit bipolar cells and modulate SAC and DSGC responses, but not in a direction-selective manner (Hoggarth et al., 2015). Furthermore, calcium imaging of bipolar cell terminals and imaging of a glutamate sensor expressed on DSGC dendrites have shown isotropic responses during moving stimulation (Yonehara et al., 2013; Chen et al., 2014; Park et al., 2014). DSGC dendrites express glutamatergic receptors symmetrically (Kwon et al., 2007; Jeong et al., 2006; Lee et al., 2017) and receive synaptic contacts from bipolar cells throughout both of the On and Off layers of their dendritic tree (Jeon

et al., 2002). Although DSGCs also receive glutamatergic inputs from VGluT3+ amacrine cells, these cells are not direction-selective and make spatially symmetrical connections onto DSGCs (Lee et al., 2014).

Direction-selective cholinergic transmission has also been considered unlikely given the current model of SAC-DSGC connectivity. Paired recordings have shown that SACs on the preferred and null sides of a DSGC can both effectively release acetylcholine with similar post-synaptic current amplitude (Lee et al., 2010). If cholinergic transmission occurs by paracrine diffusion from SAC release sites, the extensive co-fasciculation of dendrites from SACs and DSGCs preferring different directions, together with the symmetric expression of nicotinic receptors along DSGC dendrites (Lee et al., 2017; Kim and Jeon, 2014), would appear to preclude any selectivity in SAC-DSGC transmission of acetylcholine. Even if a mechanism exists to restrict released acetylcholine to particular DSGCs, the apparent symmetry of SAC-DSGC transmission in paired recordings (Lee et al., 2010; Pei et al., 2015) implies that a circuit-level mechanism must either inhibit null-direction acetylcholine release or enhance preferred-direction acetylcholine release during moving stimuli. However, during a stimulus moving in any particular direction, individual SAC dendrites simultaneously release acetylcholine onto DSGCs that prefer the direction and both acetylcholine and GABA onto DSGCs that do not. Thus, any extrinsic modulation of acetylcholine release, for example by other amacrine cells (Lee and Zhou, 2006; Zhou and Lee, 2008), must be selective for SAC release sites depending on the DSGCs they contact. Alternatively, minor undetected differences in receptor distribution or synaptic connectivity along the null-preferred axis may be present.

Given the implausibility of most mechanisms that could account for direction-selective glutamate or acetylcholine release, some studies have proposed that direction-selective EPSCs are an artifact of space clamp error (Vaney et al., 2012). The powerful inhibition evoked by null-direction stimulation may contaminate and reduce the apparent (measured) excitation. Indeed, blocking GABAergic transmission in the retina using gabazine abolishes direction selectivity in DSGC spiking and DSGC excitation (Vlasits et al., 2016). Nevertheless, gabazine may also abolish any mechanisms that lead to true direction-selective excitation, such as presynaptic (bipolar cell) inhibition. Addressing this concern, work in the Wei group using SAC-selective knockout of the vesicular GABA transporter (VGAT) found that direction selectivity of EPSCs remained in a subset of DSGCs despite absence of direction-selective inhibition (Pei et al, 2015). Direction selectivity was abolished in these cells in the presence of the nicotinic receptor antagonist DHβE or of gabazine (Pei et al, 2015). These data suggest that a component of measured direction-selective excitation in control mice is due to space clamp error, while the remainder is due to direction-selectivity in cholinergic excitation and is dependent on GABAergic transmission by non-SAC amacrine cells. Consistent with this finding, the amplitude of null-direction inhibition and the direction selectivity of excitation are not highly correlated (Percival et al., 2017), illustrating that space clamp error cannot be the only cause of apparently anisotropic EPSCs. Nevertheless, the mechanism of presynaptic modulation of acetylcholine release remains unknown.

1.6 Starburst amacrine cells - morphology

Although SACs are found in many animals, they have been best studied in rabbits and mice. Early painstaking studies in rabbits provided the foundation for modeling passive properties of SAC dendrites and are therefore useful in understanding how SACs compute direction selectivity.

SAC somata in rabbits range from 9 to 11 µm in diameter, with a small increase with increasing distance from the visual streak (Famiglietti, 1985). By contrast, their dendritic field varies from less than 200 µm in diameter at the visual streak to over 600 µm in the peripheral dorsal retina (Famiglietti, 1985). However, when normalized to the dendritic length, the branching pattern and localization of output synapses is constant throughout the retina and highly conserved among mammals (Keeley et al., 2007). Varicosities are consistently restricted to the distal 50-60% of the dendritic tree area (distal third of dendritic length), typically on branches of the 3^{rd}-6^{th} order (Famiglietti, 1985; Famiglietti, 1991). The organization of proximal dendrites is slightly more variable, with between 4 and 7 dendrites extending from the soma in most SACs (Famiglietti, 1985; Famiglietti, 1991). Interestingly, cells with fewer primary dendrites tend to exhibit extensive branching at very proximal locations (Famiglietti, 1991), so that these differences in primary dendrite number are not reflected in the overall shape of the dendritic tree (Famiglietti, 1985). An extreme example, encountered rarely in peripheral rabbit retina but commonly in primates, is a SAC with a single primary dendrite from which all other dendrites arise. It is unknown if the dendritic sectors of these SACs are sufficiently isolated to maintain distinct

directional preferences. However, the organization of the dendritic trees in these cells is otherwise typical.

SAC primary dendrites are unusually thin, ranging from 0.27 µm in diameter for cells near the visual streak to around 0.9 µm for those in the peripheral retina (Famiglietti, 1991). Branching typically begins as proximally as 10 µm from the soma in central SACs, but sometimes up to 100 µm from the soma in peripheral SACs. The dendritic tree has been classically divided into proximal, intermediate, and distal segments of roughly equal length (Famiglietti, 1991). Proximal dendrites are characterized by abrupt narrowing during their unbranched segments (Famiglietti, 1991). These proximal dendrites are the primary site of excitatory inputs from cone bipolar cells and inhibitory inputs from amacrine cells. Cone inputs are preferentially localized at small spine-like extensions of the SAC proximal dendrites, whereas amacrine inputs are nonselective (Famiglietti, 1991). In the intermediate segment of the SAC dendritic field, dendritic diameter ranges from 0.2 µm to 0.4 µm and is typically uniform. This region receives sparse inputs from cone bipolar and amacrine cells and has few varicosities, most of which do not contain vesicles (Famiglietti, 1991). The output sites of SACs are localized in varicosities of around 1 µm in diameter that are primarily found in the distal third of SAC dendrites. In rabbit, many varicosities are also postsynaptic, forming a dyadic configuration with either cone bipolar or amacrine cell input and ganglion cell dendrites (Famiglietti, 1991; Dacheaux et al., 2003). Although there is relatively less glutamatergic input onto the distal SAC dendrites, SACs depolarize in response to light stimulation anywhere in their dendritic field (Bloomfield, 1992;

Taylor and Wässle, 1995; Peters and Masland, 1996; but see Vlasits et al., 2016), indicating that these distal inputs are sufficient to drive the cell.

1.7 Starburst amacrine cells - physiology

An early model of passive current propagation in SAC dendrites (Miller and Bloomfield, 1983) showed how the unusually proximal taper of SAC processes might affect the compartmentalization of EPSPs in individual SAC sectors. In comparison to a SAC-like dendritic tree that follows Rall's 3/2 power rule of branch diameter, the thin proximal SAC dendrites in a more realistic model exhibit a substantial voltage drop, reducing the contribution of dendritic impulses to somatic potential. More refined estimates of dendritic diameter yielded an estimate of a seven-fold attenuation of voltage from a distal input measured at the soma (Famiglietti, 1991). Additionally, the relatively high input resistance due to the thin proximal dendrites increases the length constant for impulses propagating along more distal branches of a single sector (Miller and Bloomfield, 1983), such that an input at the intermediate segments would decay very little during centrifugal conduction toward varicosities and even an input at the proximal segments could modulate the potential at distal dendrites (Famiglietti, 1991). For both of these reasons, Miller and Bloomfield (1983) proposed that SACs can efficiently compute impulses within sectors but not between sectors. However, they also note that coactivation of multiple dendrites (i.e. sectors) would be expected to reduce the isolation of a non-activated dendrite in this passive model. They conclude: "…The question of a functional subunit of an amacrine is partially a network question. Are the starburst amacrine dendrites independently controlled by different synaptic inputs or are many dendrites simultaneously activated?" More

recently, the finding that dendritic sectors of a single SAC prefer distinct directions of motion (Euler et al., 2002) appeared to confirm the finding that SAC sectors operate independently, and most recent models have assumed this (Velte and Miller, 1997; Euler et al., 2002; Ozaita et al., 2004; Hausselt et al., 2007).

In adult mice, SACs do not fire action potentials that can be detected at the soma (Taylor and Wässle, 1995; Zhou and Fain, 1996), although it is not clear if they exhibit dendritic spiking. Somatic recordings show a powerful voltage-dependent outward current that limits light-evoked depolarization to around -40 mV (Taylor and Wässle, 1995). These currents reflect the high expression of the Kv3 family of voltage-gated potassium channels in the proximal SAC dendrites (Ozaita et al., 2004), which may be responsible for electrotonic isolation of SAC dendritic branches (Ozaita et al., 2004). Additionally, there is evidence that a membrane potential gradient (Hausselt et al., 2007) exists in SACs and contributes to centrifugal preference. Some studies have also proposed that a chloride gradient along SAC dendrites is set by heterogeneous expression of the chloride transporters, which could establish compartment-specific effects of GABAergic transmission (Gavrikov et al., 2003).

Circuit models of direction selectivity have also suggested that mutual inhibition between SACs (Lee and Zhou, 2006) underlies direction-selective synaptic currents in DSGCs. SACs receive inhibitory input from amacrine cells throughout their dendritic field in rabbits (Famiglietti, 1991) and on proximal portion of the dendritic field in mice (Ding et al., 2016). They express GABAA receptors (Zhou and Fain, 1995) and glycine receptors (on On SACs; Zhou and Fain, 1995),

though knockout of the a2 subunit of GABAA receptors abolishes all evoked and most spontaneous IPSCs (Chen et al., 2016). Most of the inhibitory inputs onto SACs are likely to originate from other SACs, given their extensive dendritic overlap and co-fasciculation (Famiglietti, 1991). In the On pathway, mutual inhibitory connections between SACs act to stabilize the SAC network and maintain direction selectivity during noisy stimuli (Chen et al., 2016). By contrast, during noiseless conditions, transgenic models that reduce GABA release from SACs or expression of $GABA_A$ receptors on SACs impair centrifugal preference of Off SACs, but not On SACs (Chen et al., 2016). This illustrates the differences in the computation of direction selectivity between the On and Off pathways.

Segregation between input and output sites on SACs may be expected to confer the direction selectivity circuit with a number of advantages. First, a concentration of spontaneously active synaptic inputs in the proximal dendrites reduces the local membrane resistance, creating a shunt that may contribute to isolation between dendritic sectors. Second, the lack of distal inputs would be expected to increase the length constant and reduce decay of potentials along the distal dendrites, improving activation of varicosities within a sector. Similarly, the lack of local inputs near varicosities would improve the consistency of calcium responses across varicosities within a sector, which are known to synapse onto DSGCs preferring the same direction (Brigmann et al., 2011). This may act to decrease noise in DSGC inhibition. Finally, although inhibitory and excitatory synapses are both located on proximal dendrites, the inhibitory receptive field is significantly larger than the excitatory receptive field (Lee and Zhou, 2006). Most inhibitory inputs are from other SACs, whose inputs are displaced from these synaptic sites by up to 100

μm in any direction, while excitatory inputs are from bipolar cells, which have a 40μm-diameter receptive field and whose terminals do not diverge laterally from this receptive field. Therefore, stimuli moving centripetally along a branch would first elicit inhibition, which would shunt the proximal branches and veto the subsequent excitation. By contrast, centrifugal stimuli would activate bipolar cells immediately and trigger a regenerative calcium conductance that invades the varicosities in the local sector, with much of the inhibition arriving too late to influence this event. However, it is notable that input and output segregation is reduced in rabbits (Famiglietti, 1991; Ding et al., 2016), which nevertheless exhibit similar DSGC tuning, and that centrifugal preference in mice does not require inhibitory inputs onto SACs, at least for some stimuli (Chen et al., 2016; but see Vlasits et al., 2016).

Although centrifugal preference was demonstrated by both varicosity calcium imaging and somatic current-clamp recordings in the original study of SAC direction selectivity (Euler et al., 2002), subsequent studies have observed only weak direction selectivity in somatic current-clamp recordings (Lee and Zhou, 2006; Hausselt et al., 2007; Fransen and Bourghis, 2017). This contrasts with the robust direction selectivity observed across studies using calcium imaging of SAC varicosities (Lee and Zhou, 2006; Vlasits et al., 2016; Ding et al., 2016; Chen et al., 2016). The source of this discrepancy between somatic and dendritic direction selectivity is not clear.

1.8 The SAC-DSGC synapse

Many questions remain regarding the mechanism of co-release in SACs and the mechanism of cholinergic transmission between SACs and DSGCs. Electron microscopy shows evidence for

classical synapses predominantly at sites where contacting SAC dendrites and DSGCs prefer motion in opposite directions, while the remainder of SAC dendrites are separated from DSGCs by a thin glial sheath even at sites of close apposition (Brigmann et al., 2011). This morphological asymmetry can explain why SACs on the null side of a DSGC provide more powerful GABAergic transmission than those on its preferred side (Fried et al., 2002; Lee et al., 2010; Wei et al., 2011). Nevertheless, SACs located on the preferred side of a DSGC, and therefore unable to make opposing-preference synaptic contacts, consistently transmit acetylcholine (Lee et al., 2010) and small amounts of GABA (Wei et al., 2011; Morrie and Feller, 2015) during depolarization. These observations illustrate that synaptic transmission from SACs to DSGCs does not strictly require the classical synaptic contacts seen between null-side SACs and DSGCs. However, the mechanism of GABA and acetylcholine release outside of the classical sites is unclear.

Some studies have proposed that acetylcholine is transmitted by volume transmission rather than by "wired transmission" in localized synaptic sites (Sethuramanujam et al., 2016; Brombas et al., 2017). Volume transmission is typically characterized by slow postsynaptic responses and signal divergence (Agnati et al., 1995). Dopamine (Yazula and Studholme, 1995) and other monoamines are thought to be transmitted through this mechanism in many parts of the nervous system, including the retina. The diffusion of neurotransmitter in these cases may be regulated by astrocytes and other glial cells (Agnati et al., 1995; Sykova and Chvatal, 2000) and expression of the enzymes that mediate reuptake or catalysis of these transmitters from the extracellular matrix (Sykova and Chvatal, 2000). Volume transmission often activates extrasynaptic metabotropic

receptors (Agnati et al., 1995) but can also activate ionotropic receptors. For instance, at habenulo-peduncular synapses, acetylcholine released through volume transmission acts monosynaptically on postsynaptic nicotinic receptors with slow kinetics, in stark contrast to the rapid kinetics of glutamate transmission between the same cells (Ren et al., 2011). In On-Off DSGCs, a previous study did not find any difference in latency between the GABAergic and cholinergic components during SAC stimulation (Lee et al., 2010), suggesting that acetylcholine may be acting locally rather than mainly diffusing over long distances to activate DSGCs. However, another study found that cholinergic PSPs are significantly delayed in On DSGCs (Brombas et al., 2017), suggesting potential differences in the connectivity of the two types of direction-selective cells with SACs.

The degree of spatial segregation of GABA and acetylcholine release is also unknown. In rabbit, cholinergic transmission requires higher calcium concentrations and the activity of N-type calcium channels, whereas GABAergic transmission is only partially reduced by N-type calcium channel blockade and has a lower requirement for calcium concentration (Jensen, 1995; Lee et al., 2010). Furthermore, GABAergic transmission exhibits paired-pulse depression in null- and preferred-side pairs in mice and rabbits (Lee et al., 2010; Morrie and Feller, 2015), whereas there is evidence that cholinergic transmission exhibits paired-pulse facilitation in rabbits (Lee et al., 2010). Overall, the differences in calcium dependence of acetylcholine and GABA release suggest that the two neurotransmitters are found in different vesicle pools.

An additional explanation for SAC-DSGC neurotransmission in absence of observed synaptic contacts is that a portion of neurotransmission occurs via nonvesicular, transporter-mediated release. Such nonvesicular release of GABA and other transmitters is common during development before synapse formation but has also been observed in adult neurons throughout the nervous system, including the retina (Yang and Kunes, 2004; Attwell et al., 1993; Wu et al., 2007; Demarque et al., 2002; Jones and Palmer, 2009). Transport-mediated release is generally independent of calcium concentration and SNARE proteins, but may be dependent on depolarization and sodium influx (Demarque et al., 2002; Wu et al., 2007). Given the calcium dependence of both GABA and acetylcholine release (Lee et al., 2010; but see O'Malley et al., 1992) and that vesicles are present at most SAC varicosities (Famiglietti, 2005), which are thought to be the sites of GABA release (Brigmann et al., 2011), it is likely that most release from SACs is vesicular. Nevertheless, SAC-specific knockout of VGAT in mouse retina does not fully abolish evoked GABA release from SACs (Pei et al., 2015). It is possible that the remaining small amount of GABA may be packaged by VAChT or other vesicular transporters (the vesicular monoamine transporter has been shown to load vesicles with GABA (Trisch et al., 2012)) or released by a reversal of the GABA reuptake channel. Either may be consistent with the loss in GABAergic asymmetry. Notably, it is not clear whether the VGAT-independent GABA release is a compensatory phenomenon or a wildtype mechanism uncovered by blocking VGAT-mediated GABA release.

Despite the potential importance of regulation of GABA and acetylcholine release from SACs, the role of extrinsic modulation on SAC transmitter release has not been well studied. A subset

of SAC varicosities express GABAB receptors (Zucker et al., 2005), and GABAB agonists reduce acetylcholine release (Neal and Cunningham, 1995). However, GABAB receptors are ubiquitous in the retina (Slaughter and Pan, 1992; Zucker et al., 2005), making interpretation of pharmacological experiments difficult. SACs also express metabotropic glutamate receptor 2 (mGluR2) (Koulen et al., 1996; Cai and Pourcho, 1999; Jensen, 2006; Seebahn et al., 2008). In rodent retina, expression of mGluR2 is limited to On and Off SACs and some rod amacrine cells in the outermost IPL (Seebahn et al., 2008). One pharmacological study using extracellular recordings from DSGCs found that an mGluR2 agonist abolished direction selective firing by increasing null-direction firing, while an mGluR2 antagonist slightly reduced preferred-direction firing (Jensen, 2006). Furthermore, in the presence of a cholinesterase blocker, mGluR2 agonist substantially reduced DSGC firing (Jensen, 2006). Although these results suggest that mGluR2 could modulate release of both acetylcholine and GABA from SACs, this has not been verified directly and the mechanism of this effect has not been determined.

1.9 Aims of this study

The goal of this study was to use genetic manipulations, pharmacology, electrophysiology, and two-photon calcium imaging to gain insight into the mechanisms that confer direction selectivity on SAC and DSGC dendrites. The first part of this study investigates a mechanism by which modulation of the electrotonic properties of SAC dendrites by mGluR2 alters synaptic transmission in response to moving stimuli. The second part of the study further studies the role of mGluR2, along with other properties of SACs, in centrifugal preference. The final part of the study investigates properties of the co-release of acetylcholine and GABA by SACs, the effect of

mGluR2 on acetylcholine and GABA release, and the role of acetylcholine and GABA in motion detection in the retina. Together, these findings illustrate the flexibility and modulation inherent in this circuit and suggest how it may differently integrate synaptic inputs under various environmental conditions, a critical question in circuit neurobiology.

Chapter 2: Experimental Procedures

2.1: Mice

The *Gabra2*$^{flox/flox}$ mouse line was a generous gift from Dr. Uwe Rudolph at Harvard Medical School. The mGluR2-/- mouse line (B6;129S-Grm2^{tm1Nak}*/NakRbrc)* was a generous gift from Dr. Javier González-Maeso at Virginia Commonwealth University. *Chat-IRES-Cre* mice (129S6-*Chat*$^{tm2(cre)Lowl}$/J), *Vgat*$^{flox/flox}$ mice (*Slc32a1<tm1Lowl>/J*), and floxed *tdTomato* mice (129S6-*Gt(ROSA)26Sor*$^{tm9(CAG-tdTomato)Hze}$/J) were acquired from the Jackson Laboratory. *Drd4–GFP* mice, in which posterior-preferring DSGCs are selectively labeled, are a BAC-transgenic line originally developed by MMRRC in the Swiss Webster background, and were subsequently backcrossed to C57BL/6 background. All strains were backcrossed to the *C57BL/6* background in our laboratory, and crossed to each other to create the lines used in this study.

Mice were housed in 12 hr-12 hr light-dark cycles in groups of 2-5 per cage. For electrophysiology experiments, mice of ages P21-P40 of either sex were used. Sex was tracked, but sample sizes were generally not sufficient for statistical comparisons across sex. All procedures to maintain and use mice were in accordance with the University of Chicago Institutional Animal Care and Use Committee (Protocol number ACUP 72247) and in conformance with the NIH Guide for the Care and Use of Laboratory Animals and the Public Health Service Policy.

2.2: Intravitreal injection of AAV vector

For expression of GCaMP6m in SACs, *Chat-IRES-Cre* mice aged P14-25 were anesthetized using 4-5 µL/g intraperitoneal injection of 10% ketamine/ 5% xylazine in PBS. For expression of tetanus

toxin in SACs, Chat-IRES-Cre/Drd4-GFP mice aged P14-17 were anesthetized using 3.5 µL/g intraperitoneal injection of 10% ketamine/ 5% xylazine in PBS. For expression of GCaMP6s in cells of the ganglion cell layer, C57BL/6 mice aged P18-30 were anesthetized using 5 µL/g intraperitoneal injection of 10% ketamine/ 5% xylazine in PBS. Animals were placed on their side and the periorbital region was locally anesthetized using one drop of 0.5% proparacaine HCl (Henry Schein, Melville, NY). An insulin syringe was first used to penetrate the cornea lateral to the lateral limbus, and a Hamilton syringe modified for one-handed micro-injection (Borghuis Instruments) was then inserted into the same incision and behind the lens, injecting 1µL of an AAV vector carrying GCaMP6s (University of Pennsylvania Vector Core), floxed GCaMP6m (University of Pennsylvania Vector Core), or 0.5-1µL of an AAV vector carrying floxed tetanus toxin (custom made using the University of North Carolina Viral Vector Core) into the vitreal space. This procedure was repeated for each eye. Retinas were isolated and used for imaging or recording 2-5 weeks following injection.

2.3: Whole-mount retina preparation

Mice were dark-adapted for >30 min, anesthetized using isoflurane, and then euthanized by decapitation. Under infrared illumination, retinas were isolated from the pigment epithelium at room temperature in oxygenated Ames' medium (Sigma-Aldrich, St. Louis, MO) for visual stimulation experiments or in artificial cerebrospinal fluid (aCSF) containing 119.0 mM NaCl, 26.2 mM $NaHCO_3$, 11 mM D-glucose, 2.5 mM KCl, 1.0 mM K_2HPO_4, 2.5 mM $CaCl_2$, and 1.3 mM $MgCl_2$ for dual patch clamp recording. Isolated retinas were then cut into dorsal or ventral halves and mounted ganglion-cell-layer-up on top of a 1 mm^2 hole in a small piece of filter paper

(Millipore, Billerica, MA). The orientation of the preferred direction (posterior) *of Drd4-GFP* positive neurons was noted for each piece. Retinas were kept in darkness at room temperature in Ames' medium or aCSF bubbled with 95% O_2/5% CO_2 until use (0–8 hr).

2.4: Two-photon calcium imaging

GCaMP6 imaging of SAC varicosities was performed as previously described in Chen et al. (2016). Retinas were placed in oxygenated Ames' media at 32-33°C and screened using a customized two-photon laser-scanning microscope (Bruker Nano Services Division) for expression of GCaMP6 in displaced SACs. GCaMP6 was excited by a Ti:sapphire laser (Coherent, Chameleon Ultra II, Santa Clara, CA) tuned to 920 nm, and the laser power was adjusted to avoid saturation of the fluorescent signal. To enable simultaneous visual stimulation and GCaMP6 fluorescence, a band-pass filter (Semrock, Rochester, MA) was placed on the OLED to pass blue light peaked at 470 nm, while two notched filters (Bruker Nano Surfaces Division) were placed before the photomultiplier tubes to block light of the same wavelength. The objective was a water immersion objective (60x, Olympus LUMPlanFl/IR).

Tissues in which GCaMP expression lacked nuclear exclusion were not used due to concerns about cell health (Chen et al., 2013). Only areas with sparse infection were used, often at the edge of a larger infected region, in order to allow unambiguous determination of the orientation of individual SAC dendrites. Rectangular imaging regions of length 70-180 μm and width 50-120 μm were chosen surrounding the distal tips of the SAC dendrites.

2.5: Visual stimulation

A white organic light-emitting display (OLEDXL, eMagin, Bellevue, WA; 800 × 600 pixel resolution, 60 Hz refresh rate) was controlled by an Intel Core Duo computer with a Windows 7 operating system and was presented to the retina at a resolution of 1.1 μm/pixel. Moving bar stimuli were generated by MATLAB and the Psychophysics Toolbox (Brainard, 1997).

In the plane of the retina, the OLED image was centered in the middle of the imaging window, corresponding to the tips of the imaged dendrites. In the perpendicular axis, the OLED image was focused on the photoreceptor layer. Time series of fluorescence were recorded at 30-50 Hz. After an initial 10-second period to allow the retina to adapt to the two-photon laser, moving bars were presented using the OLED. For full-field stimulation, the bars had dimensions of 220 μm x 660 μm and were presented in three trials of eight pseudorandomized directions, moving parallel to their longer dimension. Bars traversed a patch of retina that exceeded the length of the SAC receptive field by at least 150 μm in both directions.

For spatially restricted stimulation, the bars were presented in 5-10 trials of two pseudorandomized directions (centripetal and centrifugal, which were determined by dendrite orientation and verified by responses to full-field stimulation). These bars had dimensions of 132 μm x 660 μm and moved across a circular patch of retina with a diameter of 132 μm. The speed of the bar was 440 μm/s unless otherwise indicated.

Both positive- and negative-contrast moving bars were used. For positive-contrast ('bright') bars, the background light intensity was ~600 isomerizations (R*)/rod/s and the stimulus was ~6.5×10^4 R*/rod/s. For negative-contrast ('dark') bars, these values were reversed. During two-photon calcium imaging, additional source of light besides the OLED may activate photoreceptors, including the imaging IR laser at 920 nm and the GCaMP6 fluorescence emitted from the stimulated starburst amacrine cells. We consider the contribution of GCaMP6 fluorescence negligible because GCaMP6 was expressed sparsely in isolated SACs and the GCaMP fluorescence was only activated in ~ 10 varicosities at the distal tips of a SAC. The imaging IR laser, which scanned the same imaging windows, increased the background luminance in the imaging window and triggered a transient calcium response in On starburst amacrine cells at the onset of imaging. Because this IR laser-evoked response adapted within 5 seconds, we started OLED stimulation after at least 10 seconds of laser scanning. Due to the scanning laser, the background illumination at the imaging window was higher than that elsewhere in the retina during OLED stimulation. We estimate that the laser causes an equivalent illumination of about 2×10^4 R*/rod/s at 497 nm according to (Euler et al., 2009). At this level of background illumination, the rod pathway has been shown to saturate and the cone pathway mediates the light response (Borghuis et al., 2013). Since SACs and DSGCs do not receive direct input from rod bipolar cells, rod saturation is unlikely to affect the direction-selective pathway.

2.6: Imaging analysis

Fluorescence time series were analyzed offline in Prairie View software (Bruker Corporation) using elliptical regions of interest containing individual SAC varicosities. For each imaging

window, an elliptical region of interest adjacent to the varicosities but lacking GCaMP6 signal was chosen to record the background fluorescence. During a visual stimulus, a weak background impulse was detected in this region. This background signal was subtracted from fluorescence measurements of the varicosities and was also used to indicate the onset time of the stimulus. For spatially restricted visual stimulation, stimulus timing was reported by a coincident voltage pulse triggered by MATLAB and recorded by Prairie View software. Responses were background-subtracted, normalized to baseline, clipped, sorted by motion direction and averaged using Microsoft Excel and custom-written MATLAB scripts. The peak amplitude of the averaged responses to each stimulus was calculated as the maximum three-frame running average of $\Delta F/F_0$ during a 2-second period following stimulus onset, where F_0 = the mean fluorescence during the 2-second period before the stimulus and $\Delta F = F - F_0$. The time-integral of the responses was estimated as the right-sided Riemann sum of $\Delta F/F_0$ beginning at stimulus onset and ending 4 seconds later.

For stimuli that did not consistently evoke responses (those localized outside the SAC receptive field or to distant SAC dendritic sectors), response probability was calculated. To determine whether a response occurred, traces from several varicosities were averaged and a threshold of $F_0 + 3*S.D.$ was applied, where S.D. = standard deviation of the region of the ΔF trace in the 2-second period before the first stimulus. Response probability was calculated by dividing the number of evoked suprathreshold responses by the number of trials (5-10). To exclude rare spontaneous calcium events (detected in 3 of 10 cells in mGluR2 blockade), only responses beginning in the 2 seconds following stimulus onset were considered evoked.

The retinal location of the stimulus during response onset was estimated by multiplying (latency to the response at threshold) by the speed of the bar. Due to the delays inherent in phototransduction, calcium influx, and GCaMP6m activation, GCaMP6m signal onset may be expected to lag behind the bar. This lag was estimated by presenting a stationary spot of radius 50 µm that was synchronized with the fluorescence time-series acquisition. The measured latency to fluorescence onset was approximately 50 ms. For a bar moving at 440 µm/s, this corresponds to a lag of 22 µm on the retina.

To assess direction selectivity of SAC distal dendrites, we used the direction selectivity index (DSI), defined as $\frac{\Delta Fcf - \Delta Fcp}{\Delta Fcf + \Delta Fcp}$, where ΔF_{cf} is the relative fluorescence change in centrifugal motion and ΔF_{cp} is that in centripetal motion. For statistical analysis, we compared variance across varicosities on the dendrites of the same SAC versus variance across varicosities of different SACs. Since the latter was larger, we averaged DSI of all the varicosities belonging to one SAC to get a single data point, and took N in the statistical analysis to be the number of cells, which equals the number of imaging windows.

2.7: Cell targeting for electrophysiology

Cells were visualized with infrared light (920 nm) and an IR-sensitive video camera (Watec). For experiments using visual stimulation, DSGCs were targeted with the aid of two-photon microscopy in *Drd4-GFP* mice. Cell identity was confirmed physiologically by extracellular recordings of responses to moving bars or anatomically using internal solution containing 25 µM Alexa 594 to

show the distinctive bistratified dendritic morphology in the SAC sublamina of the inner plexiform layer. For experiments without visual stimulation, SACs and DSGCs were targeted using epifluorescence (X-Cite) in retinas from mice expressing *Chat-IRES-Cre*, floxed *tdTomato*, and *Drd4-GFP*. In these mice, SACs selectively express tdTomato while posterior-preferring DSGCs express GFP. Cell identity was confirmed physiologically by the presence of dual excitatory and inhibitory transmission from SACs to DSGCs and/or morphologically using internal solution containing 25 μM Alexa 594 or 25 μM Alexa 488 to show co-stratification and fasciculation of the dendrites of On SACs and On-Off DSGCs.

Alpha cells were identified by their uniquely large size (diameter ≥20μm) and characteristic sustained IPSCs during visual stimulation (van Wyk et al., 2009).

2.8: Electrophysiological recordings and data analysis

Data were acquired using PCLAMP 10 recording software and a Multiclamp 700B amplifier (Molecular Devices, Sunnyvale, CA), low-pass filtered at 4 kHz and digitized at 10 kHz. Light-evoked responses were recorded at a bath temperature of 32–33°C. Paired SAC-DSGC and SAC depolarization step experiments were performed at room temperature.

For whole-cell recordings, recording electrodes of 2.5–4 MΩ were backfilled with a cesium-based internal solution containing (from Sigma): 110 mM $CsMeSO_4$, 2.8 mM NaCl, 4 mM EGTA, 5 mM TEA-Cl, 4 mM adenosine 5′-triphosphate (magnesium salt), 0.3 mM guanosine 5′-triphosphate (trisodium salt), 20 mM HEPES, 10 mM phosphocreatine (disodium salt), 5 mM N-Ethyllidocaine

chloride (QX314), pH 7.25. To preserve potassium channel activity in SACs, $CsMeSO_4$ was replaced by 110 mM $KMeSO_4$ and TEA-Cl was excluded. For whole-cell voltage clamp recordings of SACs, synaptic blockers (from Tocris): 0.008 mM DHβE, 0.05 mM D-AP5, 0.05 mM DNQX disodium salt, and 0.005 mM D-AP4 were applied to the bath solution to block synaptic transmission in the retina. For loose cell-attached recordings, electrodes were backfilled with Ames' medium.

IPSCs evoked by visual stimulation or SAC depolarization were isolated by holding DSGCs at 0 mV. EPSCs were isolated by holding DSGCs at -60 mV. At least three repetitions of raw synaptic traces were recorded and averaged to obtain the mean response for each stimulus condition and analyzed using PCLAMP 10 software. The peak amplitude and total charge transfer of IPSCs evoked by the On edge of the moving bar (the trailing edge in dark bars) were used to calculate the direction selective index (DSI) and vector sum. DSI is defined as $\frac{P-N}{P+N}$, where P is the peak amplitude or charge transfer of IPSCs in the preferred direction, and N is that in the null direction. Reported potentials have been adjusted for a 10 mV liquid junction potential (measured).

Data from loose cell-attached recordings were analyzed using custom protocols in MATLAB. The number of spikes evoked by the On (trailing) edge of the bar was counted using MATLAB and averaged across trials in each direction. Spike count was quantified in place of spike DSI because the low spike count in mGluR2 blockade reduced the reliability of DSI calculations (Carandini and Ferster, 2000).

2.9: Analysis of SAC membrane currents

Outward currents in response to 20-ms depolarization steps in K-based internal were measured by averaging current between 10 and 20 ms during the step. Inward currents in response to depolarization steps in Cs-based internal were measured by first fitting the first 1-6 ms during the step with an exponential function, and then subtracting the peak inward current from the fitted curve. During SAC pharmacological experiments, series and membrane resistance were monitored continuously by including a 5 mV hyperpolarizing step in each sweep. Cells were discarded or experiments were discontinued if their series resistance increased by more than 20% during the recording or exceeded 40 MΩ. Series resistance compensation was not performed.

2.10: Pharmacology

For mGluR2 blockade experiments, 50-100 nM LY341495 (Tocris) was added to Ames' media or aCSF after baseline experiments. At these concentrations, LY341495 is selective for Group II mGluRs (Kingston et al., 1998). Notably, mGluR3 has not been found in the mammalian retina (Brandstätter et al., 1998). For experiments to determine targets of mGluR2 signaling, the aCSF was perfused with 500nM-1μM LY354740 (Tocris), a highly selective Group II mGluR agonist (Schoepp et al., 1997) after whole-cell recording was established, and 3 μM LY341495 was subsequently used to competitively inhibit mGluR2 activity (Kingston et al., 1998). To block voltage-gated calcium channels, 300 μM $CdCl_2$ (Sigma) or combinations of 1 μM ω-conotoxin GVIA (Abcam) and 250 nM ω-agatoxin IVA (Alomone) were added to the aCSF.

2.11: Statistical analysis

The number of experimental repeats and sample means ± s.e.m. are indicated in figure legends. In most cases, analysis of calcium imaging data was performed blind to the mGluR2 antagonist condition. Statistical comparisons were performed using Wilcoxon signed rank test for paired samples or ANOVA followed by post hoc tests (either two-tailed paired Student's *t*-test or Tukey's test, as indicated in figure legends). $P < 0.05$ was considered significant. * $p < 0.05$; ** $p < 0.01$; *** $p < 0.001$.

Chapter 3: Cross-compartmental modulation of dendritic signals for retinal direction selectivity[1]

3.1: Summary

Compartmentalized signaling in dendritic subdomains is critical for the function of many central neurons. In the retina, individual dendritic sectors of a starburst amacrine cell (SAC) are preferentially activated by different directions of linear motion, indicating limited signal propagation between the sectors. However, the mechanism that regulates this propagation is poorly understood. Here, we find that metabotropic glutamate receptor 2 (mGluR2) signaling, which acts on voltage-gated calcium channels in SACs, selectively restricts cross-sector signal propagation in SACs, but does not affect local dendritic computation within individual sectors. mGluR2 signaling ensures sufficient electrotonic isolation of dendritic sectors to prevent their depolarization during non-preferred motion, yet enables controlled multicompartmental signal integration that enhances responses to preferred motion. We find that mGluR2-mediated dendritic compartmentalization in SACs is important for the functional output of direction-selective ganglion cells (DSGCs). Therefore, our results directly link modulation of dendritic compartmentalization to circuit-level encoding of motion direction in the retina.

3.2: Introduction

Neuronal signaling relies on efficient propagation of synaptic potentials along dendrites, yet spatially restricted propagation between dendritic subdomains often underlies important dendritic

[1] This chapter is wholly reproduced from a manuscript by Koren et al., 2017. Respective contributions are detailed on page 77.

computations (Branco and Häusser, 2010). A remarkable example is the dendrites of SACs, which play a central role in generating direction selectivity of DSGCs in the mammalian retina. As an axonless interneuron, the SAC receives glutamatergic inputs from bipolar cells in the proximal dendrites (Vlasits et al., 2016) and releases neurotransmitters GABA and acetylcholine from its distal varicosities (Brecha et al., 1988; Famiglietti, 1991; Kosaka et al., 1988; O'Malley and Masland, 1989; Vaney and Young, 1988) to DSGCs (Figure 3.1A). The radial branches of a SAC are considered independent computational units that individually prefer centrifugal motion, from the soma to their distal tips (Euler et al., 2002; Hausselt et al., 2007; Miller and Bloomfield, 1983; Velte and Miller, 1997) (Figure 3.1B). This centrifugal preference has been attributed to multiple cell intrinsic and synaptic mechanisms, including the distribution of active conductances (Euler et al., 2002; Hausselt et al., 2007; Oesch and Taylor, 2010) and chloride transporters (Gavrikov et al., 2003) along the SAC dendrites, proximal targeting of glutamatergic inputs (Vlasits et al., 2016), segregation of excitatory inputs from distinct bipolar cells (Fransen and Borghuis, 2017;

Figure 3.1

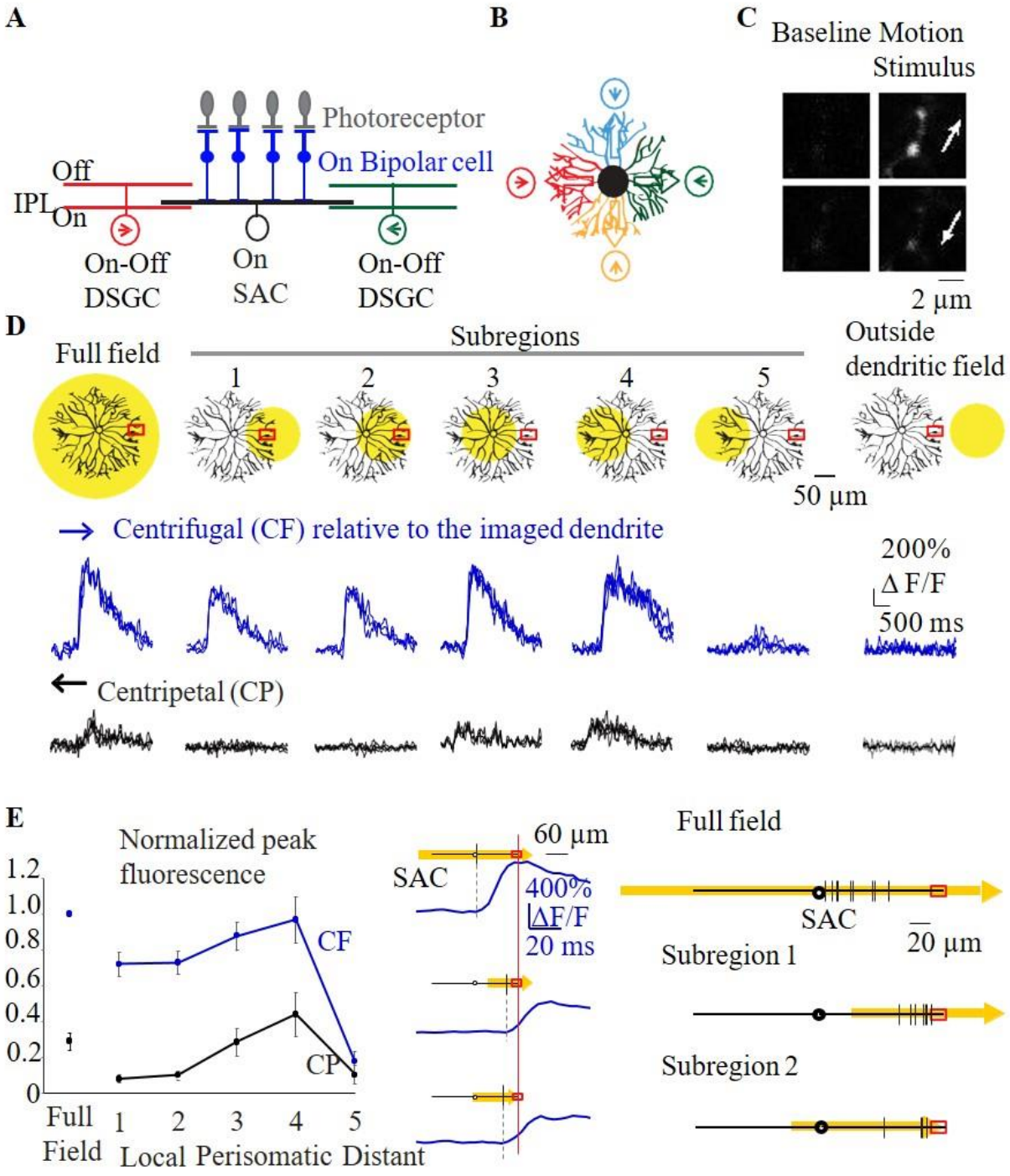

Figure 3.1. Multiple dendritic compartments contribute to centrifugal direction selectivity of SAC varicosities during linear motion (continues on next page)

G

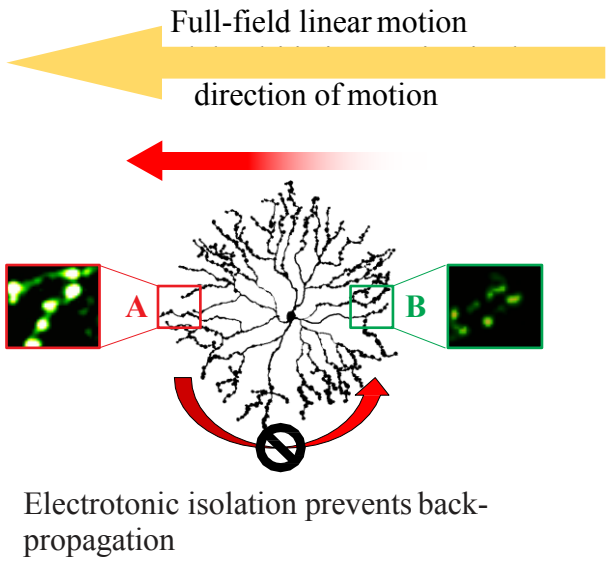

Figure 3.1 (continued). Multiple dendritic compartments contribute to centrifugal direction selectivity of SAC varicosities during linear motion

A. Schematic shows side view of the major cell types and connections involved in the On pathway of the direction selective circuit: the On SAC receives light-driven glutamatergic inputs from On bipolar cells (BP), and sends outputs to On-Off DSGCs. Inhibitory synapses onto a DSGC primarily come from SAC dendritic branches oriented in the null direction of the DSGC. PR: photoreceptor. Arrows indicate the preferred directions of the DSGCs. BP inputs onto the DSGC are not shown for clarity.

B. Schematic of the top view shows the asymmetric inhibition between SACs and DSGCs. Each SAC dendritic quadrant preferentially inhibits a subtype of On-Off DSGC whose preferred direction (arrow in circle) is antiparallel to the orientation of the SAC quadrant. Empty arrows on SAC dendrites indicate the preferred (i.e. centrifugal) directions of the SAC dendritic quadrants.

C. Example images of GCaMP6 fluorescence in distal SAC varicosities of an On SAC from a Chat-IRES-Cre mouse infected with AAV-floxed GCaMP6m at baseline and during the full-field moving bar stimulus in the centrifugal (top) and centripetal (bottom) directions (arrows). Also see Figure **3.2**.

D. Top: Schematics show the SAC dendritic areas within which the moving bar was presented (yellow filled circles) and the location of the calcium imaging window (red rectangles). Bottom: GCaMP6m fluorescence traces during centrifugal (CF) and centripetal (CP) motion under conditions shown at top. CF and CP are relative to the dendrites containing the imaging window. Dark traces represent mean values and light traces represent individual trials. See also Figure **3.3**.

E. Summary graph of peak fluorescence in SAC varicosities in different subregions evoked by motion in the CF and CP directions under the visual stimulus conditions shown in **D**. For each varicosity, responses are normalized to that during full-field motion in the CF direction. For subregion 5, peak amplitude was calculated only from trials that showed detectable responses. CF: full field: 1; subregion 1: 0.71 ± 0.07; subregion 2: 0.72 ± 0.05; subregion 3: 0.87 ± 0.08; subregion

Figure 3.1 (continued). Multiple dendritic compartments contribute to centrifugal direction selectivity of SAC varicosities during linear motion

4: 0.96 ± 0.11; subregion 5: 0.17 ± 0.06. CP: full field: 0.27 ± 0.04; subregion 1: 0.07 ± 0.02; subregion 2: 0.10 ± 0.02; subregion 3: 0.28 ± 0.08; subregion 4: 0.43 ± 0.11; subregion 5: 0.10 ± 0.07. n = 6 cells (53 total varicosities) from 6 mice. One-way ANOVA for CF direction: $F(5,25)= 54.4$, $p < 0.0001$. Tukey's post-hoc tests: Full field vs Subregion 1: $p = 0.0015$; Full field vs Subregion 2: $p = 0.0037$; Subregion 1 vs 4: $p = 0.019$; Subregion 2 vs 4: $p = 0.035$; Subregion 5 vs all stimuli: $p < 0.0001$. All other comparisons $P > 0.05$. One-way ANOVA for CP direction: $F(2,25) = 4.9$, $p = 0.0029$. Tukey's post-hoc tests: Subregion 1 vs 4: $p = 0.0048$; Subregion 2 vs 4:$p = 0.026$; Subregion 4 vs 5: $p = 0.011$. All other comparisons $P > 0.05$.
F. The onset timing of the calcium transients under different stimulus conditions. The dendritic field of the SAC is shown as black lines with the circles in the middle representing somas. The spatial extent and the direction of the moving bar stimuli is shown in yellow. Red rectangles indicate the location of the calcium imaging window. Left: Example calcium responses from one SAC. Vertical black lines on SAC dendrites indicate the spatial position of the moving bar's leading edge when the onset of calcium responses (blue traces) was detected in the varicosity in the imaging window. The calcium traces are aligned in the time axis relative to the time of the moving bar reaching the imaging window (red vertical line). Right: Summary of the onset timing of the calcium responses from multiple cells. Calculated distance from the bar's leading edge to the tip of the imaged dendrite: full field: 77 ± 6 µm, n = 9 cells; subregion 1: 18 ± 3 µm, n = 8 cells; subregion 2: 25 ± 8 µm, n = 4 cells. One-way ANOVA $F(2,18) = 38.8$, $p < 0.0001$. Tukey's post-hoc: Full field vs subregion 1: $p = 0.0001$; Full field vs subregion 2: $p = 0.0001$; subregion 1 vs subregion 2: $p = 0.72$.
G. A model of SAC dendritic processing during full-field linear motion. Sequential activation of SAC dendritic tree from right to left leads to strong centrifugal response in location A due to efficient spatiotemporal summation of depolarization along the motion trajectory. However, the strong centrifugal response in A does not propagate efficiently back to B due to electronic isolation between SAC dendritic branches.

Kim et al., 2014; but see Stincic et al., 2016), and lateral inhibition from neighboring SACs and non-SAC amacrine cells (Chen et al., 2016; Ding et al., 2016; Lee and Zhou, 2006).

As distinct computational units, the individual SAC dendritic sectors not only exhibit independent directional tuning to motion stimuli, but also connect to different postsynaptic targets. Each quadrant of the SAC dendritic tree selectively forms inhibitory synapses with one of the four subtypes of On-Off DSGCs whose preferred direction corresponds to the centripetal direction of

the SAC quadrant (Briggman et al., 2011; Fried et al., 2002; Lee et al., 2010; Wei et al., 2011) (Figure 3.1B). Selective wiring between SACs and DSGCs, together with the centrifugal directional preference of SAC dendrites, generates directionally tuned inhibition from SACs to DSGCs during linear motion that is important for the direction selectivity of DSGC spiking output.

Centrifugal direction selectivity of SAC dendritic sectors implies considerable electrotonic isolation between the sectors. Electrical isolation of SAC dendrites has been demonstrated with stationary light flashes: light spatially restricted to one circular sector of a SAC causes local activation without activating other unstimulated sectors (Euler et al., 2002). During linear motion, this is particularly important for reducing the centripetal-direction response of SAC dendrites, since it prevents propagation of depolarization from a centrifugally-stimulated SAC sector to other, weakly stimulated sectors of the same cell.

How is the strong centrifugal response of SAC dendrites generated during full-field motion? One possibility is that it arises solely from local dendritic processing within a SAC sector. Alternatively, despite considerable electrotonic isolation between SAC sectors, signal integration from multiple dendritic sectors may enhance the response of a centrifugally-stimulated branch due to favorable spatiotemporal summation (Tukker et al., 2004). These possibilities have not been examined experimentally. In the first part of this study, by comparing dendritic responses to motion stimuli crossing the full SAC receptive field with those to motion stimuli spatially restricted to different subfields, we find that multicompartmental signal integration is necessary for the strong and fast centrifugal response during full-field linear motion.

The fine balance between signal isolation and propagation between SAC dendritic sectors shapes the rules of dendritic computation in SACs. However, the regulatory mechanism that sets this balance is completely unknown. A strong molecular candidate is metabotropic glutamate receptor 2 (mGluR2), which is primarily expressed in SACs postsynaptically to bipolar cell synapses, but not in bipolar or ganglion cells (Cai and Pourcho, 1999; Koulen et al., 1996; Seebahn et al., 2008). mGluR2 activation is known to promote neuronal excitability by modulating voltage-gated conductances (Bischofberger and Schild, 1996; Hamlet and Lu, 2016; Ikeda et al., 1995; Knoflach and Kemp, 1998; Kupferschmidt and Lovinger, 2015; Saugstad et al., 1996; Taniguchi et al., 2013) and to influence spiking responses of DSGCs (Jensen, 2006). Nevertheless, the role of mGluR2 in SAC dendritic computation is unknown. In the second part of this study, we find that cross-sector signal propagation, but not local processing within a sector, is altered in the absence of endogenous mGluR2 signaling. This perturbation in SAC dendritic computation impacts the functional output of the circuit, the firing pattern of the direction selective ganglion cells, illustrating the importance of targeted modulation of spatiotemporal dendritic computation for encoding sensory information.

3.3: Results

Cross-compartmental signal integration improves the amplitude and latency of the centrifugal response of SAC dendrites during full-field linear motion

To investigate whether the centrifugal response of SAC dendrites during full-field linear motion is generated locally and independently by each dendritic sector, or involves participation from multiple dendritic compartments, we measured the motion-evoked calcium responses of On SAC

Figure 3.2

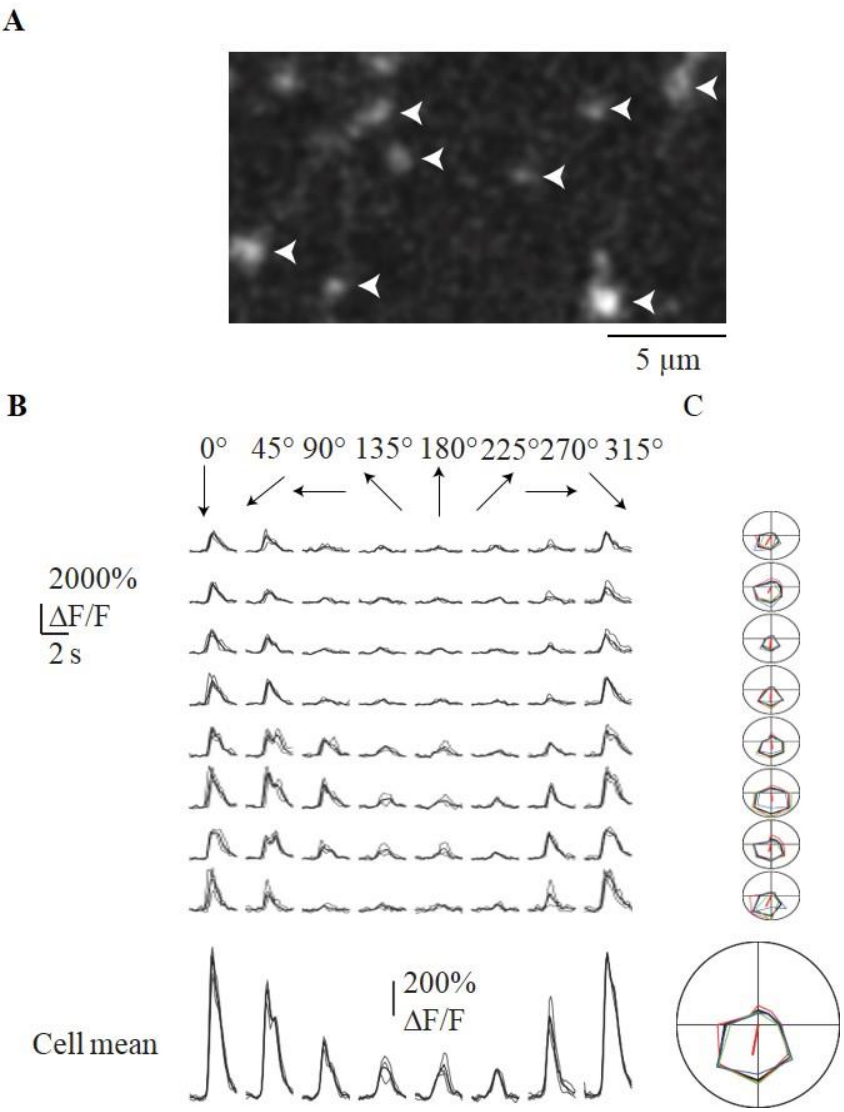

Figure 3.2: Calcium responses of imaged varicosities for a single SAC.
A.Summation projection (2 seconds) of a sample movie during a full-field centrifugal response, showing the SAC varicosities analyzed for this cell.
B. Top: Responses of the individual varicosities in A to full-field stimulation in each of 8 motion directions (indicated by arrows). Three trials of each direction are presented. Darker lines indicate mean of three trials. Bottom: Mean response of the varicosities imaged for this cell. Three trials of each direction are presented. Darker lines indicate mean of three trials.
C. Top: Tuning curves plotting the fluorescence response as a function of stimulus direction for individual varicosities. Thin colored lines indicate individual trials; thick black line indicates mean of the three trials. Thick red line indicates the vector sum of the mean response. Bottom: Tuning curve plotting the fluorescence response as a function of stimulus direction for the mean response of the varicosities imaged for this cell.

distal dendrites (Figures 3.1C and 3.2) when a moving bar stimulus was delivered to the entire SAC dendritic field, and when it was restricted to different subregions of the field. Stimulation outside the SAC dendritic field did not evoke calcium responses, indicating good spatial control of bipolar cell activation (Figure 3.1D, outside dendritic field, Figure 3.3). During full-field stimulation, a large centrifugal response was detected in distal varicosities (Figures 3.1D and 3.1E, full field), consistent with previous studies (Chen et al., 2016; Ding et al., 2016; Euler et al., 2002; Hausselt et al., 2007; Lee and Zhou, 2006; Oesch and Taylor, 2010; Vlasits et al., 2016). During subregion stimulation, we restricted the moving bar stimulus to various subregions of the SAC dendritic field while maintaining a fixed imaging site (Figure 3.1D). Stimulation restricted to the imaged dendritic sector produced larger responses in the centrifugal direction compared to those in the centripetal direction, indicating that direction selectivity can be computed locally within a dendritic sector (Hausselt et al., 2007) (Figures 3.1D and 3.1E, subregions 1 and 2, Supplemental movie 3.3). However, the amplitude of centrifugally evoked calcium transients during this local stimulation was significantly lower than that during the full-field stimulation (ANOVA $p < 0.0001$), even when the visual stimulus included proximal dendrites that receive most of the excitatory inputs (centrifugal responses in Figures 3.1D and 3.1E, full field versus subregion 2; Tukey's post-hoc test $p = 0.0037$). In addition, the onset of the centrifugal response in distal varicosities did not occur until the moving bar reached the distal tips of the dendrites during local stimulation (Figure 3.1F, subregions 1 and 2), while it occurred when the bar reached the proximal dendrites during full-field stimulation (Figure 3.1F, full field; ANOVA $p < 0.0001$; Full field vs subregion 2: $p = 0.001$). This enhanced amplitude and faster onset of calcium responses suggest

Figure 3.3

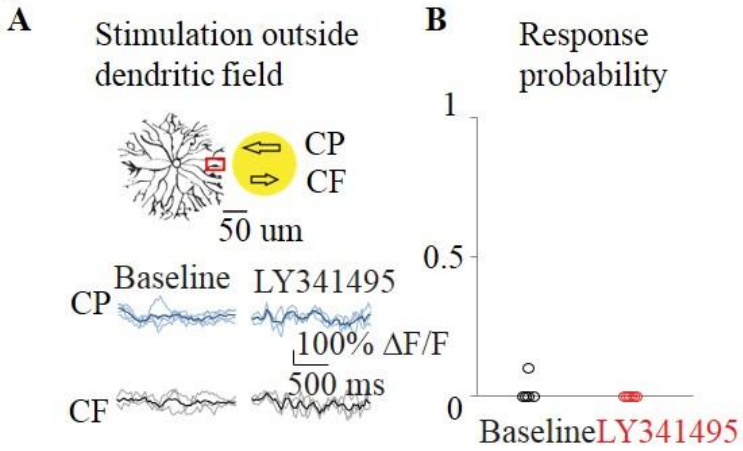

Figure 3.3. Motion stimulus outside the SAC's dendritic field does not evoke calcium response in the varicosities.
A. Schematic shows the areas within which the moving bar was presented (yellow filled circle) and the location of the calcium imaging window (red rectangle).
B. GCaMP6m fluorescence traces before and after addition of LY341495 during centrifugal (CF) and centripetal (CP) motion under the condition shown in **A**..Dark traces represent mean values and light traces represent individual trials.
C. Summary plot of response probability before and after adding LY341495 under the stimulus condition shown in **A**. n = 5 cells (45 varicosities) from 5 mice.

that multicompartmental signal integration plays a role during full-field motion in the centrifugal direction (Fig 3.1G).

When the moving bar stimulus was restricted to the perisomatic region covering either the proximal 60% of all dendritic sectors (Figure 3.1D, subregion 3) or mainly the dendritic sector on the opposite side of the imaging window (Figure 3.1D, subregion 4), strong centrifugal responses were readily detected, with an amplitude similar to that during full-field stimulation (Figures 3.1D and 3.1E, centrifugal responses of full-field versus subregions 3 and 4). Notably, the responses of varicosities in the imaging window were always stronger during motion in their centrifugal direction, regardless of the spatial extent and position of the subregion motion stimuli (Figures

3.1D and 3.1E). Therefore, both trans-somatic signal propagation and local preference of post-somatic dendrites are tuned in the direction of full-field linear motion. This likely presents a physiological advantage for the circuit, because efficient summation of the propagating signal with local excitation improves the amplitude and timing of centrifugal responses (Tukker et al., 2004) (Figure 3.1G), a computation reminiscent of coincident activation of distal dendrites and perisomatic compartments elsewhere in the nervous system (Bittner et al., 2015; Jarsky et al., 2005; Larkum et al., 2001).

Electrotonic isolation maintains the weak centripetal response of SAC dendrites

In contrast to the strong responses during motion in the centrifugal direction of the imaged dendrites, the response in the centripetal direction is weak under all stimulus conditions (Figure 3.1D and 3.1E), consistent with less effective summation of motion-evoked signals in this direction (Tukker et al., 2004). When the motion stimulus was positioned beyond the soma and covered only the distal 60% of the dendrites on the opposite side of a SAC (Figure 3.1D, subregion 5), calcium responses were evoked with significantly lower fidelity and amplitude in both centrifugal and centripetal directions (Figures 3.1D and 3.1E, subregion 5). A small calcium transient was observed in 55% of the trials when this opposite dendritic sector was stimulated in the centrifugal direction of the imaged dendrites and in 17% of the trials when it was stimulated in the centripetal direction. In contrast, the same stimulus reliably evoked stronger and centrifugally-tuned responses in the distal varicosities of the stimulated dendritic sector (Figure 3.1D, subregion 1). Therefore, the locally generated centrifugal-direction response within a dendritic sector does not propagate efficiently to the opposite, unstimulated sector due to electrotonic isolation between the sectors.

This ensures that during full-field motion, the strong centrifugal response of one dendritic sector does not contaminate the weak centripetal response of the opposite sector (Figure 3.1G).

mGluR2 blockade enhances the centripetal response of SAC dendrites during full-field motion

The importance of electrotonic isolation in minimizing the SAC's centripetal-direction responses prompted us to examine the mechanisms underlying this isolation. Compartmentalized signaling in dendrites has been attributed to interactions between synaptic inputs, active and passive dendritic conductances and dendritic morphology (Harnett et al., 2013; Johnston et al., 1997; Makara et al., 2009; Otsu et al., 2014). However, it is unclear if the electrotonic properties of SAC dendrites can be acutely modulated. Therefore, we searched for regulatory mechanisms of SAC dendritic excitability, and identified the SAC-specific mGluR2 signaling (Cai and Pourcho, 1999; Koulen et al., 1996; Seebahn et al., 2008) as a candidate. First, we tested if mGluR2 signaling affects the response of SAC varicosities to full field linear motion. The mGluR2 antagonist LY341495 consistently increased the amplitude of the full-field centripetal-direction response (Figures 3.4A, 3.4B, and 3.5). In contrast, it did not affect the centrifugal-direction response (Figures 3.4A and 3.4B), suggesting that the strong centrifugal-direction response is saturated (Lipin et al., 2015a) and cannot be further enhanced by mGluR2 blockade. As a result, the direction selectivity of SAC dendrites during full-field motion is reduced in mGluR2 blockade (Figures 3.4C and 3.5).

mGluR2 blockade selectively increases signal propagation between SAC dendritic sectors

The aberrant centripetal-direction response in mGluR2 blockade may be a result of either a general increase in SAC excitability that impacts local processing of individual dendritic sectors, or a selective reduction in electrotonic isolation between the sectors preferring different directions. In order to distinguish between these possibilities, we asked if mGluR2 signaling affects centrifugal direction selectivity within an individual dendritic sector. When the moving bar stimulus was restricted to the local dendritic sector containing the imaged varicosities (Figure 3.4D), mGluR2 antagonist LY341495 did not alter the highly directional calcium response of these varicosities (Figures 3.4D-F), indicating that mGluR2 is not required for the intrinsic centrifugal preference generated locally within a SAC dendritic sector. However, when the stimulus was restricted to the sector opposite the imaging window (Figure 3.4G), mGluR2 blockade improved the fidelity (Figures 3.4G and 3.4H, Baseline vs LY341495: $p = 0.01$, Two-way ANOVA) and amplitude (Figures 3.4G and 3.4I, $p = 0.0005$, Two-way ANOVA) of the trans-somatic calcium response. Therefore, endogenous mGluR2 signaling is important in preventing aberrant propagation of depolarization between SAC dendritic sectors without affecting local computation within the dendritic sector.

Reduced electronic isolation between SAC sectors during mGluR2 blockade is also evident when the motion stimulus is restricted to the perisomatic region covering the proximal dendrites. Under this condition, LY341495 abolished the direction selectivity of varicosity calcium responses by selectively increasing the response to stimulation in the centripetal direction for the imaged

Figure 3.4

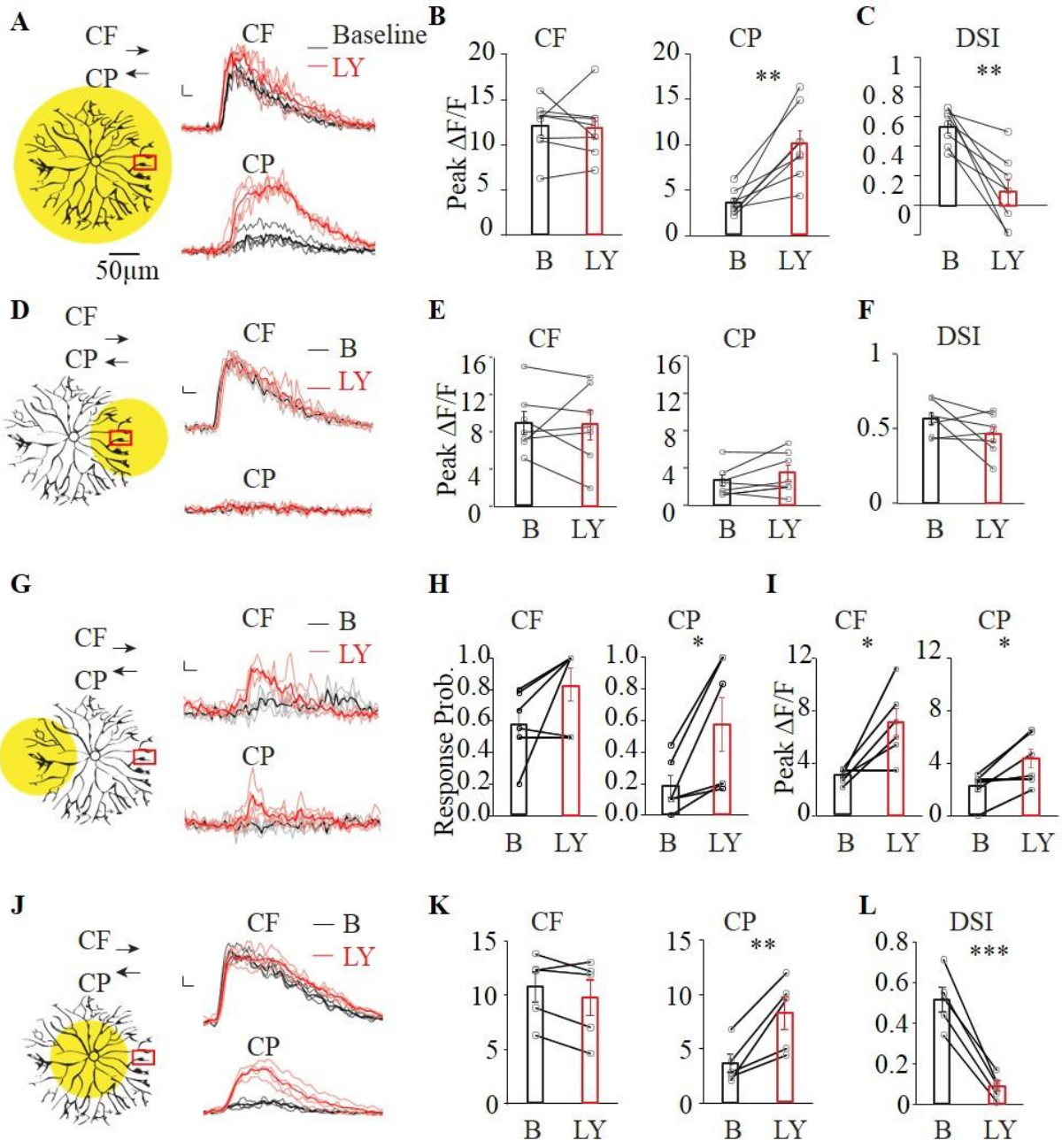

Figure 3.4. mGluR2 signaling promotes electrotonic isolation of SAC dendritic branches.
A - C. mGluR2 blockade selectively increases centripetal-direction response during full field linear motion. See also Figure **3.5**.
A. Left: same as full-field stimulus in Figure **3.1D**, schematic shows the spatial extent of the motion stimulus and the location of the calcium imaging window. Arrows indicate motion directions. Right: GCaMP6M fluorescence traces under this stimulus condition before (black) and

Figure 3.4 (cont.). mGluR2 signaling promotes electrotonic isolation of SAC dendritic branches.

after adding LY341495 (red). Dark traces represent mean values and light traces represent individual trials.

B. Summary of peak fluorescence of individual SACs before and after adding LY341495 under the condition shown in **a**. Centrifugal: baseline, 12.1 ± 1.0; LY341495, 11.8 ± 1.2; p = 0.80. Centripetal: baseline, 3.6 ± 0.5; LY341495, 10.1 ± 1.4; **p = 0.0018. n = 8 cells (97 varicosities) from 7 mice.

C. Same as **B**, summary of direction selectivity index (DSI) values. Baseline, 0.54 ± 0.04; LY341495, 0.09 ± 0.08; **p = 0.0016.

D - F. mGluR2 blockade has no effect on the SAC calcium response when the motion stimulus is restricted to the local dendritic branches containing the imaging window.

D. Left: same as subregion 1 in Figure **3.1D**, schematic shows the spatial extent of the motion stimulus and the location of the calcium imaging window. Right: GCaMP6M fluorescence traces of a varicosity before (black) and after adding LY341495 (red). Dark traces represent mean values and light traces represent individual trials.

E. Summary of peak fluorescence of individual SACs before and after adding LY341495 under the condition shown in **d**. Centrifugal: baseline, 8.9 ± 1.3; LY341495, 8.8 ± 1.6; p = 0.88. Centripetal: baseline, 2.6 ± 0.6; LY341495, 3.5 ± 0.8; p = 0.17. n = 7 cells (57 varicosities) from 6 mice.

F. Same as **e**, summary of DSI values. Baseline, 0.57 ± 0.04; LY341495, 0.46 ± 0.05; p = 0.15.

G - I: mGluR2 blockade enhances the calcium response of SAC varicosities when the motion stimulus is restricted to the dendritic sector located opposite the imaging window.

G. Left: same as subregion 5 in Figure **3.1D**, schematic shows the spatial extent of the motion stimulus and the location of the calcium imaging window. Right: GCaMP6M fluorescence traces under the stimulus condition shown on the left.

H. Summary of the response probability during motion in the centrifugal and centripetal directions of the imaged dendritic branches before and after adding LY341495 under the stimulus condition shown in **G**. Response probability is calculated as the number of trials with detectable calcium responses divided by the total number of trials (See Methods). Centrifugal: baseline, 0.55 ± 0.09; LY341495, 0.83 ± 0.11; p = 0.097. Centripetal: baseline, 0.17 ± 0.07; LY341495, 0.64 ± 0.14; *p = 0.02. n = 6 cells (53 varicosities) from 6 mice.

I. As in **G**, summary of peak amplitude of the propagated responses. Peak amplitude is calculated only from the trials with detectable calcium responses. Centrifugal: baseline, 3.0 ± 0.2; LY341495, 7.0 ± 1.1; *p = 0.016. Centripetal: baseline, 2.2 ± 0.5; LY341495, 4.3 ± 0.8; *p = 0.018.

J - L: mGluR2 blockade enhances centripetal-direction responses of SAC varicosities during perisomatic motion stimulation.

J. Left: same as subregion 3 in Figure **3.1D**, schematic shows the spatial extent of the motion stimulus and the location of the calcium imaging window. Right: GCaMP6M fluorescence traces under the stimulus condition shown on the left.

K. Summary of peak fluorescence of individual SACs before and after adding LY341495 during perisomatic stimulation (data combined for subregions 3 and 4 in Figure **3.1D**). Centrifugal: baseline, 10.7 ± 1.4; LY341495, 9.8 ± 1.7; p = 0.13. Centripetal: baseline, 3.6 ± 0.9; LY341495, 8.2 ± 1.5; *p = 0.01. n = 5 cells (39 varicosities) from 5 mice.

Figure 3.4 (cont.). mGluR2 signaling promotes electrotonic isolation of SAC dendritic branches.
L. Same as **K**, summary of DSI values. Baseline, 0.51 ± 0.06; LY341495, 0.09 ± 0.03; ***p = 0.0001.

Figure 3.5

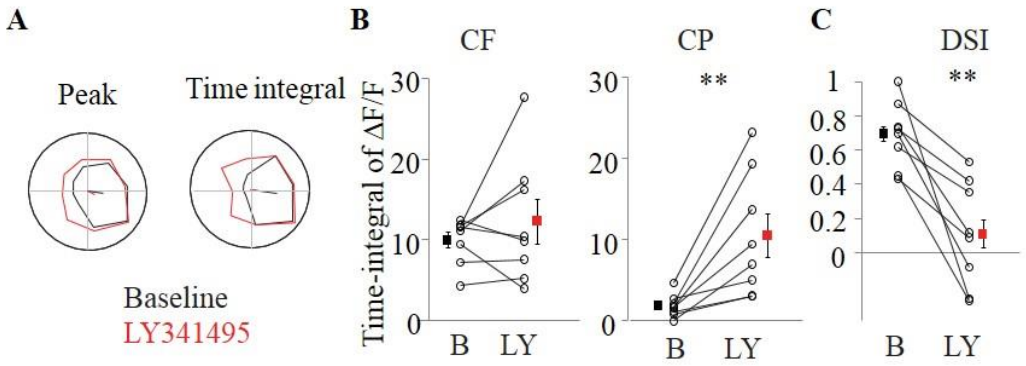

Figure 3.5. mGluR2 blockade increases the time-integral of centripetal direction calcium responses of SACs during full-field linear motion.
A. Polar plots of mean peak and time integral of GCaMP6M fluorescence in a SAC varicosity before and after adding LY341495.
B. Pairwise comparison of time-integral of ΔF/F for individual SACs before and after adding LY341495 during centrifugal and centripetal motion. Centrifugal: baseline, 10.0 ± 1.0; LY341495, 12.3 ± 2.8; p = 0.35. Centripetal: baseline, 1.9 ± 0.5; LY341495, 10.5 ± 2.7; **p = 0.008. n = 8 cells from 7 mice.
C. Same as **B**, pairwise comparison of DSI values. Baseline, 0.69 ± 0.07; LY341495, 0.11 ± 0.22; **p = 0.002.

dendritic sector (Figures 3.4J-3.4L). Since the centrifugal response was unaffected by LY341495 (Figures 3.4J and 3.4K), this illustrates that mGluR2 acts to prevent contamination of weakly-activated SAC sectors by the responses of strongly-activated sectors. Therefore, during linear motion, mGluR2 ensures that signals summate efficiently along SACs in the direction of stimulus motion without back-propagating to centripetally-stimulated varicosities (Figure 3.1G).

Figure 3.6

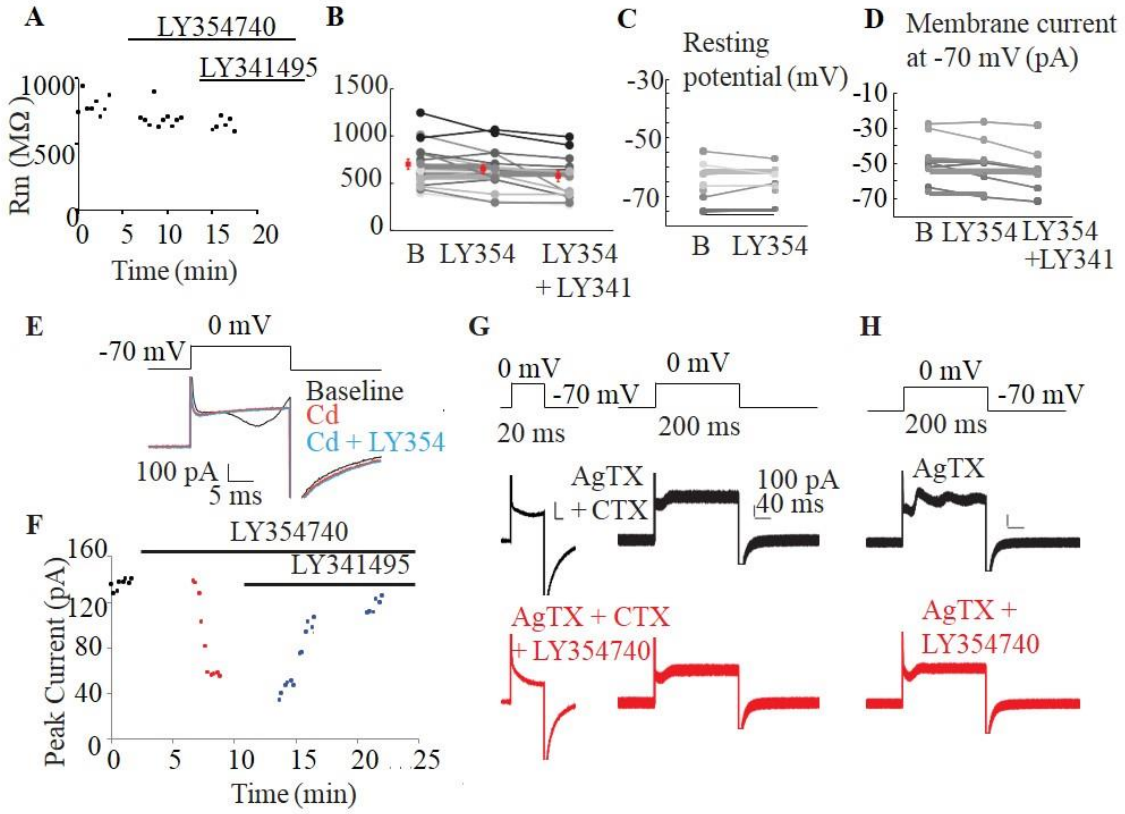

Figure 3.6. mGluR2 does not modulate resting membrane properties of SACs, but inhibits N- and P/Q-type calcium channels..

A. Plot of resting membrane resistance of a SAC at the baseline, and after sequential addition of LY354740 and then the competitive antagonist LY341495 (LY354740+LY341495).

B. Same as **A**, summary of SAC resting membrane resistance. Baseline, 691±53 MΩ; LY354740, 641±49 MΩ; LY354740+LY341495, 565±59 MΩ; One-way ANOVA p=0.34. n=18 cells; 9 mice.

C. Pairwise comparison of resting membrane potential of SACs before and after addition of LY354740. Baseline, -65.1 ± 2.6 mV; LY354740, -64.9 ± 2.1 mV; p = 0.83. n =7cells from 4 mice.

D. Plot of the amplitude of membrane currents in SACs at the holding potential of -70 mV at the baseline, and after sequential addition of LY354740 and then the competitive antagonist LY341495 (LY354740 + LY341495). Baseline, -38.7 ± 4.3 pA; LY354740, -41.2 ± 4.6 pA; LY354750 + LY341495, -43.4 ± 5.2 pA; One-way ANOVA p = 0.62. n = 9 cells from 7 mice.

E. Example voltage clamp traces of a SAC at baseline, and after sequential addition of cadmium (Cd), and then LY354740 (Cd + LY354740).

F. Plot of peak amplitude of the inward calcium current during depolarization of a SAC to 0 mV as a function of time. Application of LY354740 and LY341495 are indicated by the bars above the plot.

G. Example voltage clamp traces of a SAC during 20 ms (left) and 200 ms (right) depolarization in the presence of AgTX and CTX, and after subsequent addition of LY354740 (AgTX + CTX + LY354740). For each condition, traces represent the overlay of 10 repetitions.

mGluR2 signaling inhibits voltage-gated calcium channels in SACs

To understand the molecular mechanism underlying the effect of mGluR2 on electrotonic isolation, we searched for the ion channel targets of mGluR2 signaling in SACs while blocking synaptic transmission in the retina. We found that mGluR2 does not modulate resting membrane properties in SACs (Figures 3.6A-D). Previously, the Kv3 family of voltage-gated potassium channels had been suggested to underlie electrotonic isolation in SACs (Ozaita et al., 2004). However, we found that the cesium-sensitive voltage-gated outward conductance mediated by these channels is not affected by the mGluR2 agonist LY354740 (Figures 3.7A and 3.7B).

We next investigated if mGluR2 modulates voltage-gated calcium currents in SACs by performing voltage-clamp recording using a cesium-based internal solution (see Chapter 2). During prolonged membrane depolarization to 0 mV, a regenerative transient is triggered due to imperfect space clamp of the thin distal dendrites (Figure 3.7C). However, the latency and amplitude of the fast initial peak of this transient are highly consistent across trials (Figure 3.7C, boxed region) and reliably activated during depolarization to over -30 mV (Figures 3.7D and 3.7F). This transient is blocked by the nonselective calcium channel blocker cadmium (Figure 3.6E), or a combination of N- and P/Q-type calcium channel antagonists ω-conotoxin GVIA (CTX, 1 μM) and ω-agatoxin IVA (AgTX, 250 nM, Figure 3.7C and 3.7D), consistent with previous reports on the presence of N- and P/Q type calcium channels in rabbit SACs (Cohen, 2001; Lee et al., 2010). Application of LY354740 reversibly inhibits this calcium transient (Figures 3.7E, 3.7F and 3.6F). Furthermore, in the presence of CTX and AgTX or cadmium, application of LY354740 has no effect on the

Figure 3.7

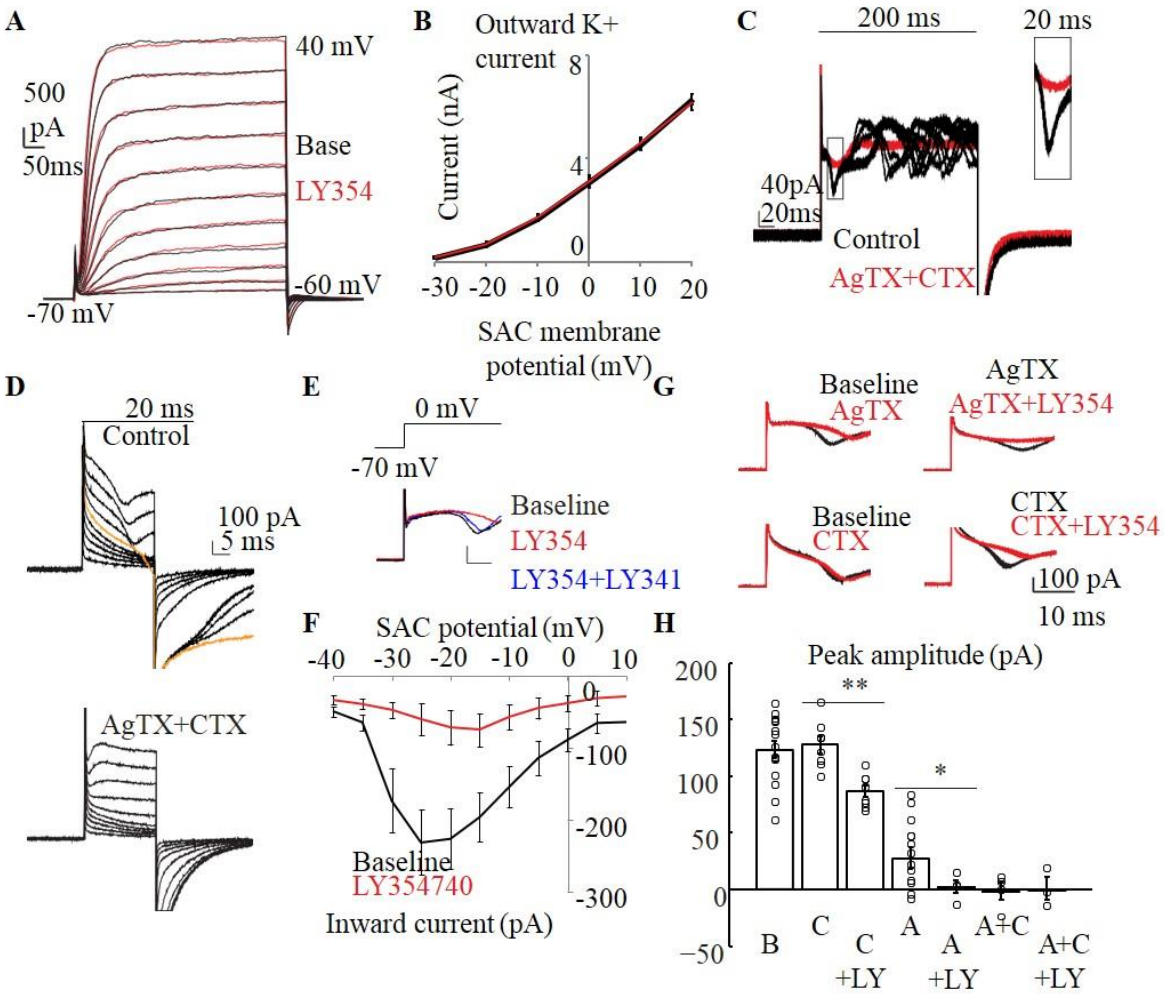

Figure 3.7. mGluR2 inhibits voltage-gated calcium channels, but not voltage-gated potassium channels in SACs.

A. Voltage clamp traces of a SAC in potassium-based internal solution during steps of depolarization at 10 mV increment before (black) and after adding the mGluR2 agonist LY354740 (red).

B. Relationship between average steady-state outward potassium current and membrane potential in SACs before (black) and after LY354740 (red). Repeated measures ANOVA p = 0.49, n = 4 cells from 3 mice.

C. Example voltage clamp traces of a SAC in cesium-based internal solution at baseline and after addition of AgTX and CTX (AgTX + CTX) during steps of depolarization from -70 mV to 0 mV for 200 ms. For each condition, traces represent the overlay of 10 repetitions. Capacitive currents are clipped for clarity. Inset shows the boxed region at higher magnification.

D. Example voltage clamp traces of a SAC at the baseline (upper), and after addition of AgTX and CTX (lower) during steps of 20 ms depolarization from -70 mV at 10 mV increment. Orange trace represents the onset of the inward calcium transient. Capacitive currents are clipped for clarity.

Figure 3.7 (cont.). mGluR2 inhibits voltage-gated calcium channels, but not voltage-gated potassium channels in SACs.
E. Example voltage clamp traces of a SAC at the baseline, and after sequential addition of LY354740 and then the competitive antagonist LY341495 (LY354740 + LY341495). Capacitive currents are clipped for clarity.
F. Relationship between peak of the inward current and membrane potential in SACs before and after LY354740. Repeated measures ANOVA **p = 0.0017, n = 9 cells from 5 mice.
G. Example traces of the same SACs before (black) and after (red) application of selective calcium antagonist and LY354740. For each condition, traces represent the overlay of 10 repetitions.
H. Summary of effects of CTX (C), AgTX (A) and LY354740 (LY) on the peak amplitude of the initial calcium transient. Baseline, 123.4 ± 7.8, n = 14 cells from 6 mice; C, 127.7 ± 7.3, n = 8 cells; C + LY, 86.7 ± 5.1, n = 8 cells; A, 27.4 ± 9.5, n = 14 cells; A + LY, 2.3 ± 5.6, n = 4 cells; A+ C, -1.5 ± 7.7, n = 4 cells; A + C + LY, 1.1 ± 9.7, n = 3 cells; C versus C + LY, **p = 0.0006; A versus A + LY, * p = 0.02.

residual currents in SACs (Figures 3.6E and 3.6G). These results indicate that mGluR2 inhibits voltage-gated calcium channels, but appears to operate independently of voltage-gated potassium channels.

To determine whether mGluR2 signaling selectively inhibits P/Q-type or N-type calcium channels, we applied AgTX or CTX individually to the bath solution in the presence of synaptic blockers. Application of AgTX significantly reduced the amplitude of the initial calcium transient (Figures 3.7G and 3.7H), and also decreased the frequency of regenerative events during prolonged depolarization (Figure 3.6H compared to Figure 3.7C), indicating a significant contribution to the calcium transients by P/Q-type calcium channels. Applying LY354740 in the presence of AgTX eliminated the residual AgTX-insensitive calcium transient, indicating mGluR2 signaling inhibits N-type calcium channels (Figures 3.7G and 3.7H). However, application of CTX alone did not change the amplitude of the initial transient, suggesting that blocking N-type calcium channels alone is not sufficient to modulate the suprathreshold regenerative calcium transient (Figures 3.7G

and 3.7H). Addition of LY354740 in the presence of CTX decreased the CTX-insensitive inward current (Figures 3.7G and 3.7H), indicating that mGluR2 also inhibits P/Q-type calcium channels.

We note that mGluR2 blockade does not directly activate synaptic calcium channels in SAC varicosities during the moving bar stimuli used in this study, because the calcium responses during local stimulation of a dendritic sector were not enhanced by mGluR2 antagonist in either the centrifugal or the centripetal directions (Figures 3.4D-F). If the mGluR2 antagonist affected synaptic calcium channels by directly activating them, the centripetal response during local stimulation would increase and the direction selectivity of a process would be impaired. We did not observe this, indicating that the mGluR2 does not directly modulate synaptic calcium channels. Instead, mGluR2 plays a highly specific role in dendritic processing of SACs by regulating trans-somatic propagation of motion-evoked activation between dendritic compartments.

mGluR2 blockade leads to enhanced but delayed inhibition onto DSGCs in the preferred direction

To test how mGluR2 blockade impacts the light response of On-Off DSGCs, we performed whole-cell voltage-clamp recordings of DSGC inhibition, which primarily comes from SAC dendrites extending in the null direction of the DSGC (Briggman et al., 2011; Fried et al., 2002; Lee et al., 2010; Wei et al., 2011) (Figure 3.8A). During full-field motion in the preferred direction of a DSGC, inhibitory postsynaptic currents (IPSCs) are weak because the presynaptic SAC dendritic sector that releases GABA onto that DSGC is minimally activated by motion in the centripetal direction (Figure 3.8A, left schematic). Since mGluR2 blockade enhances centripetal responses in

Figure 3.8

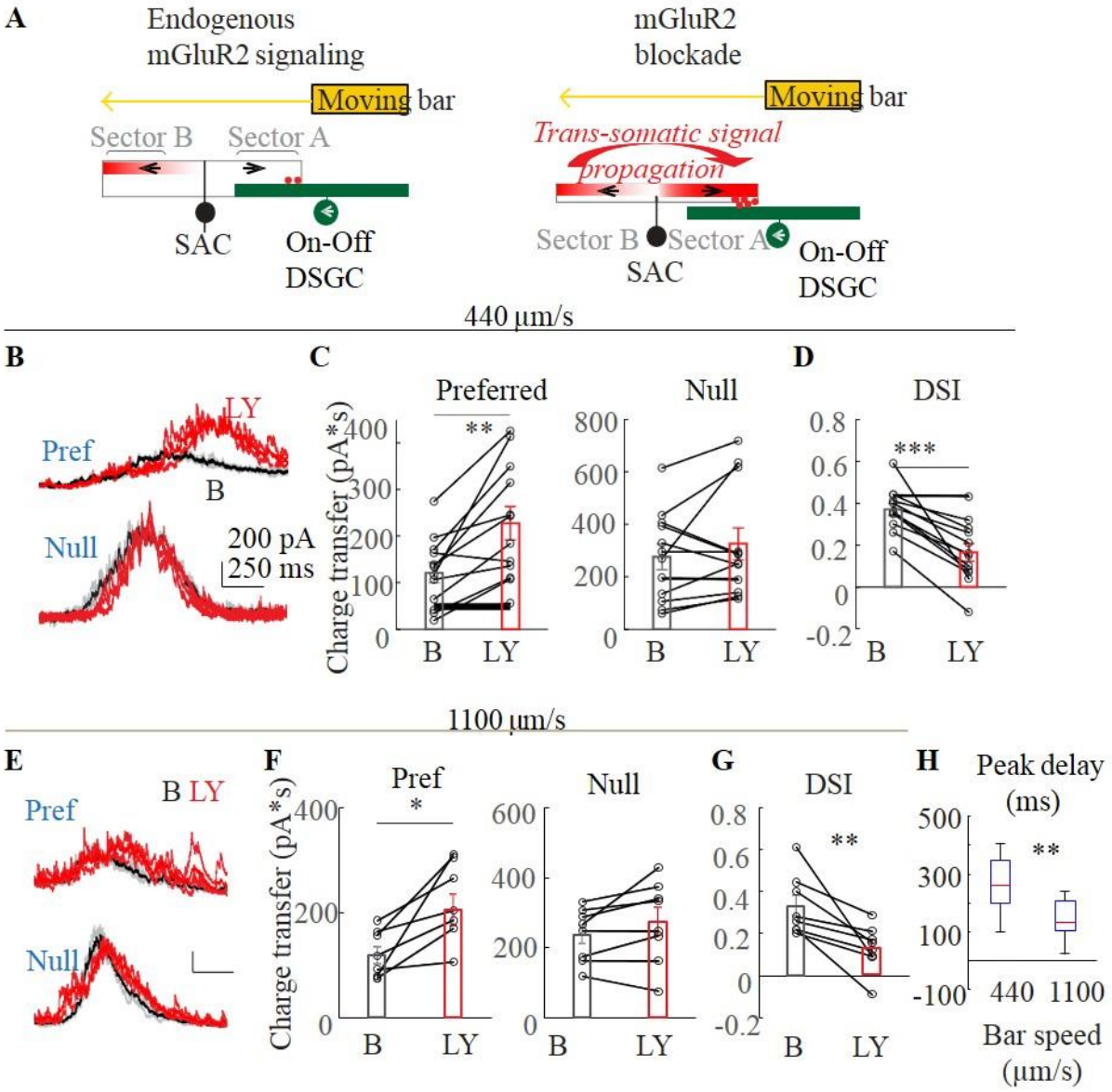

Figure 3.8. mGluR2 blockade causes an enhanced but delayed preferred-direction inhibition onto DSGCs.

A. A model of mGluR2-dependent dendritic compartmentalization in SACs. Left: During endogenous mGluR2 signaling, SAC dendritic branches are more isolated from each other. A bar moving in the preferred direction of the DSGC (leftward) triggers minimal GABA release (red dots) from the centripetally activated sector A of the SAC. Subsequent activation of sector B in the centrifugal direction does not propagate efficiently to sector A to trigger GABA release. Right: During mGluR2 blockade, electrotonic isolation between SAC branches is reduced. Therefore, the

Figure 3.8 (cont.). mGluR2 blockade causes an enhanced but delayed preferred-direction inhibition onto DSGCs.
strong centrifugal response of sector B propagates more efficiently to sector A. This leads to enhanced dendritic activation of sector A and more GABA release onto the DSGC during motion in the DSGC's preferred direction.
B – D. DSGC IPSCs before and after adding LY341495 at the bar speed of 440 µm/s.
B. Example On components of IPSC traces of DSGCs in a wild type mouse evoked by a dark bar moving in the preferred and null directions at a bar speed of 440 µm/s before (black) and after (red) adding LY341495. Dark traces represent mean values and light traces represent individual trials. Also see Figures **3.9B-D** for IPSC data evoked by a bright bar.
C. Summary of charge transfer of IPSCs in the preferred and null directions at the speed of 440 µm/s in wild type mice. Preferred: baseline, 121.8 ± 21.6 pA·s; LY341495, 227.5 ± 36.0 pA·s;**p = 0.002. Null: baseline, 275.9 ± 48.9 pA·s; LY341495, 325.7 ± 60.8 pA·s; p = 0.23. n = 12 cells from 5 mice. Also see Figures **3.9B-D**.
D. As in **C**, summary of DSI values for IPSCs in wild type mice at the bar speed of 440 µm/s. Baseline, 0.37 ± 0.03; LY341495, 0.17 ± 0.04; *** p = 0.0001.
E – G. DSGC IPSCs before and after adding LY341495 at the bar speed of 1100 µm/s.
E. As in **B**, example IPSC traces of DSGCs at the bar speed of 1100 µm/s.
F. As in **C**, summary of charge transfer of IPSCs at the bar speed of 1100 µm/s. Preferred: baseline, 118.0 ± 15.8 pA·s; LY341495, 204.6 ± 29.9 pA·s; *p = 0.01. Null: baseline, 236.9 ± 26.8 pA·s; LY341495, 274.1 ± 41.1 pA·s; p = 0.13. n = 8 cells from 5 mice.
G. As in **D**, summary of DSI values for IPSCs at the bar speed of 1100 µm/s. Baseline, 0.33 ± 0.05; LY341495, 0.13 ± 0.04; ** p = 0.008.
H. Boxplot of the temporal delay of IPSC peak due to LY341495 application in wild type mice at the bar speed of 440 um/s and 1100 um/s. Mean ± SEM: 440 um/s, 289 ± 39 ms; 1100 um/s, 147± 20 ms; **p = 0.005. n = 12 cells from 7 mice. Also see Figure **3.9A**. Also see Figure **3.12** for the effect of LY341495 on DSGCs from mGluR2 KO mice and alpha RGCs.

SAC varicosities due to back-propagation (Figures 3.4A-C), we expect that motion in the preferred direction will produce greater GABA release onto DSGCs, albeit with an increased latency (Figure 3.8, right schematic). As expected, when LY341495 was applied, the preferred-direction On IPSCs exhibited an enhanced but delayed component (Figures 3.8B and 3.8C). The latency of this enhanced component (289 ± 39 ms, for bar speed of 440 µm/s, Figures 3.8H and 3.9A) roughly corresponds to the time necessary for the moving bar to travel one SAC dendritic radius (127 ± 17 µm). Also as expected, the null-direction IPSCs were not significantly affected by LY341495 (Figures 3.8B and 3.9A), consistent with saturated centrifugal-direction calcium responses in

Figure 3.9

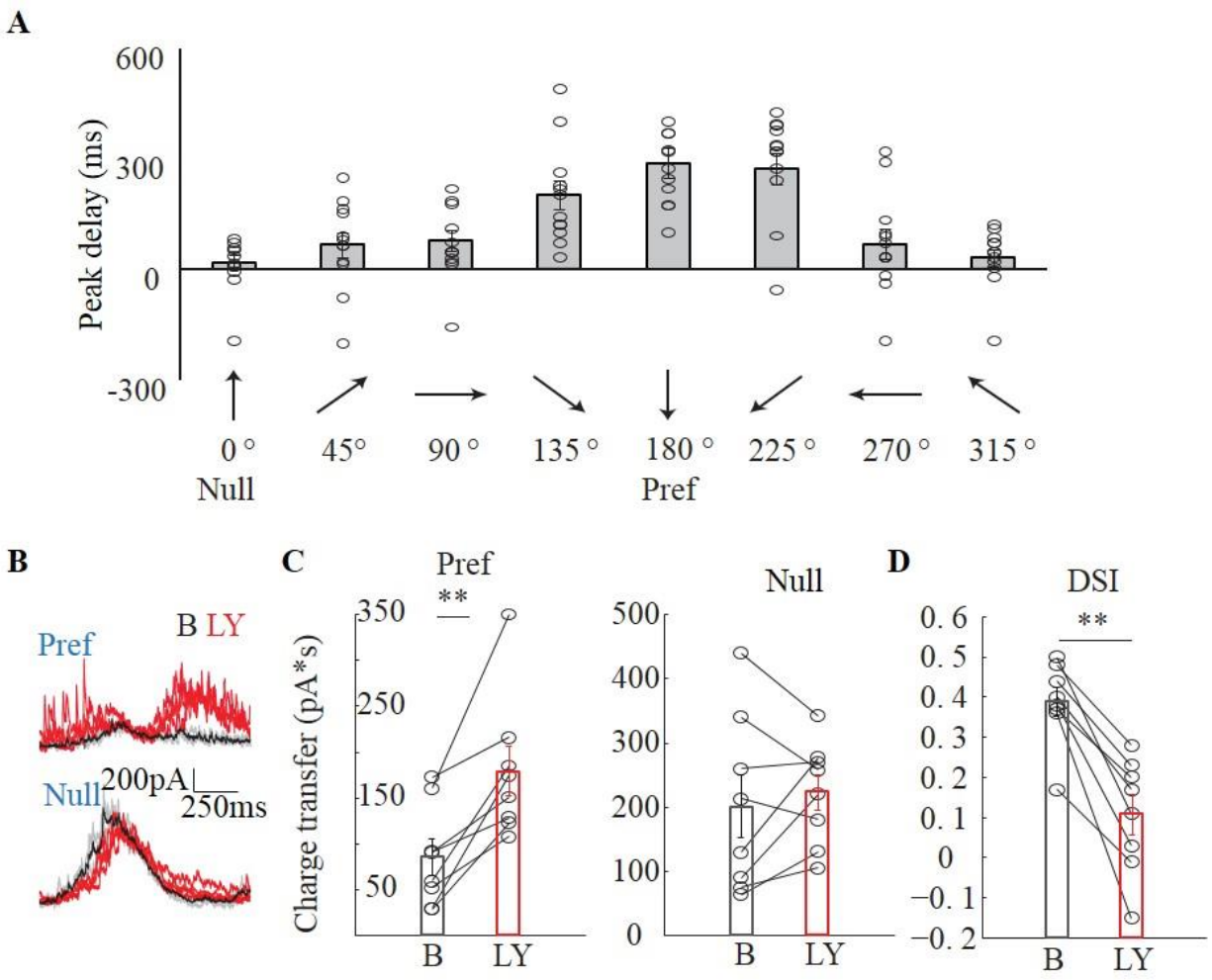

Figure 3.9. mGluR2 blockade causes an enhanced but delayed preferred-direction inhibition onto DSGCs.

A. Delay of IPSC peak in the presence of LY341495 as a function of motion direction. The null direction is set to 0° for all cells. Bars indicate mean delay; data points for individual cells represented by open circles. One way-ANOVA $F(7;88) = 9.89$, $p < 0.0001$. Tukey's post-hoc test: 0° (17 ± 22 ms) vs 135° (202 ± 29 ms): $p = 0.0073$. 0° vs 180° (289 ± 39 ms): $p < 0.0001$. 0° vs 225° (274 ± 42 ms): $p < 0.0001$. 45° (66 ± 35 ms) vs 180°: $p = 0.0005$. 45° vs 225°: $p = 0.0015$. 90° (79 ± 30 ms) vs 180°: $p = 0.0012$. 90° vs 225°: $p = 0.0035$. 135° vs 315° (32 ± 24 ms): $p = 0.018$. 180° vs 270° (69 ± 40 ms): $p = 0.0006$. 180° vs 315°: $p < 0.0001$. 225° vs 270°: $p = 0.0019$. 225° vs 315°: $p = 0.0001$. All other comparisons $p > 0.05$. n = 12 cells from 7 mice.

B-D. IPSCs during a bright moving bar stimulus

B. Example On components of IPSCs of a DSGC in a wild type mouse evoked by a bright bar moving in the preferred and null directions at a bar speed of 440 µm/s before (black) and after

Figure 3.9 (cont.). mGluR2 blockade causes an enhanced but delayed preferred-direction inhibition onto DSGCs.
(red) adding LY341495. Dark traces represent mean values and light traces represent individual trials.
C. Summary of charge transfer of IPSCs in the preferred and null directions at the speed of 440 µm/s in wild type mice. Preferred: baseline, 86.1 ± 19.6 pA·s; LY341495, 179.8 ± 27.4 pA·s; **p = 0.002. Null: baseline, 201.5 ± 48.5 pA·s; LY341495, 223.0 ± 28.1 pA·s; p = 0.52. n = 12 cells from 5 mice.
D. As in **C**, summary of DSI values for IPSCs in wild type mice at the bar speed of 440 µm/s. Baseline, 0.39 ± 0.04; LY341495, 0.11 ± 0.05; *** p = 0.0003.

SACs (Figure 3.4) and saturated null-direction inhibition in DSGCs (Lipin et al., 2015b). Consequently, mGluR2 blockade decreases the direction selectivity of DSGC inhibition (Figure 3.8D). Similar results were obtained when the contrast of the moving bar was reversed (Figures 3.9B-D). This effect is produced by LY341495 acting specifically on mGluR2 in SACs, because the drug has no effect on the strength and timing of IPSCs in mGluR2 knockout mice (Figures 3.10A-G), nor on IPSCs of alpha retinal ganglion cells in wild type mice, a cell type that is not synaptically connected to SACs (Figures 3.10J and 3.10K).

Since the timing of sequential activation of opposite SAC sectors during full-field stimulation depends on the speed of a moving stimulus, we tested the effect of mGluR2 blockade at a higher bar speed. We found enhanced preferred-direction inhibitory inputs onto DSGCs and reduced direction selectivity of inhibition similar to those seen during the lower bar speed (Figures 3.8E-G). However, the latency of the preferred-direction IPSC peak at this speed was reduced, since the faster moving bar activates opposite sectors more quickly (Figures 3.8E and 3.8H, 147 ± 20 ms, for bar speed of 1100 µm/s), equivalent to a spatial offset of ~ 1.3 SAC radius (162 ± 22 µm). Therefore, mGluR2 blockade in SACs selectively increases preferred-direction inhibition onto

Figure 3.10

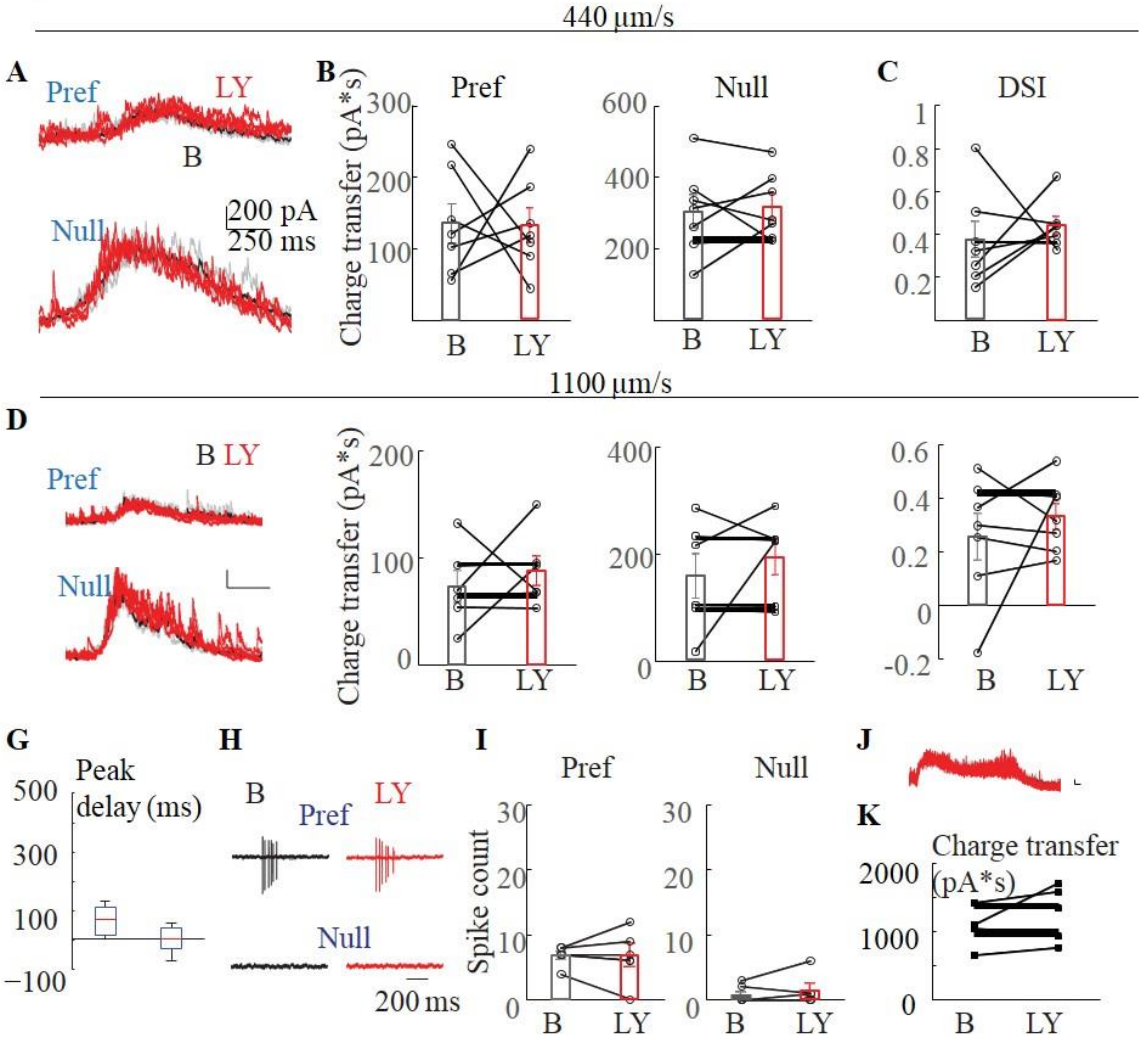

Figure 3.10. mGluR2 agonist has no effect on DSGC IPSC and spiking in mGluR2 KO mice or alpha ganglion cells in wild type mice.

A-I: IPSC and spiking activity of DSGCs in mGluR2 KO mice. A-C. IPSCs of DSGCs at a bar speed of 440 µm/s.

A. Example On components of IPSC traces of DSGCs in an mGluR2 KO mouse evoked by a dark bar moving in the preferred and null directions at a bar speed of 440 µm/s before (black) and after (red) adding LY341495. Dark traces represent mean values and light traces represent individual trials.

B. Summary of charge transfer of IPSCs in the preferred and null directions at the speed of 440 µm/s in mGluR2 KO mice. Preferred: baseline, 135.4 ± 27.5 pA•s; LY341495, 131.9 ± 24.3 pA•s; p = 0.94. Null: baseline, 303.2 ± 46.0 pA•s; LY341495, 318.4 ± 35.0 pA•s; p= 0.72. n = 7 cells from 5 mice.

C. Summary of DSI values for IPSCs in mGluR2 KO mice at the bar speed of 440 µm/s. Baseline, 0.37 ± 0.08; LY341495, 0.44 ± 0.04; p = 0.57.

Figure 3.10 (cont.). mGluR2 agonist has no effect on DSGC IPSC and spiking in mGluR2 KO mice or alpha ganglion cells in wild type mice.
D-F. IPSCs of DSGCs at a bar speed of 1100 µm/s.
D. As in **A**, example IPSC traces of DSGCs in an mGluR2 KO mouse at the speed of 1100 µm/s.
E. As in **B**, summary of inhibitory charge transfer at 1100 µm/s in mGluR2 KO mice. Preferred: baseline, 72.4 ± 15.0 pA•s; LY341495, 87.6 ± 14.1 pA•s; p = 0.51. Null: baseline, 159.6 ± 41.5 pA•s; LY341495, 193.3 ± 32.1 pA•s; p = 0.42. n = 6 cells from 4 mice.
F. As in **C**, summary of DSI values for IPSCs at the speed of 1100 µm/s in mGluR2 KO mice. Baseline, 0.26 ± 0.09; LY341495, 0.33 ± 0.05; p = 0.46.
G. Boxplot of the temporal delay of IPSC peak due to LY341495 application in mGluR2 KO mice at the bar speed of 440 mm/s and 1100 mm/s. Mean ± SEM: 440 mm/s, 35 ± 48 ms, n = 7 cells from 5 mice; 1100 mm/s, 1 ± 19 ms. n = 6 cells from 4 mice.
H. Example traces of DSGC spikes evoked by the bar speed of 1100 µm/s in the preferred and null directions in an mGluR2 KO mouse before and after adding LY341495.
I. Summary plot of DSGC spike count in mGluR2 KO mice at the bar speed of 1100 µm/s. Preferred: baseline, 6.8 ± 0.6; LY341495, 6.7
± 1.6; p = 0.88. Null: baseline, 0.8 ± 0.5; LY341495, 1.3 ± 1.0; p = 0.40. n = 6 cells from 3 mice.
J-K: IPSCs from alpha ganglion cells in wild type mice.
J. Example IPSC traces of an Off-alpha retinal ganglion cell in a wild type mouse during the moving bar stimulus at the bar speed of 1100 µm/s before and after adding LY341495. Dark traces represent mean values and light traces represent individual trials.
K. Pairwise comparison of charge transfer for motion-evoked IPSCs in alpha retinal ganglion cells before and after addition of LY341495. Baseline, 1124 ± 142; LY341495, 1264 ± 181; p = 0.33. n = 5 cells from 2 mice.

DSGCs by enabling propagation of dendritic signals between SAC dendritic sectors that are tuned to different motion directions.

mGluR2 blockade reduces DSGC spiking in the preferred direction at higher motion speed

To test if mGluR2 blockade is functionally relevant to the ultimate output of the retinal direction selective circuit, we examined the spiking activity of DSGCs during perfusion of LY341495. We hypothesized that the enhanced but delayed preferred-direction inhibition during mGluR2 blockade decreases DSGC firing rate. Since SACs release both acetylcholine and GABA to DSGCs, we first examined the effect of mGluR2 antagonist on DSGC EPSCs. In contrast to the increased IPSCs, we found no significant change in the peak EPSC or overall excitatory charge

transfer during moving stimuli in the presence of LY341495 (Figures 3.11B and 3.11C), presumably because centripetally-activated SAC dendrites only contribute to a small fraction of the total excitatory inputs onto DSGCs (Figure 3.11A, also see Discussion). In order for delayed IPSCs to impact DSGC spiking, the two must temporally coincide. Therefore, we compared temporal relationship among the evoked excitatory and inhibitory charge transfer and firing rate of DSGCs. In baseline conditions, inhibitory charge transfer in response to a bar moving at 440 μm/s was delayed by 100-200 ms relative to the excitatory charge transfer (Figures 3.12A and 3.12B) consistent with previous studies (Pei et al., 2015; Taylor and Vaney, 2002). The statistically significant effect of LY341495 on IPSCs evoked at this speed began after 70% of the excitatory charge transfer and 77% of DSGC spiking had already occurred (Figure 3.12B). By contrast, the baseline inhibitory charge transfer in response to a bar moving at 1100 μm/s was coincident with the excitatory charge transfer (Figures 3.12C and 3.12D). Because of the reduced latency of the aberrant inhibition at faster stimulus speed, the effect of mGluR2 blockade on IPSCs began after only 49% of the excitatory charge transfer and 59% of DSGC firing had occurred (Figure 3.12D). Consistent with this result, LY341495 reduced DSGC firing during an 1100 μm/s stimulus, predominantly while IPSCs were increased (Figure 3.12D); by contrast, there was no statistically significant reduction in DSGC firing during a 440 μm/s stimulus (Figure 3.12B).

The effect of LY341495 on DSGC firing gradually increased with increasing stimulus speed between 440 μm/s and 1760 μm/s, consistent with a mechanism based on the degree of temporal overlap of EPSCs with enhanced IPSCs (Figure 3.12E). The mGluR2 antagonist had no effect on DSGC firing rate in the KO mice (Figures 3.10H and 3.10I), further validating our

Figure 3.11

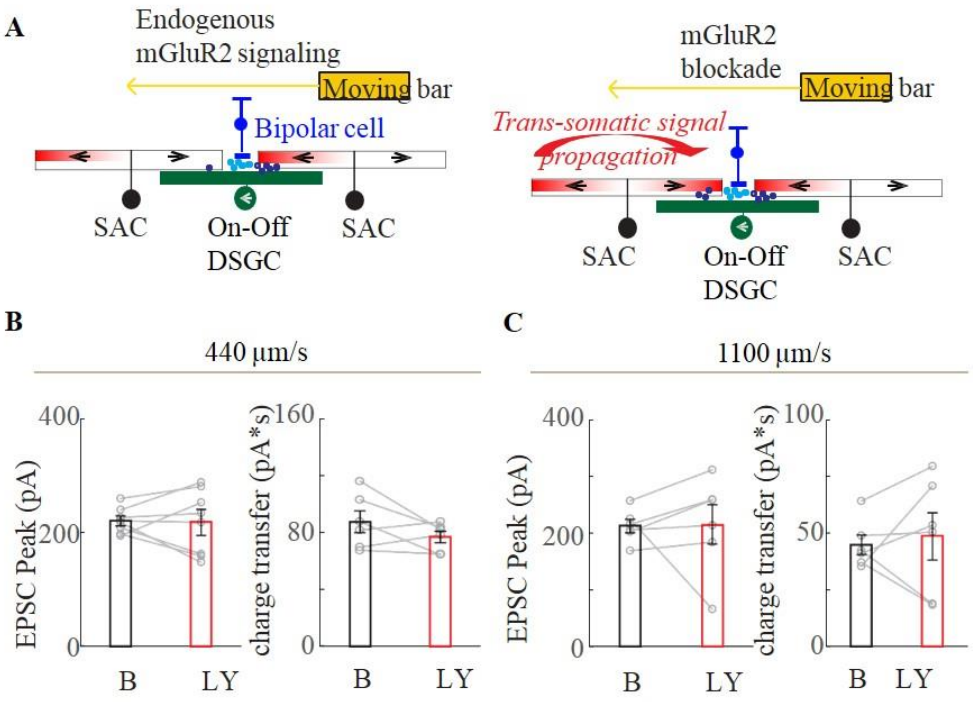

Figure 3.11. mGluR2 blockade does not significantly change preferred-direction excitation onto DSGCs.

A. A model of the effect of mGluR2 blockade on DSGC excitation. The total excitation comes from two sources: glutamate (light blue dots) released from bipolar cells and acetylcholine (dark blue dots) from SACs. SACs form cholinergic synapses with DSGCs in an isotropic pattern. During mGluR2 blockade, enhanced trans-somatic propagation of depolarization in SACs causes increased acetylcholine release only from the centripetally activated SAC sectors, but not from centrifugally activated sectors. The glutamate release is not affected. Therefore, in contrast to the inhibitory inputs, the effect of mGluR2 blockade on the overall excitatory inputs is less pronounced. Also see Discussion.

B. Summary of EPSC peak amplitude and charge transfer in the preferred direction at the speed of 440 µm/s before and after adding LY341495. Peak: baseline, 220.2 ± 8.9; LY341495, 217.4 ± 22.8; p = 0.89, n=7 cells from 5 mice. Charge transfer: baseline, 87.5 ± 7.8; LY341495, 76.8 ± 4.0; p = 0.19.

C. Summary of EPSC peak amplitude and charge transfer in the preferred direction at the speed of 1100 µm/s before and after adding LY341495. Peak: baseline, 212.2 ± 11.8; LY341495, 215.5 ± 34.8; p = 0.93, n = 6 cells from 4 mice. Charge transfer: baseline, 44.8 ± 4.3; LY341495, 48.5 ± 10.4; p = 0.70.

Figure 3.12

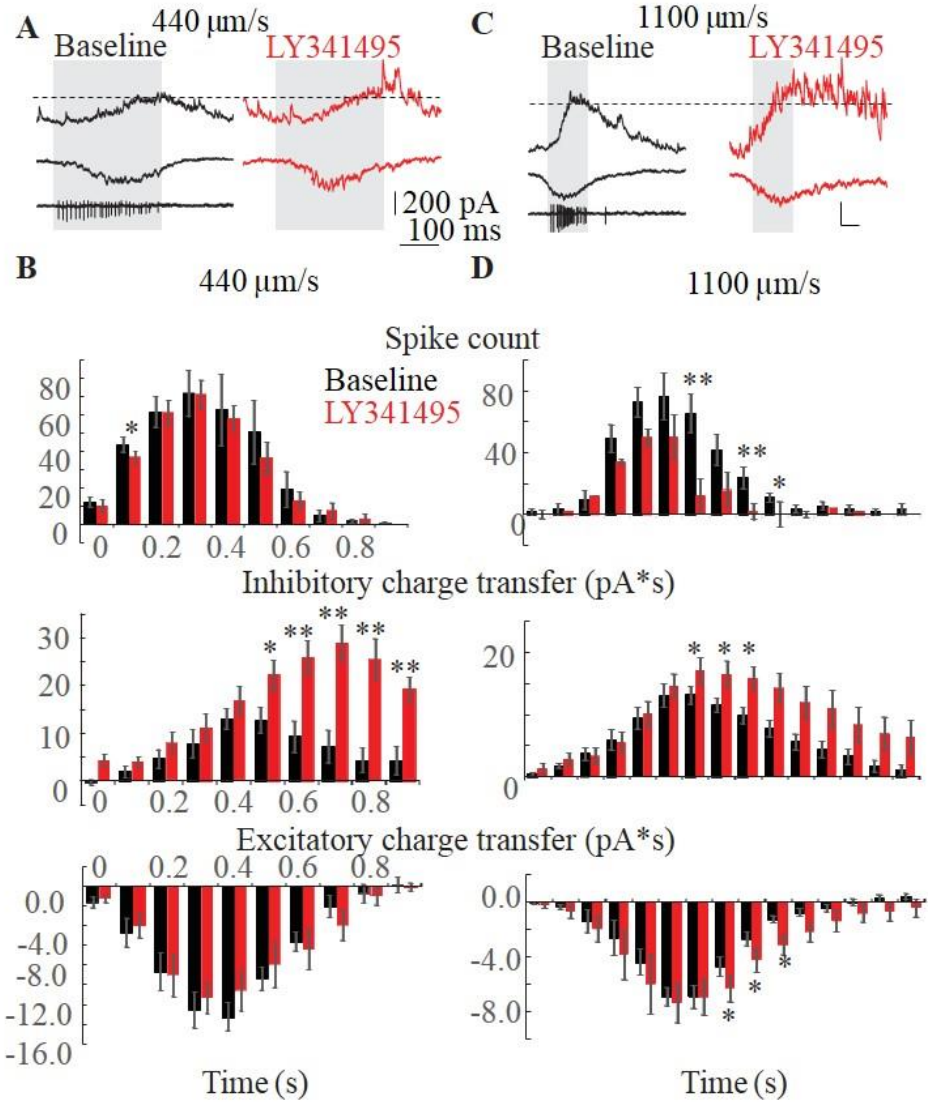

Figure 3.12. mGluR2 blockade decreases preferred-direction spiking of DSGCs at higher bar speed (continues on next page).

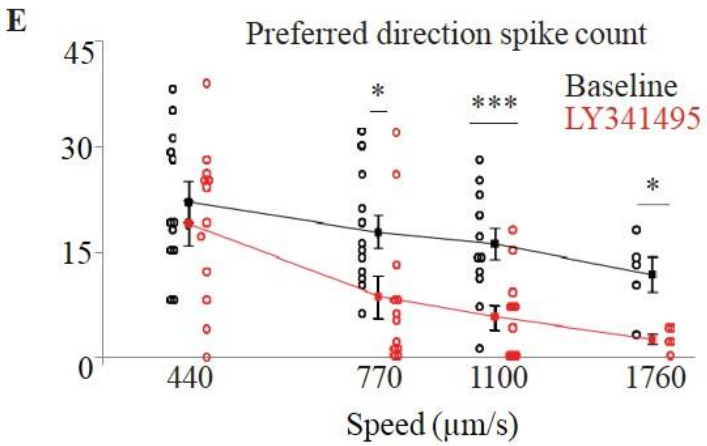

Figure 3.12 (cont.). mGluR2 blockade decreases preferred-direction spiking of DSGCs at higher bar speed.

A. Example loose cell-attached and whole-cell recordings of a DSGC showing IPSC (upper), EPSC (middle) and spiking (lower left) in the baseline condition (left) and the IPSC and EPSC from the same cell after adding LY341495 (right) evoked by a bar moving in the preferred direction at the bar speed of 440 µm/s. Shaded area represents the temporal window of spiking activity at the baseline condition. Dashed line indicates the peak IPSC level at baseline condition. The LY341495-enhanced IPSC component lags behind spiking activity.

B. Summary histograms of DSGC spike count (upper), inhibitory charge transfer (middle) and excitatory charge transfer (lower) before and after adding LY341495 at the speed of 440 µm/s. Spiking: n = 9 cells; inhibition: n = 6 cells; excitation: n = 6 cells. Spiking: 0.1 – 0.2 s: *p = 0.02. Inhibition: 0.5 – 0.6 s: *p = 0.035; 0.6 - 0.7 s: **p = 0.004; 0.7 – 0.8 s: **p = 0.003; 0.8 – 0.9 s: **p = 0.005; 0.9 – 1.0 s: **p= 0.003.

C. As in **A**, example loose cell-attached and whole-cell recordings of a DSGC showing IPSC (upper), EPSC (middle) and spiking (lower left) in the baseline condition (left) and the IPSC and EPSC from the same cell after adding LY341495 (right) evoked by a bar moving in the preferred direction at the bar speed of 1100 µm/s. A portion of he LY341495-enhanced IPSC component coincides with spiking activity.

D. As in **B**, summary histograms of DSGC spike count (upper), inhibitory charge transfer (middle) and excitatory charge transfer (lower) before and after adding LY341495 at the speed of 440 µm/s. Spiking: n = 11 cells; inhibition: n = 8 cells; excitation: n = 8 cells. Spiking: 0.30-0.35 s: **p = 0.001; 0.40 – 0.45 s: *p = 0.008; 0.45 – 0.50 s: *p = 0.015. Inhibition: 0.30 – 0.35 s: *p = 0.029; 0.35 – 0.40 s: *p = 0.023; 0.40 – 0.45 s: *p = 0.019. Excitation: 0.35 – 0.40 s: * p = 0.037; 0.40 – 0.45: *p = 0.042; 0.45 – 0.50 s: *p = 0.015; 0.50 – 0.55 s: *p = 0.049.

E. Summary plot of preferred direction spike count before and after adding LY341495 at different speeds. Horizontal (speed) axis is in log scale. Mean ± SEM: 440 µm/s: baseline, 21.9 ± 2.9; LY341495, 18.9 ± 3.2; p = 0.42, n = 12 cells; 770 µm/s: baseline, 17.7 ± 2.9; LY341495, 8.5 ± 3.0; *p = 0.035, n = 12 cells; 1100 µm/s: baseline, 16.0 ± 2.2; LY341495, 5.6 ± 1.8; *** p = 0.0001, n = 12 cells; 1760 µm/s: baseline, 11.6 ± 2.5; LY341495, 2.4 ± 0.7; *p = 0.01, n = 5 cells.

pharmacological approach. Together, these data illustrate that the reduction in DSGC firing during mGluR2 blockade is speed-dependent and is due to aberrantly large IPSCs. This indicates that mGluR2-dependent dendritic computation in SACs is particularly important for the generation of strong preferred-direction DSGC spiking at higher motion speed, suggesting a role for mGluR2 signaling in the broad speed tuning of On-Off DSGCs.

3.4: Discussion

Our findings highlight the importance of regulated interaction between dendritic subdomains in dendritic computation, even for strongly isolated and functionally distinct dendritic compartments. While many current models assume that centrifugal direction selectivity of SAC dendrites is independently computed within individual dendritic sectors, our results demonstrate that direction selectivity of SAC dendrites during full-field motion arises from the delicate balance between electrotonic isolation and cross-compartmental signal integration. Signal integration from the entire dendritic tree primes and amplifies the response to centrifugal motion, while electrotonic isolation attenuates the response to centripetal motion.

A role for multicompartmental signal integration in the centrifugal direction confirms a prior modeling study that predicted efficient summation in the centrifugal direction at the distal SAC dendrites due to temporal coincidence of local excitation with the "global" signal spreading from the rest of the dendritic tree (Tukker et al., 2004). In contrast, the local signal in the centripetally-stimulated distal dendrites does not coincide with the temporally delayed global signal, leading to little summation (Tukker et al., 2004). The global signal in the centripetally-stimulated dendrites

is highly suppressed by mGluR2-mediated electrotonic isolation, which prevents the subsequent strong activation of the opposite, centrifugally-stimulated sector from back-propagating and contaminating the centripetal response of the original sector.

In our study, neither the centrifugal responses in SAC varicosities nor the resultant null-direction IPSCs in DSGCs were significantly affected by LY341495, illustrating that the SAC centrifugal response is robust to the decrease in multicompartmental integration caused by mGluR2 signaling at our stimulus conditions. This indicates that favored spatiotemporal integration across SAC dendrites is capable of evoking maximal GABA release from SACs at the endogenous level of mGluR2 signaling. This finding is consistent with nonlinearities in the SAC response to whole-field motion demonstrated in previous studies, which found that SAC GABA release and DSGC direction selectivity are saturated for a wide range of stimulus contrasts and speeds (Amthor and Grzywacz, 1991; Grzywacz and Amthor, 2007; Lipin et al., 2015b). By contrast, we find that the SAC centripetal response is significantly modulated by mGluR2 signaling, illustrating that dendritic nonlinearities can enable modulation of dendritic responses in a direction-selective manner (Figure 3.13). However, we cannot rule out that mGluR2-dependent changes in dendritic integration could affect the centrifugal response during other stimulus conditions.

Optimized balance between signal isolation and cross-compartmental integration is subject to neuromodulation via mGluR2 signaling. mGluR2 activation inhibits N- and P/Q-types of voltage-gated calcium channels in SACs. These calcium channels have been shown to participate in synaptic release of acetylcholine and GABA from SACs in the rabbit (Lee et al., 2010). However,

Figure 3.13

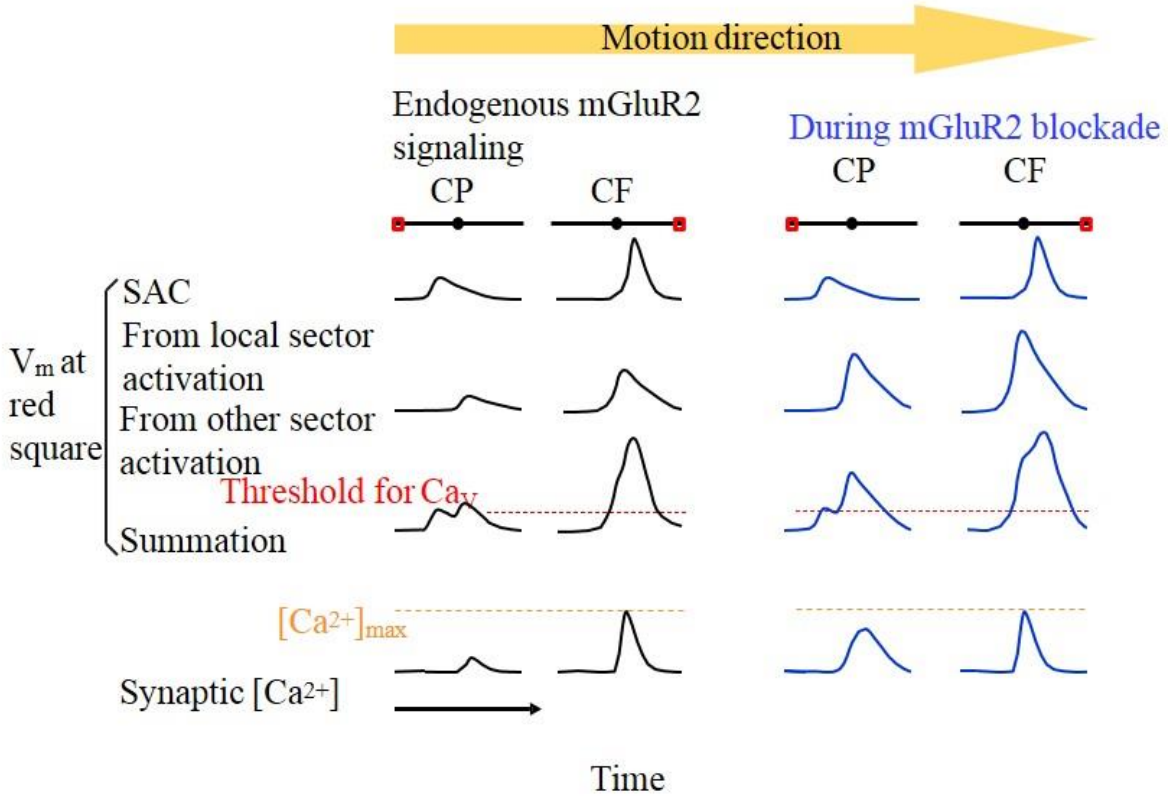

Figure 3.13. A model of the effect of mGluR2 blockade on SAC dendritic activation during full field motion.
The dendritic field of the SAC is shown as black lines with the circles in the middle representing somas. The traces represent the Vm or calcium response over time at the varicosities indicated by red rectangles. Vm from local sector activation refers to the membrane depolarization caused by activation of only the dendritic sector containing the red square. mGluR2 blockade does not affect the component of depolarization from local sector activation (see Figure **3.4B**). Vm from other sector activation refers to membrane depolarization at the red square caused by activation of the rest of the dendritic tree, which is enhanced by mGluR2 blockade (see Figure **3.4C**). Vm summation refers to the arithmetic sum of the responses from local sector and other sector stimulation. The threshold for voltage-dependent Ca^{2+} channel activation is shown as red dashed line. Synaptic [Ca^{2+}] saturates at the level indicated by the orange dashed line. CF calcium response is saturated at the varicosities and therefore cannot be further enhanced by mGluR2 blockade.

when endogenous mGluR2 signaling is blocked, we did not detect an increase in calcium responses

during local stimulation within the dendritic sector, indicating that endogenous mGluR2 signaling

does not directly inhibit synaptic calcium channels and synaptic transmission under our stimulus conditions. Instead, this mechanism controls a subpopulation of calcium channels specifically involved in trans-somatic signal propagation. This specificity may be a consequence of the segregation of proximal glutamatergic input sites from distal neurotransmitter release sites on SAC dendrites (Vlasits et al., 2016). For example, proximally-localized mGluR2 may gate the trans-somatic propagation of depolarization without affecting depolarization and calcium influx in distal varicosities. Because glutamatergic inputs are mostly located on proximal SAC dendrites, mGluR2-dependent inhibition of voltage-gated calcium channels likely acts in concert with other cell-intrinsic and synaptic mechanisms that are targeted to the proximal dendritic region of the SAC to promote electrotonic isolation between dendritic sectors. These mechanisms include proximal expression of Kv3 channels (Ozaita et al., 2004) and enriched inhibitory inputs onto the proximal dendrites from neighboring amacrine cells (Ding et al., 2016).

Pharmacological blockade of mGluR2 signaling in our study preferentially impacted SACs in the direction selective circuit, since mGluR2 expression is mainly restricted to SACs in rodents (Koulen et al., 1996; Seebahn et al., 2008), and the mGluR2 promoter has been used to drive GFP expression selectively in On and Off SACs in a transgenic mouse line (Watanabe et al, 1998; Wang et al, 2007). Besides SACs, rod amacrine cells, presumably A17 amacrine cells, exhibit weak immunofluorescence for mGluR2 (Koulen et al., 1996; Seebahn et al., 2008). However, lack of mGluR2 in the rod amacrine cells is unlikely to contribute to the effect we observed, since the rod pathway is saturated under the photopic visual stimulus condition in our study. The selective expression pattern of mGluR2 in rodents is in contrast to that in the cat or rabbit, which has been

reported to include the horizontal and multiple types of amacrine cells (Cai and Pourcho, 1999; Jensen, 2006).

mGluR2-dependent dendritic computation in SACs is important for the DSGC spiking output that is conveyed from the retina to the brain during preferred-direction motion. This effect appears to rely on speed-dependent coincidence between excitatory and inhibitory inputs. Most GABAergic synapses onto a DSGC arise from SAC dendrites that prefer motion in the null direction of the DSGC. The somata of these SACs are mostly located on the null side of the DSGC. To elicit enhanced IPSCs onto a DSGC during preferred-direction motion in mGluR2 blockade, the stimulus must activate the more distant sectors of these SACs. Therefore, the latency of enhanced IPSCs during mGluR2 blockade depends on the speed of motion. At lower speeds, the increase of IPSC during mGluR2 blockade lags the excitation and spiking, and therefore has little effect on the firing rate of DSGCs. At higher speeds, the mGluR2-dependent change in IPSC occurs with a shorter latency, and overlaps more with the temporal window of excitation and spiking. As a result, mGluR2 blockade exerts a greater impact in DSGC spiking at higher stimulus speeds. While we cannot rule out the possibility that additional mechanisms play a role in reducing DSGC spiking during high-speed motion in mGluR2 blockade, the temporal correspondence of enhanced IPSCs and spiking reduction strongly suggests a causal link.

In addition to GABA release, SACs provide cholinergic excitation to DSGCs. However, mGluR2 blockade has a less noticeable effect on the EPSCs of DSGCs. Several factors may contribute to this result. First, EPSCs of DSGCs contain an mGluR2-insensitive bipolar component mediated

by ionotropic glutamate receptors. Second, the cholinergic inputs onto DSGCs come from SAC dendrites oriented in all directions, but only the centripetally activated dendrites show increased calcium transients during mGluR2 blockade. Therefore, only a subset of cholinergic inputs onto DSGCs during preferred direction motion could be affected by mGluR2 blockade, while the majority of GABAergic inputs are enhanced by mGluR2 blockade. Third, since acetylcholine release from SACs has been shown to require higher calcium concentration than GABA release (Lee et al., 2010), it is possible that back-propagation during mGluR2 blockade is less efficient in enhancing cholinergic ESPCs compared with GABAergic IPSCs onto DSGCs. Furthermore, even when an increase is detected in the decaying phase of EPSCs at the speed of 1100 μm/s, it is insufficient to enhance spiking due to the concomitant increase of IPSC that appears to overturn the excitatory effect.

Endogenous mGluR2 signaling, which is tied to glutamate release, might serve as a safeguard to prevent excess signal propagation across dendritic sectors during strong glutamatergic excitation through ionotropic receptors. Thus, SAC dendrites represent an intriguing example where the dendritic computation algorithm dynamically adjusts to input conditions through activity-dependent neuromodulation. We believe that our study will initiate future studies on the optimization of dendritic computation rules by neuromodulatory systems. A deeper understanding on this topic is important for delineating and modeling input-output relationships of individual neurons and neural networks, and ultimately, to link dendritic processing to behavior.

Author contributions

D.K. conducted the experiments in all Figures and the data analysis. J.G. and W.W. conducted experiments in Figures 3 and S4. D.K. and W.W. designed the experiments and wrote the paper.

Chapter 4: Mechanisms of direction selectivity in SACs

4.1: Endogenous mGluR2 signaling in the Off pathway of direction selectivity

Our previous study (Chapter 3) indicated that On direction selectivity is modulated by mGluR2 activity in SACs. The Off SAC layer also expresses mGluR2 (Jensen, 2006), but On and Off direction selectivity are computed separately (Kittila and Massey, 1995), with some inherent differences in circuitry and function (Chen et al., 2016). Therefore, we asked if the Off component of direction selectivity is similarly mediated by mGluR2 signaling.

We recorded light-evoked IPSCs in DSGCs during bars moving in either the preferred or null direction. In baseline conditions, Off IPSCs were highly direction-selective in their amplitude (Figures 4.1A and 4.1B) and charge transfer (Figures 4.1C and 4.1D). However, in the presence of LY341495, IPSCs evoked by preferred-direction motion significantly increased in amplitude (Figure 4.1A), reducing the direction selectivity index of the IPSCs (Figure 4.1B). This indicates that mGluR2 blockade elicits aberrant preferred-direction inhibition onto DSGCs from Off SACs, as it does from On SACs (Chapter 3). This increased preferred-direction inhibition occurred with a significant delay compared to the baseline preferred-direction inhibition (Figure 4.2A). We further probed the properties of this delayed inhibition, finding that it is activated only during motion in the preferred or near-preferred directions (Figure 4.2B) and exerts a similar effect on the DSI of inhibition at different speeds (Figure 4.2C). The delay of inhibition in LY341495 was speed-dependent (Figure 4.2D), consistent with GABA release arising from null-side SAC dendrites activated by backpropagation of depolarization of opposite SAC sectors.

Figure 4.1

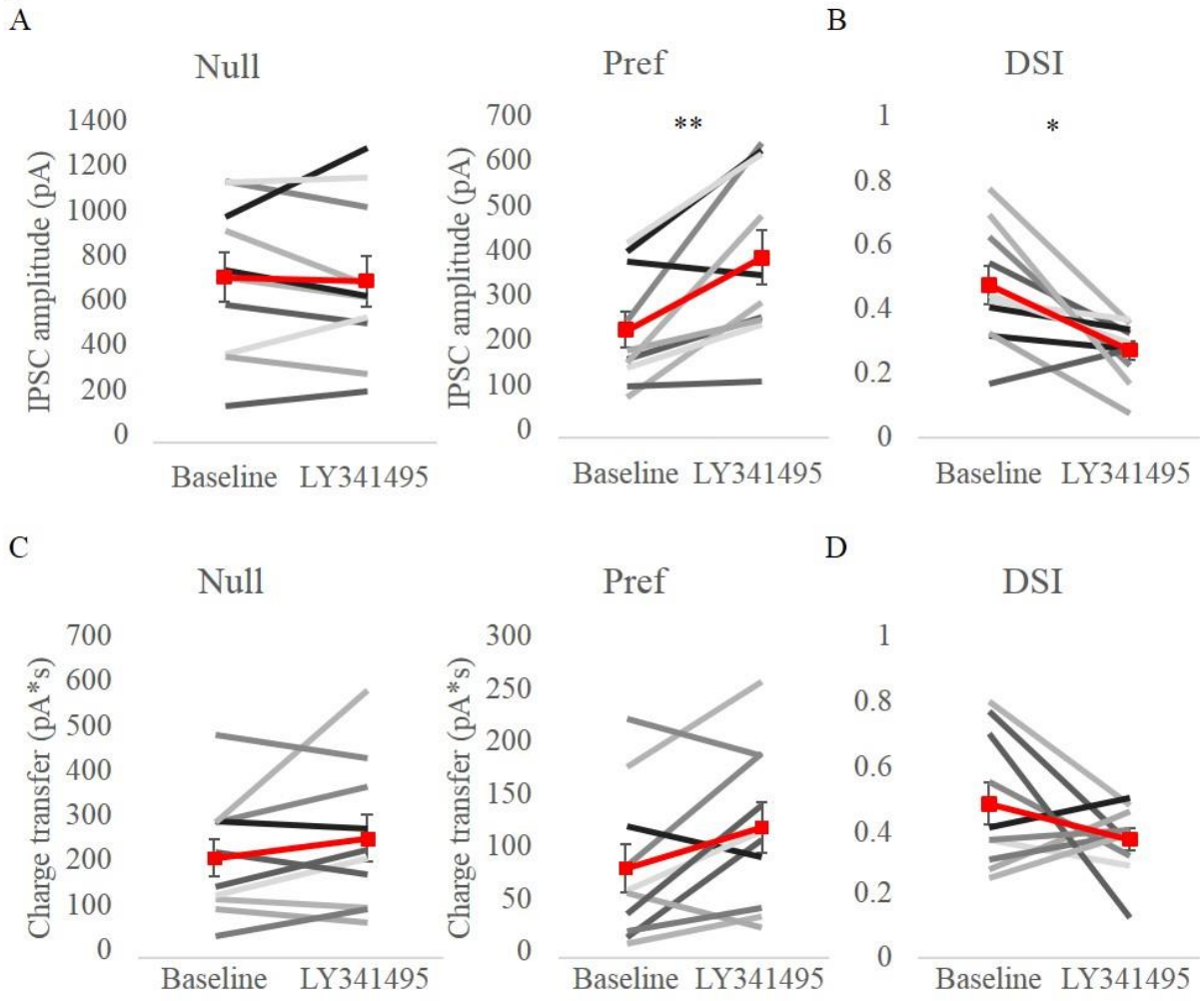

Figure 4.1: Reduced direction selectivity of Off IPSCs during mGluR2 blockade
A: Summary of the amplitude of IPSCs evoked by null-direction (left) or preferred-direction (right) motion of a luminance decrement (the leading edge of a "dark bar"). Red points and line indicate mean ± SEM. Null: Baseline 719 pA ± 107 pA; LY341495 703 pA ± 110 pA; p = 0.79. Preferred: Baseline 237 pA ± 40 pA; LY341495 393 pA ± 59 pA; **p = 0.005.
B: Summary of DSI of the cells in A. Baseline 0.48 ± 0.06; LY341495 0.27 ± 0.03; * p = 0.01.
C: Summary of the charge transfer of IPSCs, as in A. Null: Baseline 220 pA*s ± 41 pA*s; LY341495 262 pA*s ± 51 pA*s; p = 0.22. Preferred: Baseline 84 pA*s ± 22 pA*s; LY341495 123 pA*s ± 24 pA*s; p = 0.06.
D: Summary of DSI of the cells in C. Baseline 0.48 ± 0.07; LY341495 0.37 ± 0.03; p = 0.21.

However, the delay in inhibition evoked by motion at greater stimulus speed was not significant (Figure 4.2D) in the Off component. The reason for this lack of delay is unclear, but may involve the difficulty of reliably voltage-clamping the distant Off dendrites.

Figure 4.2

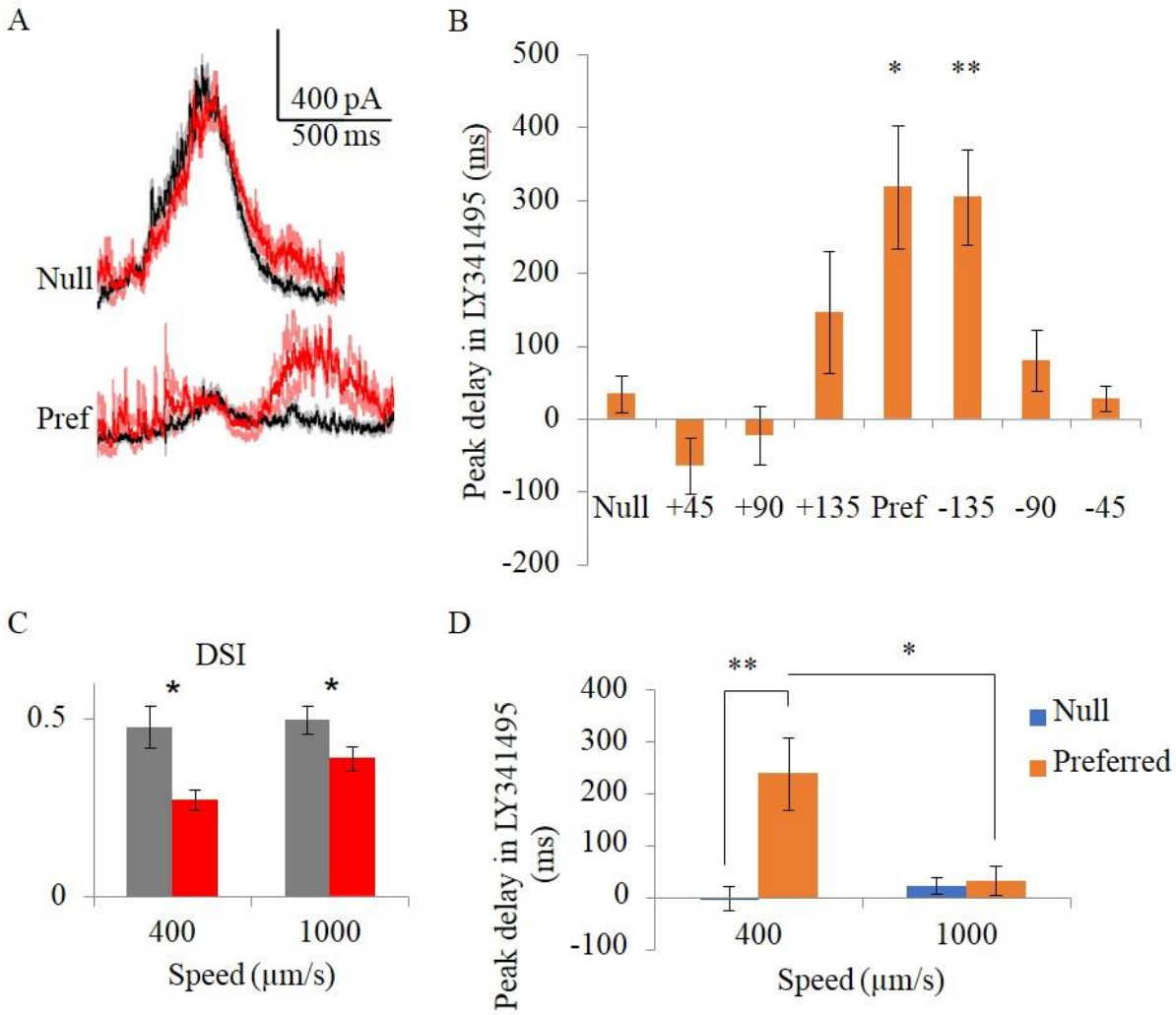

Figure 4.2: Aberrant Off inhibition during preferred-direction motion is speed dependent
A: Example traces of DSGC IPSCs in response to null- or preferred-direction motion in baseline conditions (black) or during mGluR2 blockade by bath application of LY341495 (red). Black and red traces show the mean of 3 trials. Gray and pink traces show the mean ± SEM of the baseline and LY341495 conditions, respectively. Note delayed inhibition evoked by preferred-direction motion.
B: Peak delay of the Off component of DSGC IPSCs, calculated as the peak time in the presence of LY341495 subtracted by the peak time in baseline conditions, in response to 8 moving stimulus directions.
C: Comparison of the reduction of IPSC direction selectivity during bath application of LY341495 at two different stimulus speeds.
D: Summary of the peak delay in the presence of LY341495 for both null and preferred direction motion at two different stimulus speeds.

Because the effect of LY341495 on On DSGC spiking is dependent on stimulus speed (Chapter 3), we performed extracellular recordings from DSGCs during stimulation with moving bars of various speeds. As in the On component, the Off component showed a reduction in the number of spikes evoked by preferred-direction spiking at 1100 µm/s but not at 440 µm/s (Figure 4.3). Together, these experiments suggest that mGluR2 acts similarly in On and Off SACs to influence direction selectivity of On-Off DSGCs.

Figure 4.3

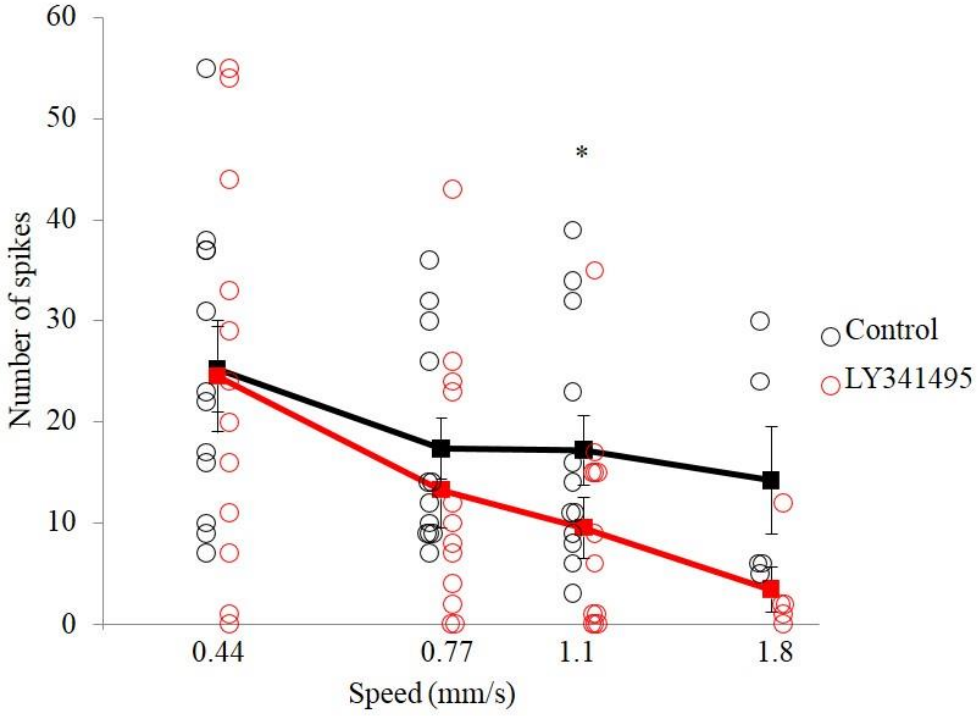

Figure 4.3: mGluR2 blockade reduces DSGC preferred-direction firing in the Off component. Plot of number of spikes evoked by preferred-direction motion (average of 2-3 trials per cell) at different speeds in baseline conditions (Control) or in the presence of LY341495. Stimulus speed is plotted on a log axis.

4.2: mGluR2 signaling improves direction selectivity of SAC-DSGC in noisy conditions

One potential modulatory function of inhibitory synaptic input to SACs is to provide homeostatic regulation of responses in a noisy visual environment, so as to maintain sensitivity to motion regardless of extraneous stimuli (Chen et al., 2016). Since mGluR2 also provides a functionally inhibitory input to SACs and might be expected to operate in parallel with ionotropic activation of glutamate receptors, we tested the effect of endogenous mGluR2 signaling on gain control in SAC dendrites during noisy stimulation. Noise was provided by randomized flashes which approximated the extent of a bipolar cell receptive field in size and occurred in the background the moving stimulus (Figure 4.4A). We found that mGluR2 blockade by LY341495 uncovered increased inhibition in DSGCs during preferred-direction motion at low or medium noise luminance (Figures 4.4B and 4.4D), which resulted in a similar reduction in direction selectivity of responses at these noise levels as in uniform background conditions (Figures 4.4C and 4.4E). However, there was no significant increase in IPSCs evoked by null-direction stimuli in noisy conditions in mGluR2 blockade. These results indicate that mGluR2 provides similar levels of gain control in SAC dendrites in many different visual conditions, including in more physiological, "noisy" background.

4.3: Distinct mechanisms underlie SAC dendritic processing during centripetal and centrifugal motion

The finding that cross-compartmental signal integration plays a role in dendritic direction selectivity in SACs (Chapter 3) suggests that responses of SAC dendrites to centripetal motion

Figure 4.4

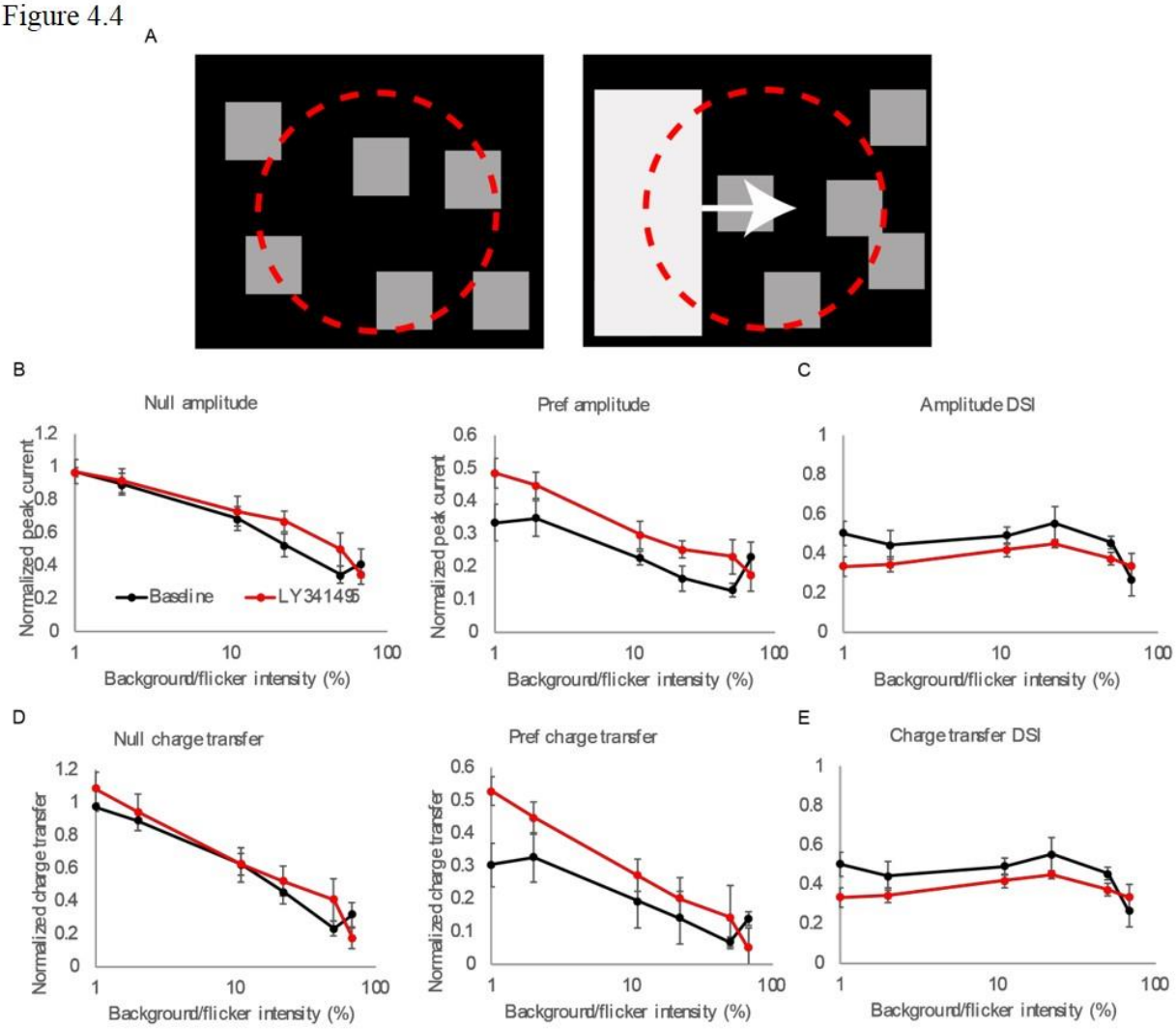

Figure 4.4: mGluR2 signaling improves direction selectivity of inhibition in noisy conditions

A: Schematic of noisy stimulus (gray squares on black background). Left: a 10-second period of randomly appearing 55 µm x 55 µm squares of uniform luminance was presented to the retina prior to stimulus onset. Right: A moving bar appeared and moved across the receptive field of a DSGC (relative size indicated by red circle).

B: Amplitude of IPSCs evoked by the moving bar in either the preferred or null direction of a DSGC as a function of the relative intensity of the flickering background (log scale) in baseline and mGluR2 blockade. 100% intensity means that the noise was the same brightness as the moving bar.

C: Direction selectivity of inhibition (see methods) of the cells in B.

D: Charge transfer of IPSCs in B.

E: Direction selectivity of the charge transfer in D.

propagate more readily than the larger responses to centrifugal motion, but the mechanism for this effect is unknown. Three candidate mechanisms to explain anisotropic cross-somatic propagation are synaptic inhibition of SACs (Lee and Zhou, 2008; Chen et al., 2016), metabotropic glutamate signaling (Chapter 3), and voltage-gated potassium channels (Ozaita et al., 2004), all of which are thought to impact primarily the proximal dendrites in mice (Ding et al., 2016; Vlasits et al., 2016; Ozaita et al., 2004) and therefore might affect electrotonic isolation. We tested the effect of each mechanism using current-clamp recordings from the SAC soma during centripetally- or centrifugally-moving stimuli.

First, we asked if synaptic inhibition of On SACs affects centrifugal preference of somatic currents. To this end, we performed recordings from wildtype SACs and SACs which selectively lose expression of $GABA_A$ receptors because of a loss of the a2 subunit (Gabra2; Chen et al., 2016). We stimulated the cells with alternating expanding or contracting rings centered about the SAC soma (Figure 4.5A). SACs responded to expanding (centrifugal) stimuli with a sharp but transient depolarization and to contracting (centripetal) stimuli with a sustained response (Figure 4.5B). Wildtype SACs showed a small but significant centrifugal preference in the amplitude of their response (Figure 4.5C) and a pronounced centripetal preference in the area of the response (Figure 4.5D). SACs from Gabra2 mice showed similar levels of centrifugal preference of amplitude and centripetal preference of area (Figures 4.5C and 4.5D). Although it is possible that residual synaptic inhibition via glycine receptors or non-a2-containing $GABA_A$ receptors may be present in SACs from Gabra2 mice, the contribution of these is likely minor (Chen et al., 2016).

Figure 4.5

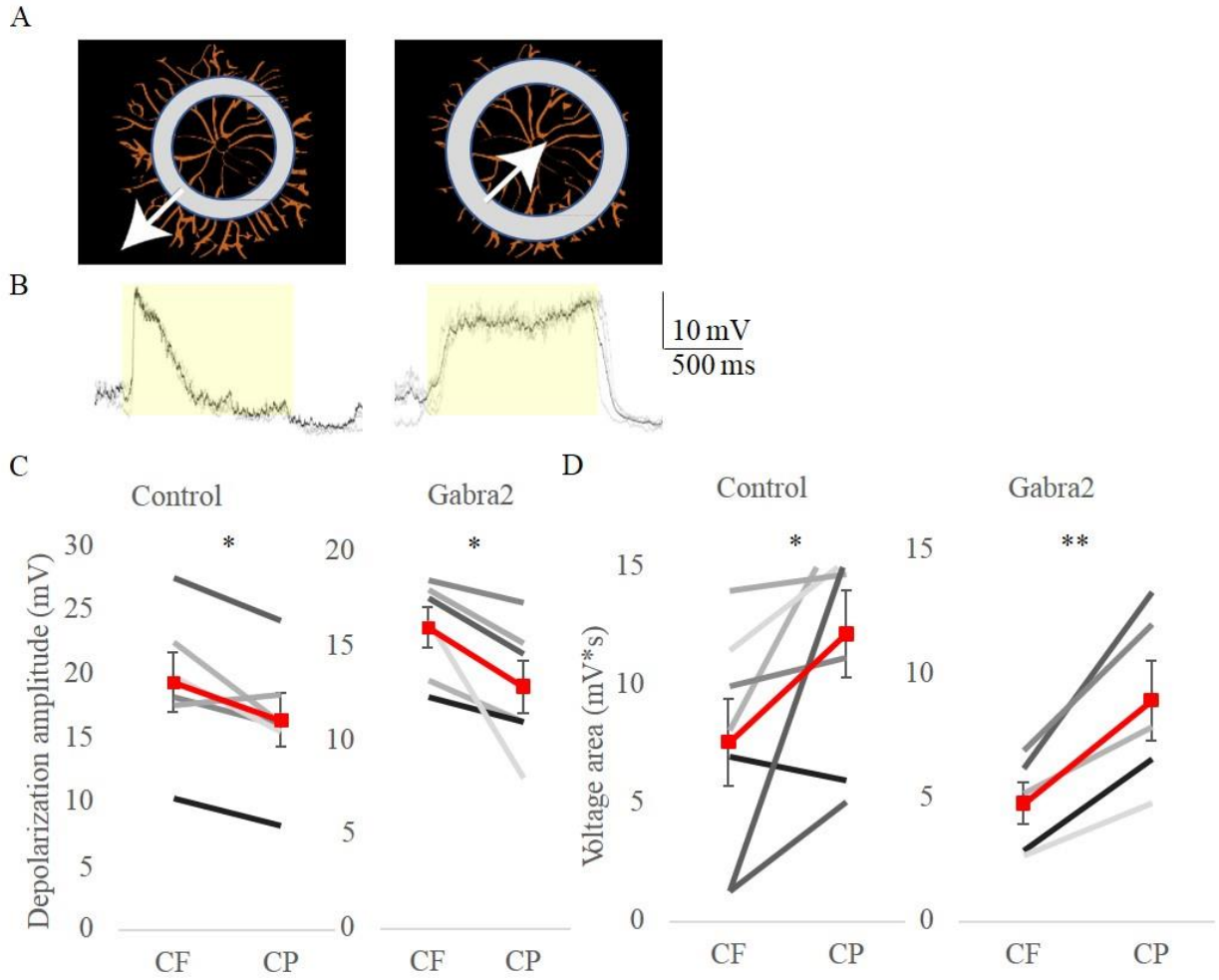

Figure 4.5: GABAergic inhibition of SACs is not required for radial DS in SACs
A: Schematic showing visual stimuli used to test radial direction selectivity. Annuli centered on the SAC soma moved either centrifugally (left) from the center, or centripetally (right).
B: Current clamp responses of a SAC to the visual stimuli shown in A. Gray lines indicate 3-4 individual repetitions. Black line indicates mean response. Yellow rectangle indicates the time during which the stimulus was moving. Note the sustained response to centripetal motion.
C: Summary of SAC response amplitude during centripetal (CP) or centrifugal (CF) stimuli in control and Gabra2 conditional knockout mice. Control: CF 19.4 mV ± 2.3 mV; CP: 16.4 mV ± 2.1 mV; *p = 0.030; N = 6 cells from 2 mice. Gabra2: CF 16.0 mV ± 1.1 mV; CP: 12.9 ± 1.4 mV; *p = 0.035; N= 6 cells from 3 mice.
D: Summary of SAC voltage area during centripetal (CP) or centrifugal (CF) stimuli in control and Gabra2 conditional knockout mice. Control: CF 7.6 mV*s ± 1.8 mV*s; CP: 12.2 mV*s ± 1.8 mV*s; *p = 0.036; N = 7 cells from 3 mice. Gabra2: CF 4.8 mV*s ± 0.9 mV*s; CP: 8.9 mV*s ± 1.6 mV*s; **p = 0.0099; N = 5 cells from 2 mice.

Therefore, these data suggest that synaptic inhibition of SACs is not required for efficient summation of centrifugal input or for efficient propagation of centripetal input. To test the role of mGluR2 on impulse propagation in SAC dendrites, we first clarified the mechanism of the effect of endogenous mGluR2 on voltage-gated calcium currents in SACs. At physiological conditions (compared to the blockade of ionotropic transmission in the retina, as in Figure 3.3), large synaptic conductance changes due to spontaneous excitatory and inhibitory input onto SACs reduces the quality of voltage-clamp recordings. Nevertheless, we found that application of LY341495 consistently reduced the threshold for activation of the calcium current (Figures 4.6A and 4.6B) during a short stimulation pulse. This indicates that mGluR2 is tonically activated by bipolar cells during dark-adapted conditions, and that voltage-gated calcium channels are inhibited by endogenous levels of mGluR2 activation in SACs.

Like ring stimuli, spatially restricted moving bars can be used to probe centrifugal and centripetal responses. We used spatially restricted bars to test the role of mGluR2 to avoid conflating the role of mGluR2 in multicompartmental integration with its role in propagation of responses in individual SAC sectors. In baseline conditions, the amplitude of SACs responses to bars restricted to one SAC sector exhibited centrifugal preference, while their voltage area exhibited centripetal preference (Figures 4.7A-D), similarly to responses to moving ring stimuli (Figure 4.5). Interestingly, following bath application of LY341495, the amplitude of SAC responses lost centrifugal preference due to a pronounced increase in the amplitude of centripetal responses (Figures 4.7A and 4.7B). This is consistent with the role of mGluR2 in modulating forward propagation of moving stimuli as described in Chapter 3. By contrast, the voltage area of

Figure 4.6

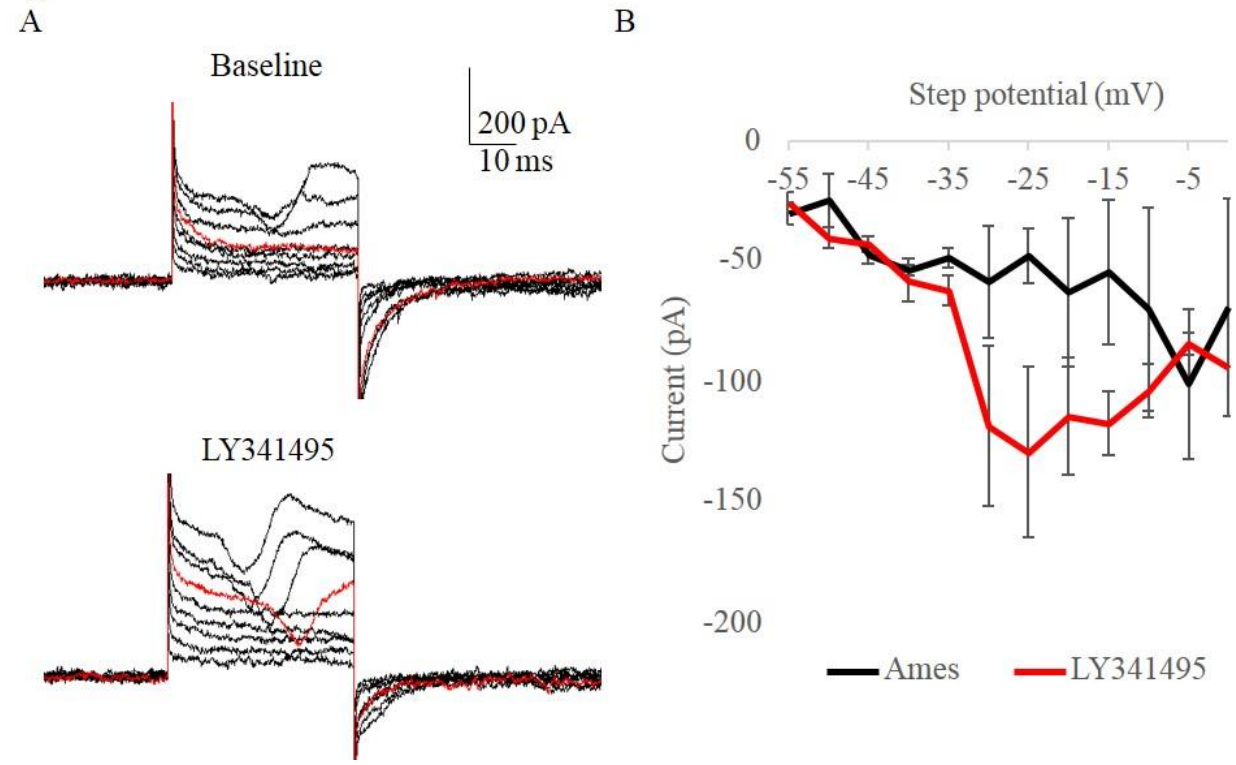

Figure 4.6: Endogenous mGluR2 signaling modulates voltage-gated calcium channels
A: Example traces during stepwise depolarization of the same SAC in voltage clamp from -60 mV to -15 mV (5 mV steps) in baseline conditions and in the presence of bath-applied LY341495. No blockers of ionotropic transmission were included in the bath. Internal solution contained blockers of sodium and potassium channels (see methods). Red trace highlights the response to the -30 mV step, which elicited a calcium current in the presence of LY341495 but not at baseline.
B: Current-voltage relationship of the inward current in baseline (Ames solution) and in the presence of LY341495. N = 4 cells from 2 mice.

responses in LY341495 maintained centripetal preference (Figure 4.7C), although there was a significant reduction in this anisotropy compared with the baseline conditions (Figure 4.7D) due to an increase in the voltage area of centrifugal responses (Figure 4.7C). Thus, mGluR2 signaling accounts for the small centrifugal preference in response amplitude measured at the soma, but is not required for the centripetal preference in the sustained component of depolarization. This finding suggests that other mechanisms are involved in the rapid decay of responses to centrifugal motion.

Figure 4.7

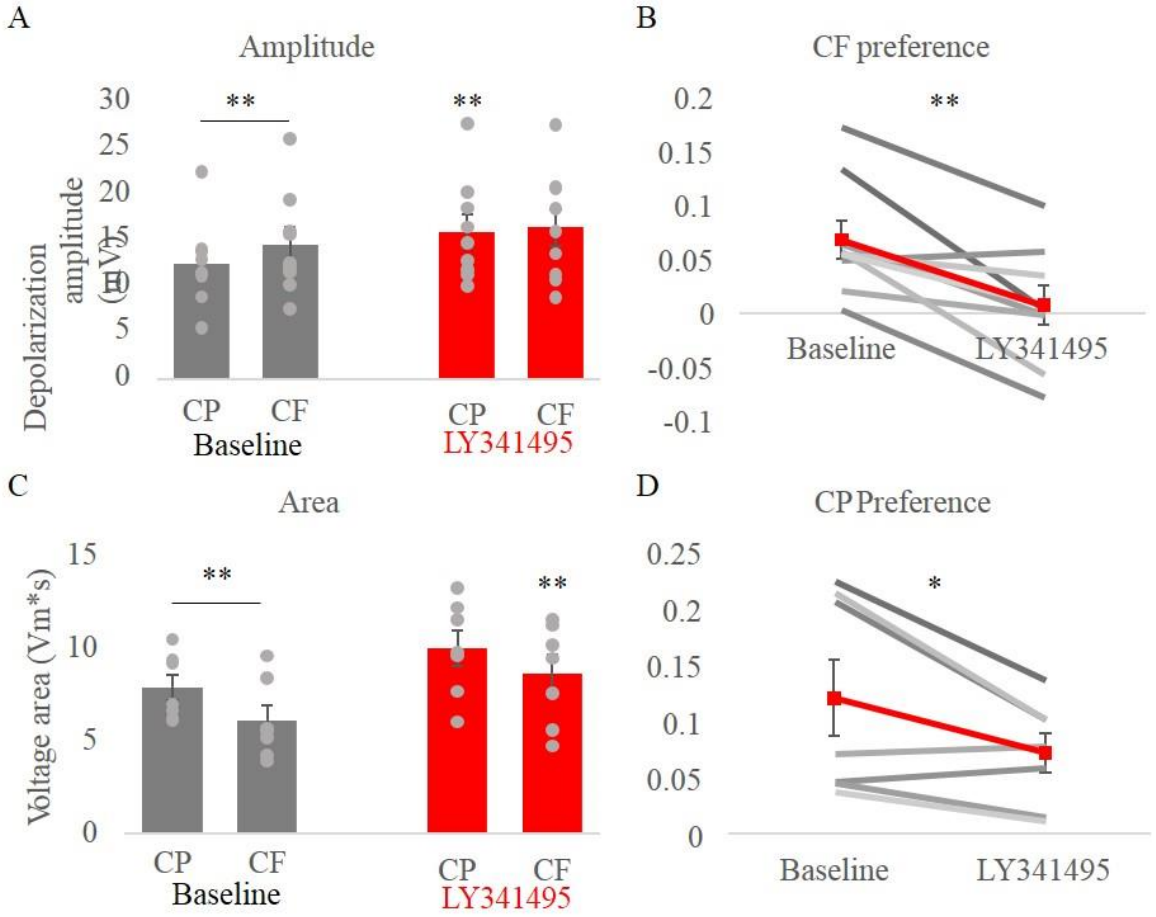

Figure 4.7: mGluR2 blockade abolishes DS of response amplitude but not area in SACs. A: Summary of depolarization amplitude evoked by a centripetal (CP) or centrifugal (CF) moving bar that traversed a single SAC sector in baseline conditions (K internal) and in mGluR2 blockade by LY341495. 3-5 trials averaged for each condition. Baseline: CP: 12.3 mV ± 1.5 mV; CF: 14.5 mV ± 1.8 mV; LY341495 CP: 15.9 mV ± 1.9 mV; CF: 16.3 mV ± 2.0 mV. Baseline CP vs CF ** p = 0.009. Baseline CP vs LY341495 CP ** p = 0.003; N = 9 cells from 4 mice.
B: Summary of centrifugal preference of response amplitude for the cells in A in baseline conditions and mGluR2 blockade. Centrifugal preference is reported as the log of the ratio of CF response to CP response. Baseline: 0.069 ± 0.018; LY341495: 0.007 ± 0.018; ** p = 0.004; N = 9 cells from 4 mice.
C: Summary of depolarization area evoked by a CP or CF moving bar as in A. Baseline: CP: 7.9 mV*s ± 0.7 mV*s; CF: 6.1 mV*s ± 0.8 mV*s; LY341495 CP: 10.0 mV*s ± 1.0 mV*s; CF: 8.6 mV*s ± 1.0 mV*s. Baseline CP vs CF: ** p = 0.003. Baseline CF vs LY341495 CF: ** p = 0.008; N = 7 cells from 3 mice.
D: Summary of centripetal preference of response area for cells in C in baseline conditions and mGluR2 blockade. Centripetal preference reported as the log of the ratio of CP response to CF response. Baseline: 0.12 ± 0.03; LY341495: 0.07 ± 0.02; * p = 0.045; N = 7 cells from 3 mice.

Given that mGluR2 signaling and GABAergic inhibition do not appear to be important for the more rapid decay of centrifugal responses, we hypothesized that voltage-gated potassium channels may play a role. We therefore tested the role of voltage-gated potassium channels on dendritic integration in SACs. We recorded from SACs using internal solution containing TEA and cesium, which block Kv3 channels (Ozaita et al., 2004), the dominant voltage-gated potassium channels in SACs. In the absence of Kv channel activity, both centrifugal preference in response amplitude and centripetal preference in response area were abolished (Figures 4.8A-D). Comparison to SACs recorded using potassium-based internal suggests that the loss of selectivity is likely due to increased amplitude of centripetal responses and more sustained depolarization during centrifugal responses (Figures 4.8A and 4.8C). In the absence of voltage-gated potassium channel activity, LY341495 did not significantly modulate responses to moving stimuli, except for a reduction of the amplitude of centrifugally-evoked responses (Figure 4.8A). However, LY341495 induced frequent spontaneous calcium spikes (Figure 4.8E), which are not observed in cesium-based internal during endogenous levels of mGluR2 signaling or in potassium-based internal regardless of mGluR2 signaling levels. This suggests that mGluR2 blockade improves conduction of dendritic impulses in the absence of Kv channel activity under our recording conditions. However, mGluR2 blockade does not increase light-evoked depolarization, perhaps because significant depolarization in the absence of Kv channels inactivates voltage-gated calcium channels.

Together, these data indicate that both the centrifugal preference of depolarization amplitude and the centripetal preference of the sustained component of depolarization may be modulated by

Figure 4.8

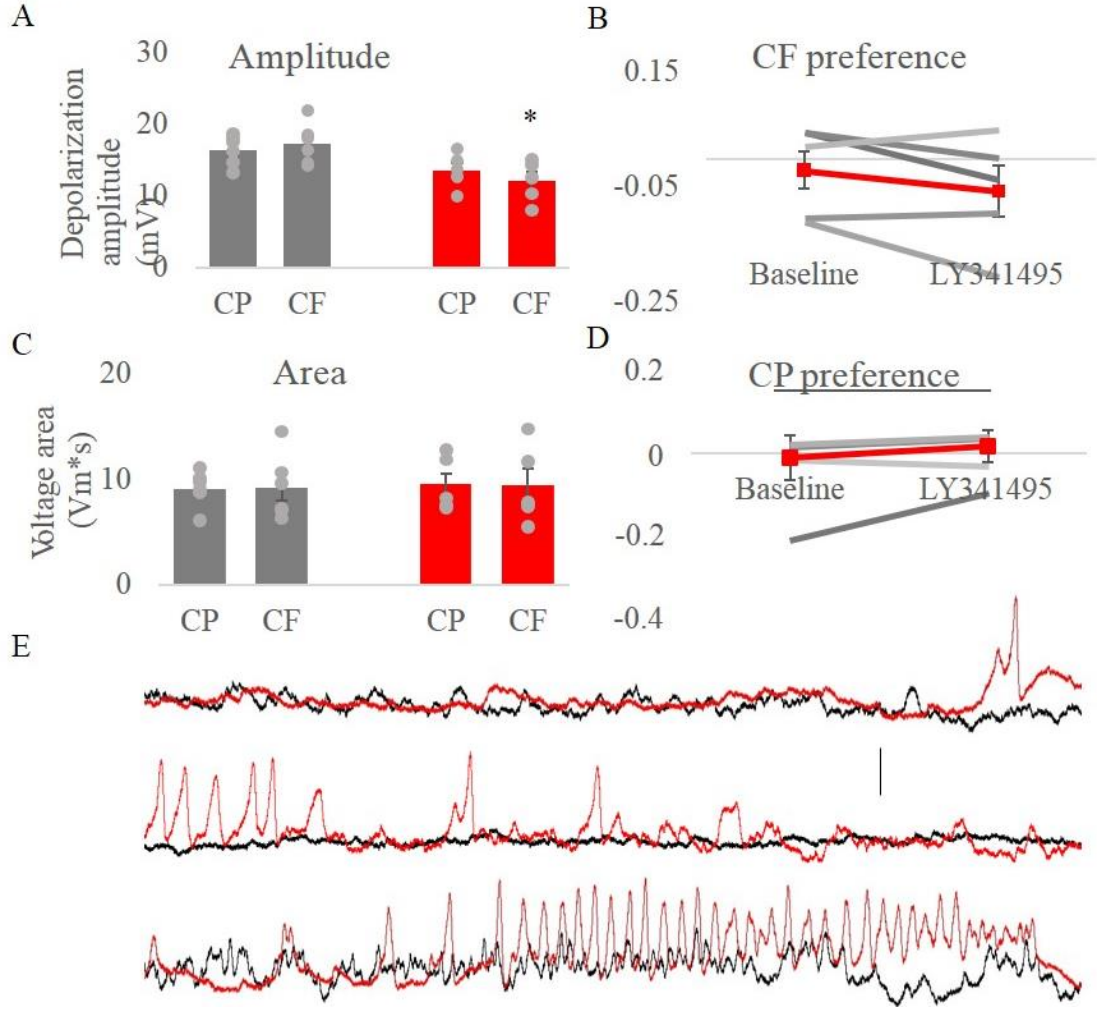

Figure 4.8: Blockade of SAC Kv channels abolishes DS of response amplitude and area
A: Summary of depolarization amplitude evoked by a centripetal (CP) or centrifugal (CF) moving bar that traversed a single SAC sector. Internal solution contained blockers of Kv channels. 3-5 trials averaged for each condition. Baseline: CP: 16.4 mV ± 0.9 mV; CF: 17.3 mV ± 1.2 mV; LY341495 CP: 13.6 mV ± 1.1 mV; CF: 12.1 mV ± 1.3 mV. Baseline CF vs LY341495 CF ** p = 0.001; N = 6 cells from 3 mice.
B: Summary of centrifugal preference of response amplitude for the cells in A. CF preference is reported as the log of the ratio of CF response to CP response. Baseline: -0.02 ± 0.03; LY341495: -0.06 ± 0.04; N = 6 cells from 3 mice.
C: Summary of depolarization area evoked by a CP or CF moving bar as in A. Baseline: CP: 9.2 mV*s ± 0.7 mV*s; CF: 9.3 mV*s ± 1.3 mV*s; LY341495 CP: 9.6 mV*s ± 1.1 mV*s; CF: 9.5 mV*s ± 1.5 mV*s. N = 6 cells from 3 mice.
D: Summary of centripetal preference of response area for cells in C in baseline conditions and mGluR2 blockade. CP preference reported as the log of the ratio of CP response to CF response. Baseline: -0.01 ± 0.06; LY341495: 0.02 ± 0.04; N = 6 cells from 3 mice.

Figure 4.8 (cont.)
E: Spontaneous recordings from three SACs (internal solution blocking Kv) at baseline and in mGluR2 blockade

mechanisms that regulate electrotonic isolation in SAC dendrites. Voltage-gated potassium channels and mGluR2-mediated inhibition of voltage-gated calcium channels operate in concert to precisely regulate the degree of propagation of visual stimuli, depending on their direction of motion.

Chapter 5: Synaptic transmission between SACs and DSGCs

5.1: GABA and acetylcholine release by SACs requires VAMP2

We first asked if transmission of GABA and acetylcholine in wild-type mice requires calcium-dependent vesicle release. We used an AAV vector to express the tetanus toxin light chain and a GFP reporter under the control of the ChAT promoter in isolated SACs (see Chapter 2). Tetanus toxin is a potent cleaver of synaptobrevin/vesicle associated membrane protein 2 (VAMP2), which is required for classical synaptic neurotransmission (Verderio et al., 1999). However, VAMP2 is not required for some forms of vesicle exocytosis: spontaneous release in some synapses occurs via other SNARE proteins (Verderio et al., 1999; Hua et al., 1998; Shin et al., 2012). We performed paired recordings between SACs expressing the tetanus toxin light chain, as evidenced by their GFP fluorescence, and nearby DSGCs which exhibited substantial dendritic overlap with these SACs. We found that stimulation of SACs expressing the tetanus toxin light chain never evoked GABAergic or cholinergic PSCs in these DSGCs, despite their dendritic overlap and the evoked calcium currents in these SACs (n = 5 pairs, including 3 null-side pairs, from 4 mice) (Figure 5.1). This suggests that evoked release of both GABA and acetylcholine operates in a vesicular manner and requires the action of VAMP2.

5.2: Preferred-direction GABA release is delayed

A previous study in rabbits showed that there is no systematic difference in the latency of GABAergic and cholinergic transmission at the SAC-DSGC synapse (Lee et al., 2010), but it is not clear if the same is true in mice. Furthermore, given the difference in the synaptic

Figure 5.1

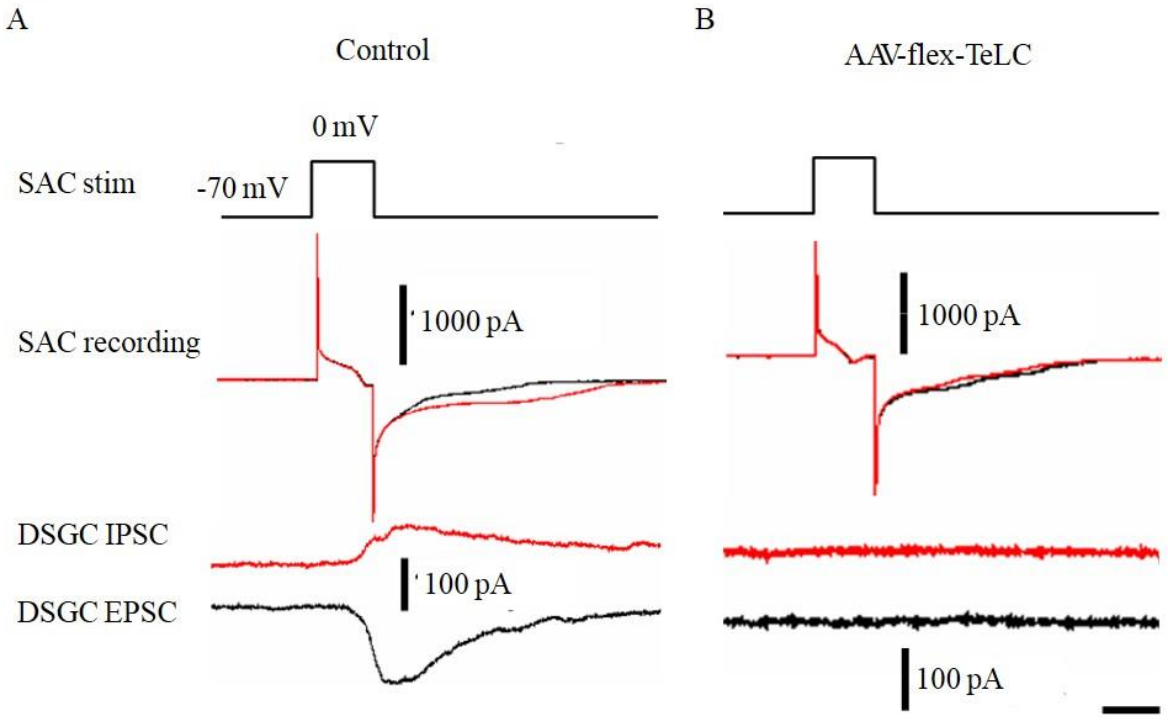

Figure 5.1: Tetanus toxin blocks evoked transmission from SACs to DSGCs
A: Control SAC-DSGC voltage-clamp recording in wildtype retina showing that SAC depolarization induces a delayed inward current in SACs that coincides with the onset of GABAergic and cholinergic PSCs in a connected DSGC.
B: Paired recording of a SAC infected with flexed tetanus toxin light chain (AAV-flex-TeLC) and a nearby DSGC. Two-photon imaging confirmed extensive dendritic overlap between the SAC and DSGC (not shown). SAC depolarization induces a delayed inward current in SACs, as in A, but no GABAergic or cholinergic PSCs are detected.

architecture between null-side and preferred-side SAC and DSGC connections (Brigmann et al., 2011), it is possible that the latency of GABA and/or acetylcholine transmission is isotropic. To answer these questions, we performed paired recordings between SACs and DSGCs on either the null or preferred side (Figure 1.1C) to compare the onset of post-synaptic currents during SAC stimulation. We recorded only from pairs located 80-120 µm apart in order to maximize dendritic overlap on only one side of the SAC (Figure 1.1C). We used a sensitive threshold (2*S.D.) to detect the onset of a postsynaptic response during the SAC depolarization step.

Surprisingly, we found a statistically significant isotropy in the timing of release (Figure 5.2A). It is not clear if cholinergic transmission exhibits a difference in latency between the null and preferred-side pairs ($p = 0.06$), but GABAergic transmission occurred about 3.5 ms later for preferred-side pairs than null-side pairs ($p = 0.004$) (Figure 5.2A). Furthermore, individual pairs showed a bias in the relative latency of the two neurotransmitters depending on their orientation (Figure 5.2B). In preferred-side pairs, EPSCs began 1.0 ± 0.5 ms earlier than IPSCs ($n = 15$), with a median difference of 0.5 ms. In null-side pairs, IPSCs began 0.7 ± 0.4 ms earlier than EPSCs ($n = 16$), with a median difference of 1.1 ms (Null vs preferred $p = 0.031$) (Figure 5.2B). Notably, there was no detectable bias if preferred- and null-side pairs were combined for analysis (median latency difference: 0.1 ms, $p = 0.43$), and 43% of pairs showed sub-millisecond latency difference between EPSCs and IPSCs, consistent with the previous study in rabbits (Lee et al., 2010).

We next asked if the threshold for release of GABA and acetylcholine differed, and whether the relationship was isotropic. There was no statistically significant difference in the threshold for release of acetylcholine and GABA, and there was no significant difference between the threshold of null- and preferred-side pairs (Figure 5.2C). This average threshold was around -25 mV, comparable to the threshold for the voltage-gated calcium current (Figure 3.7). Throughout these recordings, PSCs were never observed in the absence of a SAC calcium current. Thus, in contrast to the isotropic latency differences between acetylcholine and GABA release, the threshold for release during electrical stimulation of SACs is spatially uniform, consistent with dependence on the voltage-gated calcium current in SACs.

Figure 5.2

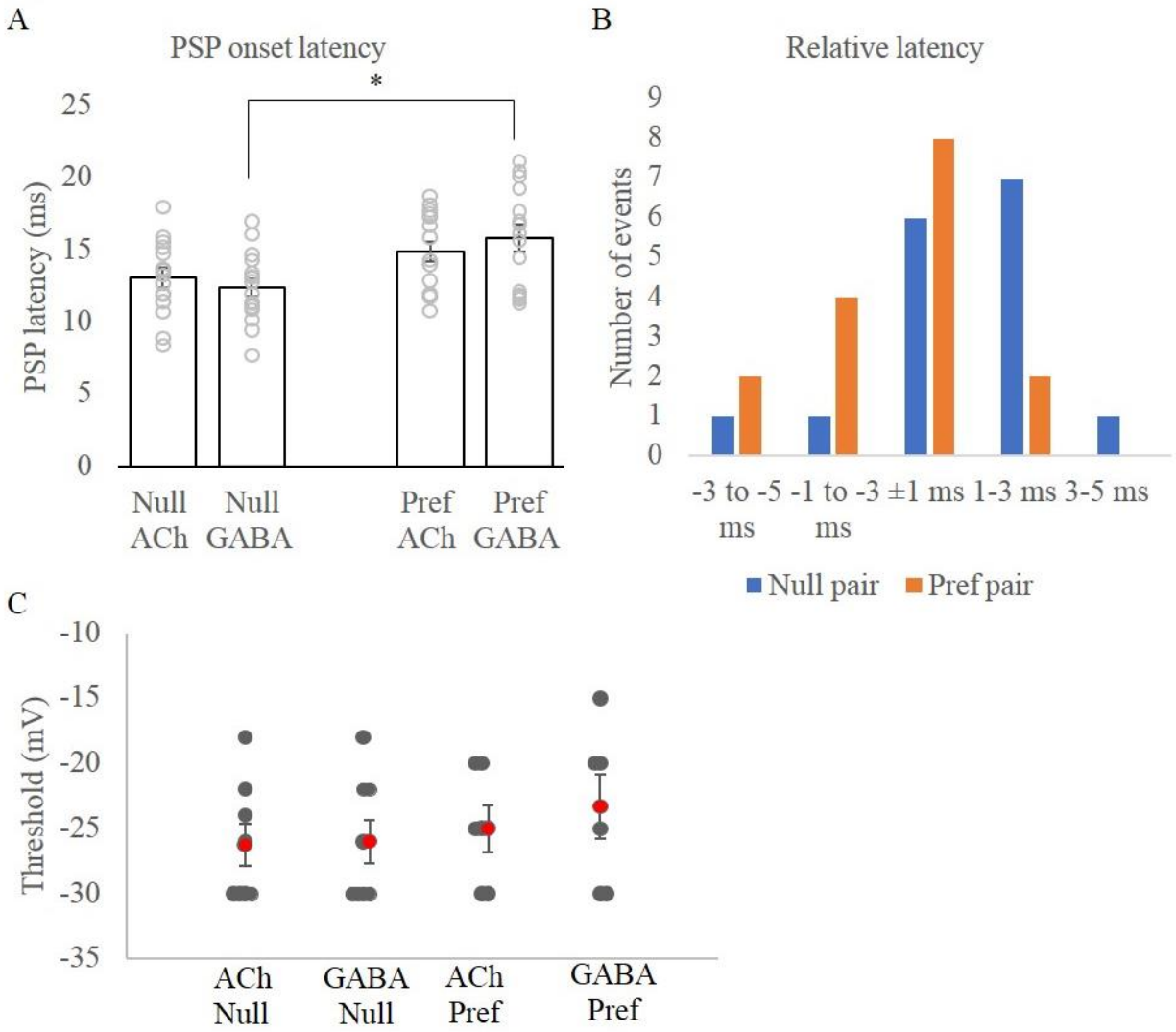

Figure 5.2: Properties of neurotransmitter co-release from SACs
A: Summary of onset latency for cholinergic EPSCs or GABAergic IPSCs onto DSGCs following depolarization of either a null- or preferred-side SAC to 0 mV. Null ACh: 13.1 ms ± 0.7 ms, N = 16 pairs; Null GABA: 12.4 ± 0.6 ms, N = 16 pairs; Preferred ACh: 14.9 ms ± 0.7 ms, N = 16 pairs; Preferred GABA: 15.9 ms ± 0.9 ms, N = 15 pairs. Two-factor ANOVA ACh vs GABA: $F(1,56) = 0.01$, $p = 0.92$. Null vs preferred: $F(1,56) = 13.09$, $p = 0.006$. Post-hoc Null GABA vs Preferred GABA * $p = 0.004$.
B: Distribution of relative PSP latency (cholinergic – GABAergic) for null- or preferred-side pairs. The median preferred pair exhibited a relative latency of -0.5 ms (cholinergic transmission preceding GABAergic); the median null pair exhibited a relative latency of 1.1 ms.
C: Summary of the SAC depolarization threshold for release, measured by sequentially increasing voltage steps in SACs during paired recordings until PSPs were detected at the DSGC. Two-factor ANOVA Null vs Preferred: $F(1,24) = 1.07$, $p = 0.31$; ACh vs GABA: $F(1,24) = 0.21$, $p = 0.65$.

5.3: Cholinergic transmission is potentiated in a GABA-dependent manner

In the above experiments, cholinergic transmission was measured by clamping the DSGC at the reversal potential for inhibitory currents (-60 mV) and GABAergic transmission was measured by holding the DSGC at the reversal potential for excitatory currents (0 mV). Thus, the DSGC was repeatedly depolarized for 6-10 seconds and then repolarized for 10-20 seconds, as in previous studies that measured SAC-DSGC transmission in voltage clamp (Wei et al., 2011; Pei et al., 2015; Chen et al., 2016). Interestingly, we noted that, using this protocol, the cholinergic currents during the second and subsequent SAC stimuli were significantly greater than during the first stimulus, which occurred prior to DSGC depolarization (Figure 5.3A). Therefore, we asked if the DSGC depolarization might be modulating cholinergic transmission. When the SAC was stimulated repeatedly without depolarization of the DSGC, cholinergic transmission was constant (Figure 5.3B, n = 4); subsequent DSGC depolarization caused potentiation (Figure 5.3B, n = 4). When the DSGC was depolarized before the first SAC stimulus, cholinergic PSCs in response to subsequent SAC stimuli were consistent (Figure 5.4C, n = 5). Finally, evoked GABAergic PSCs, which were measured by depolarizing the DSGC, did not potentiate (Figure 5.4D, n = 5). Together, these experiments suggest that depolarization of the DSGC triggers potentiation of cholinergic transmission.

We next asked whether cholinergic potentiation was isotropic. We found that cholinergic currents evoked by stimulation of either preferred- or null-side SACs exhibited potentiation, ranging from 88% ± 22% in preferred-side pairs to 46% ± 11% in null-side pairs (Figure 5.3E), and the difference was not statistically significant. In order to understand the mechanism of this

Figure 5.3

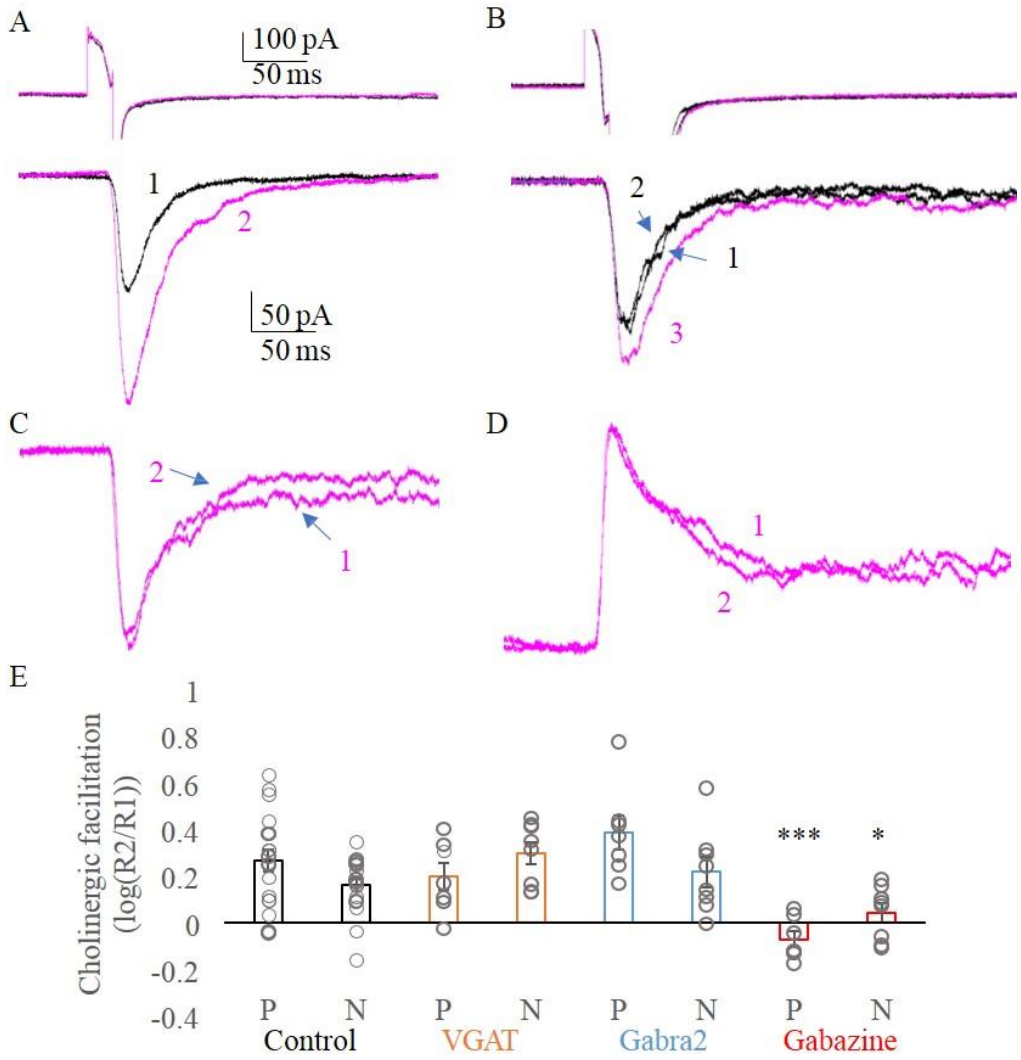

Figure 5.3: Potentiation of nicotinic transmission by DSGC depolarization
A-D: Representative traces illustrating properties of cholinergic potentiation. Black traces are pre-depolarization of DSGC; fuchsia traces are post-depolarization. Numbers indicate the temporal order of recordings. SAC responses clipped for clarity.
A: SAC (top) and DSGC recording (bottom) during SAC stimulation prior to DSGC depolarization (1) and following DSGC depolarization (2).
B: SAC (top) and DSGC recording (bottom) during repeated SAC stimulation prior to DSGC depolarization (1 and 2) and following DSGC depolarization (3).
C: DSGC recording during repeated SAC stimulation following DSGC depolarization.
D: IPSC recording from DSGC during repeated SAC stimulation (DSGC depolarized to 0mV).
E: Summary of EPSC facilitation, reported as log of the ratio of EPSC amplitude following DSGC depolarization to EPSC amplitude prior to DSGC stimulation, for several mouse lines and conditions. $F(7, 72) = 6.45$, $p < 0.0001$. Post-hoc: Gabazine vs Control Preferred: *** $p < 0.0001$; Gabazine vs Control Null: * $p = 0.0016$.

Figure 5.4

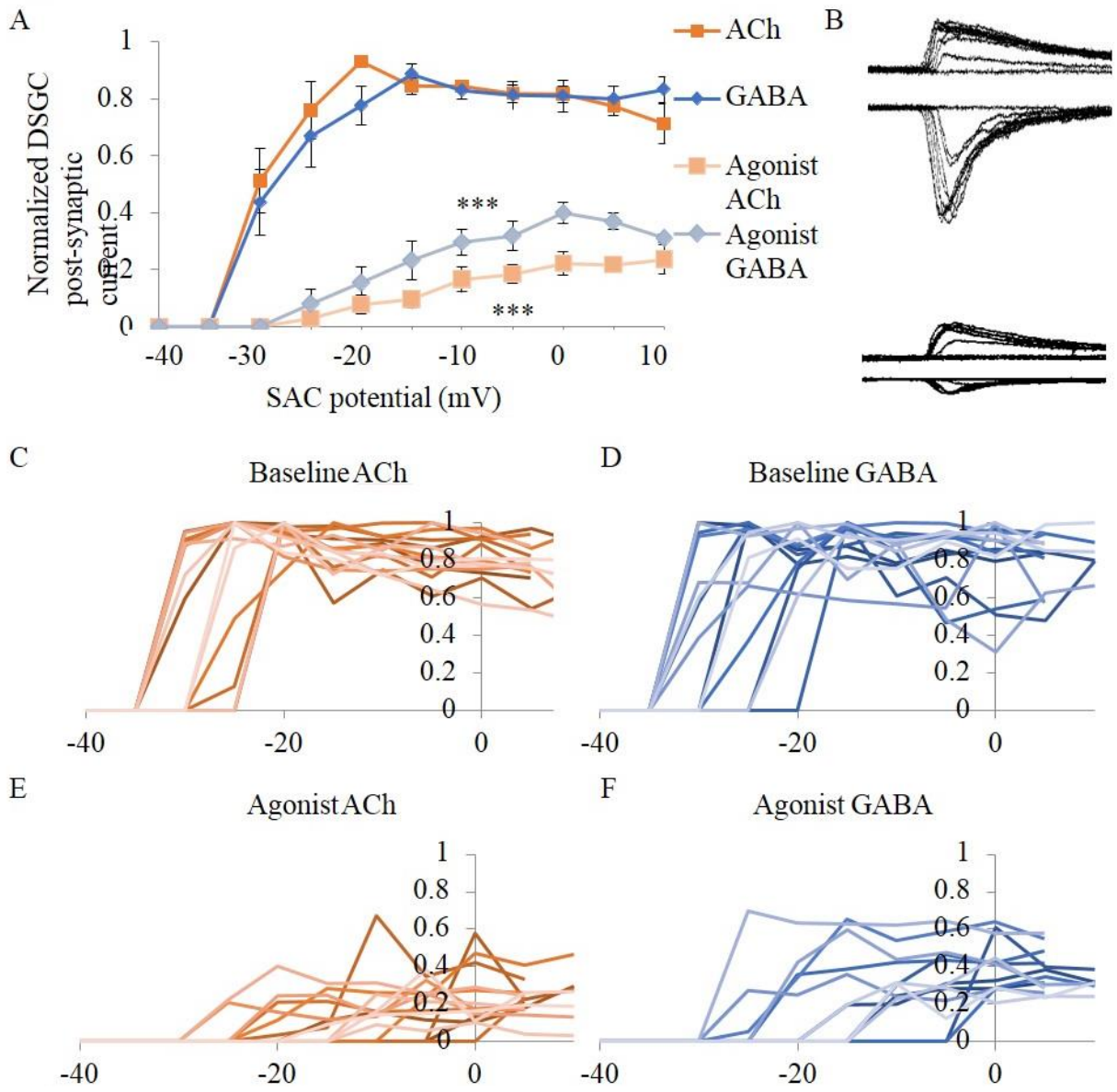

Figure 5.4: mGluR2 agonist reduces evoked release of GABA and acetylcholine

A: Quantification of the relationship between presynaptic (SAC) depolarization steps and post-synaptic (DSGC) GABAergic and cholinergic currents under baseline conditions and in mGluR2 agonist. For each SAC-DSGC pair, GABAergic and cholinergic PSCs were normalized to the respective maximum PSC. ***Repeated measures ANOVA $p < 0.0001$ for both GABA and acetylcholine.

B: Example post-synaptic traces from a single pair, corresponding to increasing SAC voltage steps in baseline conditions (top) and in the presence of mGluR2 agonist (bottom).

C-F: Quantification of normalized post-synaptic currents as a function of SAC depolarization step, as in A, but for individual pairs. Note that release is all-or-none in most cells.

potentiation, we performed paired SAC-DSGC recordings in retinas from transgenic mice which lacked the a2 subunit of GABAA receptors in SACs, and therefore receive little or no ionotropic inhibition (Chen et al., 2016). As in wildtype mice, potentiation was noted in both the preferred-side (148% ± 47%) and null-side (67 ± 27%) configurations (Figure 5.3E). We also analyzed previous paired experiments published in Pei et al. (2015) to determine the effect of a lack of VGAT expression in SACs. Again, potentiation was observed in preferred-side (59% ± 23%) null-side (101% ± 24%) pairs (Figure 5.3E). These results suggest that potentiation of the cholinergic current by depolarization of the DSGC does not require GABA receptors on SACs or GABA release by SACs. To test if inhibitory transmission other than that involving SACs contributes to cholinergic potentiation, we analyzed paired recordings performed in the presence of the bath-applied antagonist of the GABAA receptor antagonist gabazine (dataset from Zhe Pei, unpublished). Surprisingly, gabazine prevented potentiation of preferred- (-15% ± 7%) and null-side (11% ± 11%) cholinergic transmission (Figure 5.3E). These data suggest that activation of GABAA receptors, but possibly not on SACs or by GABA released from SACs, is required for the potentiation of cholinergic transmission. Furthermore, the modulation of potentiation by gabazine provides additional evidence that this potentiation is not an artifact of recording.

5.4: mGluR2 signaling can modulate release of GABA and acetylcholine

We have previously shown that mGluR2 signaling modulates the unclamped currents triggered by depolarization in SACs, which are mediated by P/Q-type and N-type calcium channels (Figure 3.7). These currents are time-locked to neurotransmission of GABA and acetylcholine

(Figures 3.7 and 3.5; Lee et al., 2010). We therefore investigated whether mGluR2 signaling also alters SAC-DSGC transmission triggered by these evoked events. Bath application of the mGluR2 agonist LY354740 significantly reduced the amplitude evoked PSCs of both acetylcholine and GABA during SAC depolarization (Figures 5.4A and 5.4B), as well as increasing the potential threshold for release (Figures 5.4A-F, 5.5A, and 5.5B). Therefore, exogenous mGluR2 activation can sufficiently block voltage-gated calcium currents in SACs to reduce neurotransmitter release.

In the conditions used for paired recording, ionotropic transmission in the retina is blocked or substantially reduced (see Chapter 2). Bath application of LY341495 in these conditions did not affect GABAergic or cholinergic transmission between preferred- or null-side pairs (Figure 5.6A-D), illustrating that there is little or no tonic activation of mGluR2, consistent with low or no tonic activation of bipolar cells. We therefore used application of LY341495 to competitively inhibit mGluR2 activation by LY354740, to verify that the effects of mGluR2 signaling on SAC-DSGC transmission are reversible and mGluR2-dependent. We found that the threshold for acetylcholine release and the amplitude of evoked cholinergic EPSCs were significantly and reversibly modulated by LY354740 (Figures 5.5A and 5.5C). The threshold for GABA release and amplitude of evoked IPSCs were also modulated by LY354740, but were not significantly reversed by mGluR2 blockade (Figures 5.5B and 5.5D). A direct comparison of the effect of LY354740 on cholinergic and GABAergic PSCs in individual pairs showed a consistently greater reduction of cholinergic transmission in both null- and preferred-side pairs (Figure 5.5E), as well as a significantly greater recovery of cholinergic transmission by bath application of

Figure 5.5

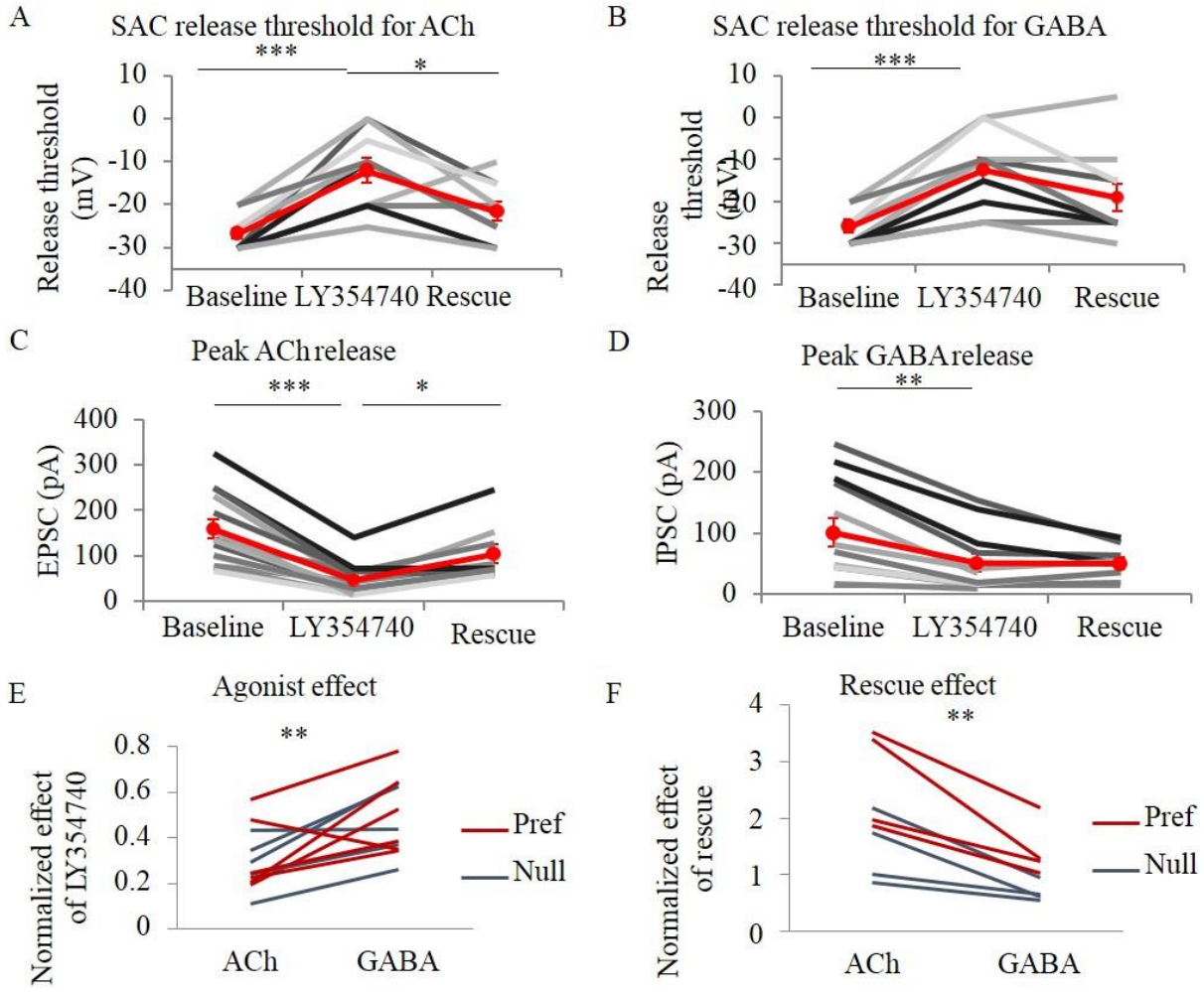

Figure 5.5: Differential effect of mGluR2 signaling on acetylcholine and GABA
A and B: Release threshold (SAC potential at which PSCs were first detected in DSGCs) in baseline conditions, in the presence of mGluR2 agonist, and following rescue with competitive antagonist LY341495. Repeated measures ANOVA $p < 0.001$.
C and D: Maximal PSCs recorded during stepwise SAC depolarization from -70 mV to +10 mV in baseline conditions, in the presence of mGluR2 agonist, and following rescue with LY341495. Repeated measures ANOVA: ACh: $p = 0.004$; GABA: $p = 0.014$.
E: The effect of mGluR2 agonist on maximal PSCs, reported as a ratio of the maximal PSC in mGluR2 blockade and the maximal PSCs in baseline conditions. Pref and Null pairs separated by color. ** $p = 0.004$ for effect on ACh vs GABA. Null vs Pref comparison nonsignificant.
F: The effect of rescue on maximal PSCs, reported as a ratio of the maximal PSC in the presence of LY34145 and the maximal PSCs in mGluR2 agonist. ** $p = 0.002$ for differential effect on ACh and GABA. Null and Preferred comparison nonsignificant.

Figure 5.6

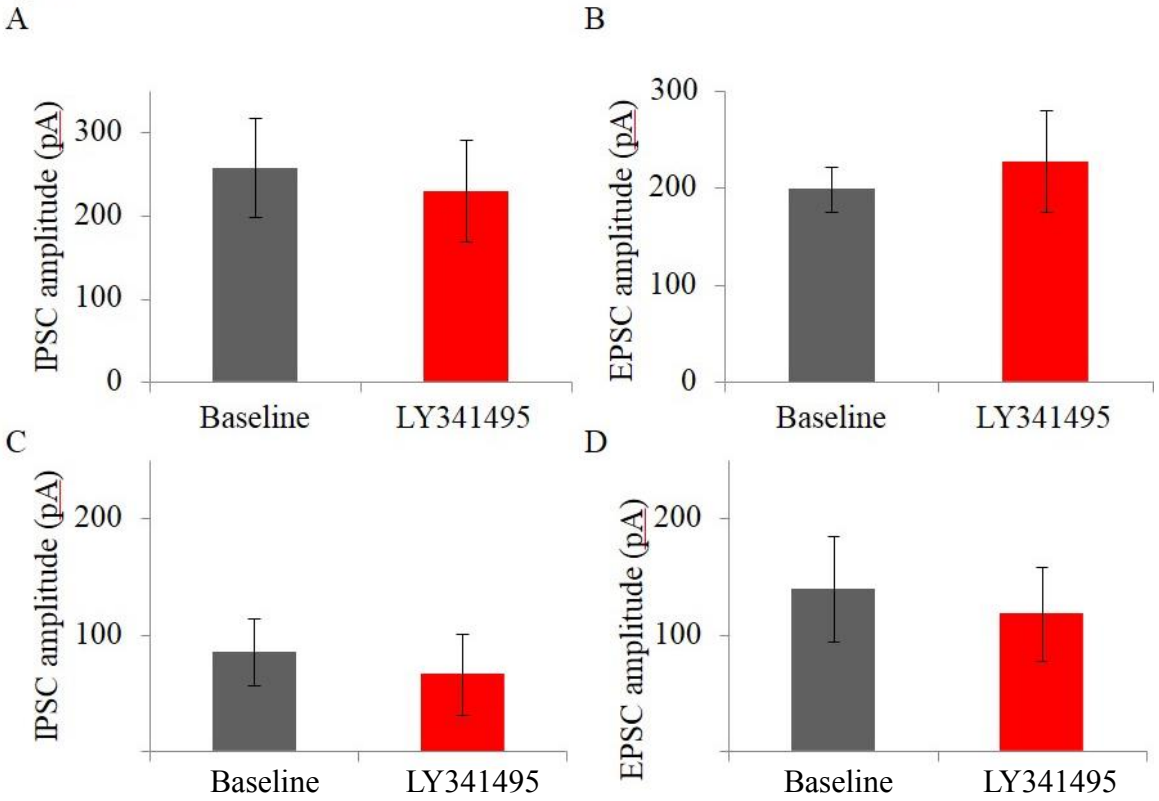

Figure 5.6: mGluR2 blockade has no effect on SAC-DSGC transmission in conditions blocking ionotropic glutamatergic receptors throughout the retina

A: Summary of the amplitude of IPSCs measured in DSGCs in response to depolarization of null-side SACs to 0 mV in baseline conditions and during mGluR2 blockade. Baseline: 258 pA ± 60 pA; LY341495: 230 pA ± 61 pA; p = 0.14; n = 4 pairs from 3 mice.

B: Summary of the amplitude of EPSCs measured in DSGCs in response to depolarization of null-side SACs as in A. Baseline: 199 pA ± 23 pA; LY341495: 228 pA ± 52 pA; p = 0.47; n = 3 pairs from 2 mice.

C: Summary of the amplitude of IPSCs measured in DSGCs in response to depolarization of preferred-side SACs to 0 mV in baseline conditions and during mGluR2 blockade. Baseline: 85 pA ± 29 pA; LY341495: 66 pA ± 34 pA; p = 0.52; n = 4 pairs from 3 mice.

D: Summary of the amplitude of EPSCs measured in DSGCs in response to depolarization of preferred-side SACs as in C. Baseline: 139 pA ± 46 pA; LY341495: 118 pA ± 40 pA; p = 0.08; n = 3 pairs from 3 mice.

LY341495 (Figure 5.5F). Together, these results indicate that release of acetylcholine by SACs is more sensitive to mGluR2-dependent inhibition of the voltage-gated calcium events. This is

consistent with the higher calcium concentration required for acetylcholine release (Lee et al., 2010).

5.5: Reduction of SAC release in mGluR2 agonist impairs direction selectivity of DSGCs

We next asked if exogenous mGluR2 signaling could also reduce light-evoked responses of SACs. We performed whole-cell recordings of DSGC PSCs evoked by moving bar stimulation. Application of LY354740 nearly completely eliminated IPSCs during motion in any direction (Figures 5.7A and 5.7C) and blocked the direction selectivity of IPSCs (Figure 5.7C). In addition, LY354740 partially blocked, but did not completely eliminate, light-evoked EPSCs onto DSGCs (Figure 5.7B). This is consistent with a complete blockade of acetylcholine release, since some excitatory input onto nasal-preferring DSGCs is glutamatergic (Figure 1.1). Therefore, exogenous activation of mGluR2 in SACs impairs SAC-DSGC neurotransmission of both GABA and acetylcholine during moving stimulation.

We tested the effect of mGluR2 on the DSGC spiking response. DSGCs responded to moving light bars with direction-selective firing, which became non-directional in most cells following application of LY354740 (Figures 5.8A-C) due to an increase in spiking evoked by null-direction motion (Figures 5.8A and 5.8B). Application of LY341495 partly rescued direction selectivity in these cells (Figures 5.8A-C). These results are consistent with a previous study using mGluR2 agonists in extracellular recordings from DSGCs (Jensen, 2006). Together, these results indicate that high levels of mGluR2 signaling can block voltage-gated calcium conductance in SACs during physiological stimulation, which abolishes direction selectivity in DSGCs.

Figure 5.7

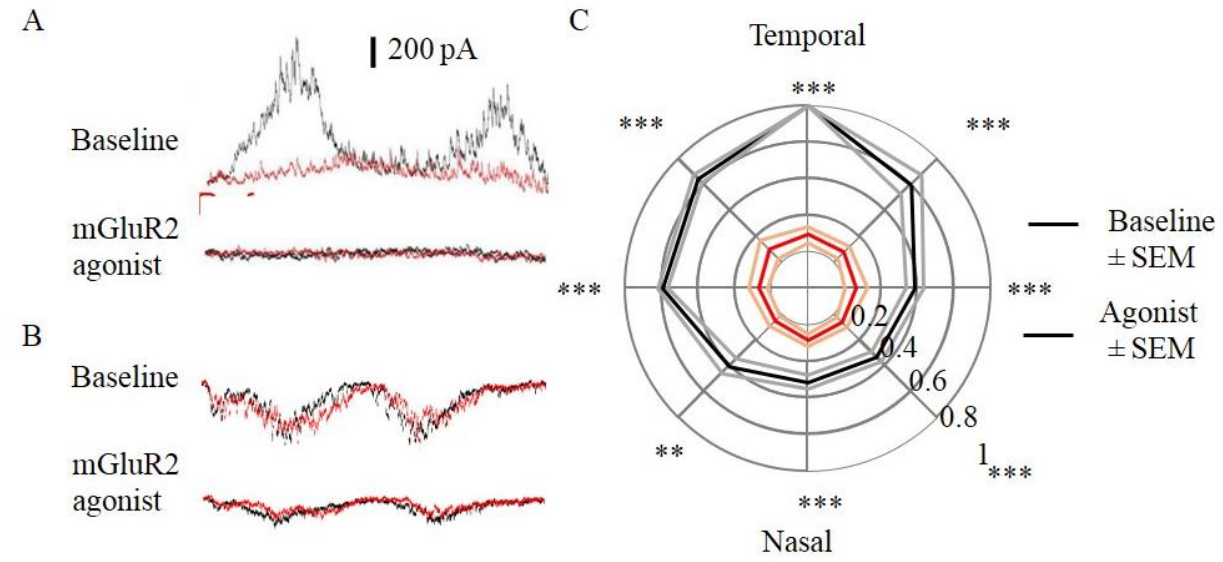

Figure 5.7: mGluR2 agonist blocks most IPSCs and EPSCs onto DSGCs during moving bar stimulation
A: Example traces of IPSCs recorded from a DSGC during motion in the null (black) or preferred (red) directions during baseline (top) or in the presence of mGluR2 agonist (bottom).
B: Example traces of EPSCs recorded from a DSGC during motion in the null (black) or preferred (red) directions during baseline (top) or in the presence of mGluR2 agonist (bottom). Same scale as in A.
C: Averaged tuning curves of IPSCs such as in A plotted as a function of motion direction in baseline condition (black) and in the presence of mGluR2 agonist (red). Gray and pink lines indicate SEM. Responses are normalized to the average response to motion in the temporal (null) direction in baseline conditions.

5.6: Calcium imaging in the GCL illustrates role of GABA release from SACs

Although it is well accepted that elimination of GABA release by SACs abolishes most direction selectivity in the retina (Pei et al., 2015), it is unknown if there are subtypes of DSGCs that do not require GABA release by SACs. Furthermore, it is unknown if orientation selectivity depends on SACs. As a strategy to increase throughput to detect rare retinal cell types, we expressed GCaMP6s in cells located in the GCL via an AAV vector (see Chapter 2). GCaMP6s activity was imaged using a two-photon microscope, which revealed large patches of labeled neurons (Figure 5.9A). Reliable responses could be evoked by visual stimulation, allowing

Figure 5.8

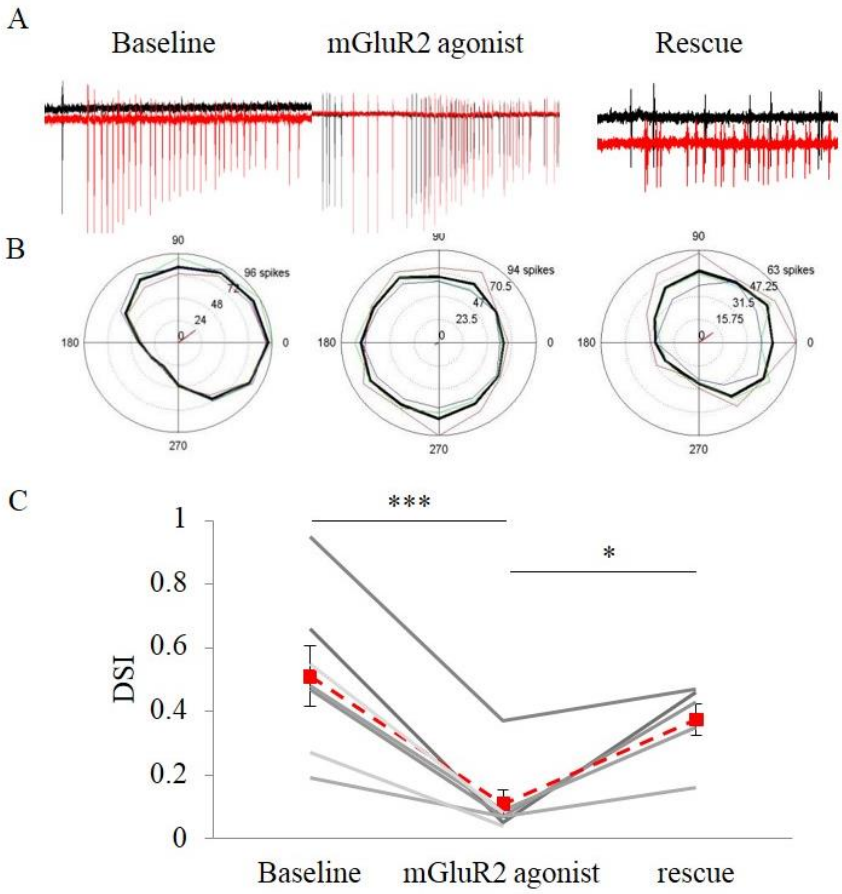

Figure 5.8: mGluR2 agonist blocks direction selectivity by increasing null-direction spiking
A: Example traces of the On component of spiking of a DSGC during moving bar stimulation in the null (black) or preferred (red) direction at baseline conditions (left), in the presence of mGluR2 agonist (center), and following rescue with competitive mGluR2 antagonist (right).
B: Tuning curves showing the spiking as function of motion direction, measured by presenting 3 trials of moving bars in 8 different directions, for a single DSGC in the conditions described in A. Individual trials are indicated by the thin colored lines, and the black line indicates average of the trials.
C: Summary of the direction selectivity index of DSGCs in baseline, mGluR2 agonist, and rescue conditions. Repeated measures ANOVA $p < 0.0001$.

identification of direction-selective and non-selective cell types (Figure 5.9B). A simultaneous extracellular recording of one DSGC during visual stimulation and calcium imaging showed good correspondence between spiking and fluorescence (Figures 5.9C and 5.9D). Imaging of a large number of cells in wildtype mice and mice in which SACs selectively lost VGAT

Figure 5.9

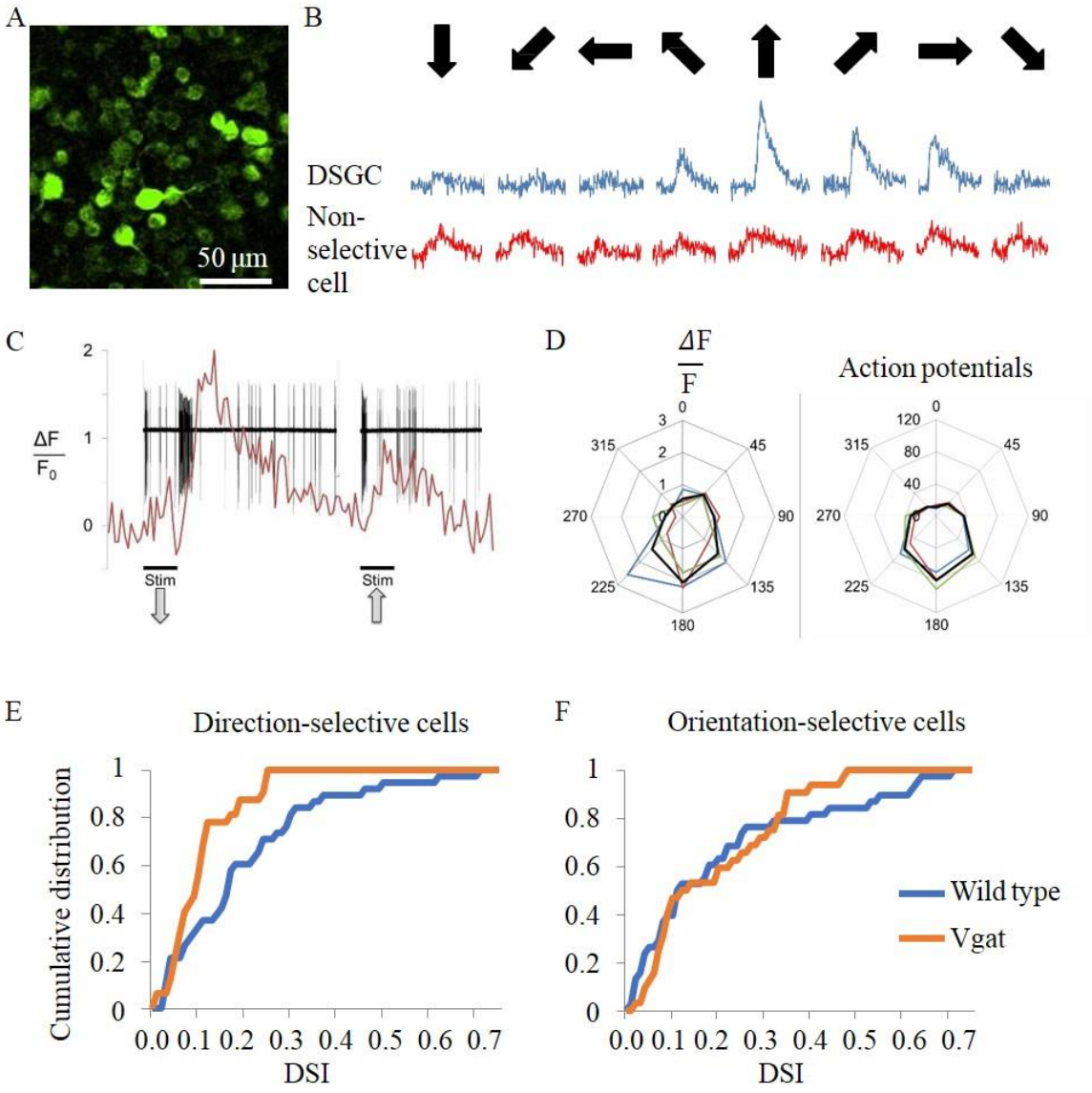

Figure 5.9: Calcium imaging of DSGCs and OSGCs
A: Two-photon image of cells in the ganglion cell layer expressing GCaMP6s.
B: Example calcium responses by motion direction of a DSGC and a non-selective cell
C: Spike recording (black) overlaying simultaneously imaged calcium response in a DSGC during a stimulus in its preferred (left) and null (right) direction.
D: Tuning curve of calcium response (left) and spiking (right) of the cell in C. Red, green, and blue lines indicate individual trials of 8 directions. Black line indicates average of the trials.
E and F: Cumulative distribution of direction selectivity (E) and orientation selectivity (F) of 632 cells from 6 wildtype mice and 251 cells from 1 VGAT mouse.

(Pei et al., 2015) showed that loss of GABA release from SACs shifted the distribution of direction-selective cells (Figure 5.9E). In control mice, about 40% of imaged cells exhibited DSI (direction selectivity index) above 0.2. By contrast, preliminary data from a VGAT mouse showed few cells with DSI above 0.2 (Figure 5.9E). The distribution of orientation selectivity does not appear to be perturbed by absence of VGAT in SACs (Figure 5.9F). These data were incorporated in a study that connected a deficit of retinal direction selectivity to motion sensitivity in the superior colliculus (Shi et al., 2017).

Chapter 6: Discussion

6.1: Mechanism of centrifugal preference

To summarize our findings on SAC direction selectivity, distal-to-proximal activation of one SAC sector is unfavorable for depolarization at the varicosities, approximately equally effective to the opposite direction for depolarization at the soma, and strongly preferred for propagation of depolarization to the post-somatic dendrites. Such a compartment-specific effect of a particular set of inputs suggests the complex interaction of several mechanisms, both cell-intrinsic and cell-extrinsic, in generating direction selectivity.

The biophysical mechanisms that underlie centrifugal preference in SAC dendrites are still unclear, but calcium imaging in SAC varicosities during spatially restricted moving stimuli (Chapter 3) suggest a re-evaluation of one potential mechanism. Anatomical studies using serial electron microscopy (Kim et al., 2014; Greene et al., 2016) have suggested that a Reichardt detector-like microcircuit formed by two spatially segregated and kinetically distinct bipolar cell inputs contributes to direction selectivity in On and Off SACs. In that model, bipolar cells synapsing on proximal SAC dendrites (type 2 on Off SACs and type 7 on On SACs) provide sustained release of glutamate while those synapsing on more distal SAC dendrites (type 3a for Off SACs and type 5 for On SACs) provide transient glutamate release (reviewed in Borst and Helmstaedter, 2015). Therefore, a stimulus moving in the proximal to distal direction would cause favorable spatial summation of signals, while a stimulus moving in the opposite direction would cause a prolonged but blunted depolarization (see Figure 6.1C, top). In disagreement with

this model, a physiological and modeling study showed that local activation of bipolar cells throughout the SAC dendritic field elicited responses with similar kinetics (Stincic et al., 2016). However, that study did not record responses at distal SAC dendrites.

In our calcium imaging study, SAC varicosities sometimes responded to stimulation of only the opposite sector of the cell, especially in mGluR2 blockade. The Reichardt detector-like presynaptic model posits that the directional preference relies on the order of activation of distinct bipolar inputs, and therefore suggests that responses to opposite-sector stimulation should occur preferentially during outward motion (Figure 6.1B, 3 to 4). Instead, we found that responses at the varicosities to opposite-side stimulation prefer the same linear direction as responses to same-sector stimulation (Figure 3.4 and Figure 6.1B, 4 to 3). That is, the linear preferred direction of a SAC dendritic branch is spatially intransient (Figure 6.1B and Figure 6.1C, bottom). This result suggests that, at least for On SACs, centrifugal preference is computed not based on the order of activation of distinct types of bipolar cell synapses but based on the order of activation of SAC dendritic compartments. During physiological conditions, we found that centrifugal responses to whole-field stimuli are triggered just before the moving stimulus directly activates the post-somatic dendritic sector, suggesting that trans-somatic signals are crucial for priming SAC dendrites for a centrifugal response. Because a stimulus moving toward the soma causes a somatic depolarization that is slow and sustained, spatial summation is favored at postsomatic sites, consistent with our hypothesized post-synaptic mechanism of generating direction selectivity (Figure 3.13). However, these experiments do not rule out the possibility

Figure 6.1

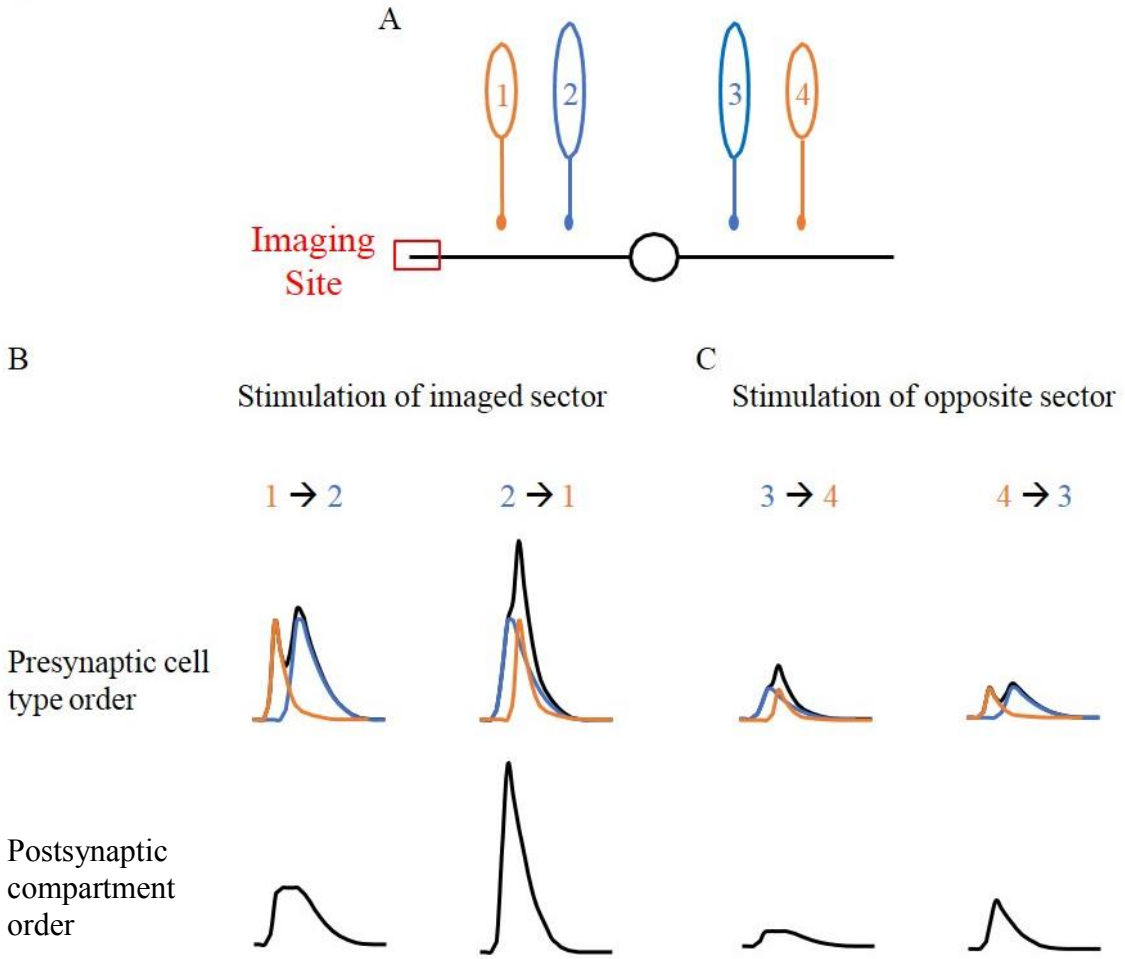

Figure 6.1: Two models to explain SAC centrifugal preference

A: Schematic show ing a SAC (black) with two dendritic sectors (represented by lines) extending from the soma in opposite directions and bipolar cell inputs (blue and orange). Proximal bipolar cells (blue, 2 and 3) are thought to exhibit sustained response kinetics, while distal bipolar inputs (orange, 1 and 4) are thought to exhibit transient kinetics.

B: Traces indicate hypothetical membrane potential at the imaging site. In one model (Presynaptic cell type order), the order of activation of distinct bipolar cell types determines direction selectivity. Centripetal stimulation of the imaged sector (1 to 2) activates these inputs in an unfavorable order, such that the inputs do not coincide. By contrast, centrifugal stimulation (2 to 1) causes effective spatial summation. In another model, postsynaptic mechanisms favor sequential activation of the proximal and distal compartments. Both models predict centrifugal preference during stimulation of the imaged branches.

C: During stimulation of the opposite sector relative to the imaging site, the presynaptic model predicts more effective summation during outward motion (3 to 4) than during inward motion (4 to 3). However, the postsynaptic model predicts that the opposite order of activation, the direction preferred by the imaged dendrite, would trigger a larger depolarization. This model most closely matches the data from stimulation of the opposite sector in Figure 3.4.

that presynaptic mechanisms can contribute to centrifugal preference under some conditions (for instance, stimuli localized to a single dendritic sector).

As reported in some other studies (Lee and Zhou, 2006; Hausselt et al., 2007; Fransen and Bourghis, 2017), current-clamp recordings from SAC somata show only weak direction selectivity to stimuli restricted to a single SAC sector. These nearly isotropic somatic responses contrast with the robust direction selectivity seen at distal SAC varicosities using calcium imaging during the same moving stimuli. In this study, we found that this relative isotropy in response amplitude at the soma is maintained in the absence of ionotropic inhibition of SACs, in the absence of voltage-gated potassium channels in SACs, and in the absence of mGluR2 signaling. In fact, the latter two conditions show little or no centrifugal preference. Therefore, it is likely that intrinsic mechanisms, such as unfavorable dendritic branching patterns, prevent the strong centrifugal responses in distal SAC dendrites from back-propagating toward the soma.

One plausible mechanism to explain electrotonic isolation of SACs is that voltage-gated potassium channels expressed proximally in SACs (Ozaita et al., 2004) are selectively activated by the higher-amplitude centrifugal response and therefore selectively block back-propagation of this centrifugal response. Bidirectional gain modulation has been reported as a consequence of interplay between voltage-gated potassium and calcium channels in invertebrate neurons that share similarities with SACs (Laurent, 1993). At low potentials, synaptic input is conducted passively and can modulate the membrane potential linearly. Increased depolarization leads to sublinear integration of synaptic input because of the activation of voltage-gated potassium

channels. It is possible that the weak depolarization in SAC dendrites during centripetal motion propagates faithfully because it does not significantly activate Kv channels, while the powerful centrifugal depolarization triggers perisomatic voltage-gated potassium channels (Ozaita et al., 2004), limiting the somatic depolarization. Our data somewhat support this hypothesis, because blocking Kv channels selectively prolongs the centrifugal response at the soma. However, further experiments using calcium or voltage imaging at proximal dendritic locations in SACs are needed to verify this mechanism.

Other mechanisms, including a hypothesized potential gradient along SAC dendrites (Hausselt et al., 2007) may also play a role in compartment-specific responses. This potential gradient is thought to depend on ionotropic input from tonic activation of bipolar cells (Sethuramanujam and Slaughter, 2015), but a role for mGluR2 in setting this gradient has not been ruled out. Manipulations used in this study, including mGluR2 and Kv channel blockade, are likely to affect any resting membrane potential gradients. Therefore, the precise mechanism by which these manipulations exert their effects are not clear. Still, the differential effect of mGluR2 and Kv channel blockade on responses to centripetal motion suggest that these signals play distinct roles in maintaining electrotonic isolation and controlling the degree of impulse propagation.

If the amplitude of somatic depolarization is nearly isotropic, how does centripetal conduction preferentially activate post-somatic propagation? Our data indicate that endogenous mGluR2 signaling partly impedes this propagation. The most likely explanation, given current clamp recordings, is that the sustained depolarization following centripetal stimulation is a more

efficient trigger for the post-somatic calcium spike than the transient centrifugal response, perhaps because it enables summation with local post-somatic excitatory inputs over a longer period of time. However, this has not yet been tested.

The role of mGluR2 in SACs is intriguing because tonic release of glutamate by bipolar cells is modulated by visual conditions (Sethuramanujam and Slaughter, 2015). These findings suggest that the electrotonic isolation of SACs, and therefore compartmentalization of dendritic signals, are sensitive to the visual environment. For instance, it is possible that mGluR2 activation alters the sensitivity of SAC branches bidirectionally in a homeostatic mechanism: reduced glutamate release could lead to increased excitability and cross-compartmental integration to enhance responsiveness, while increased glutamate release could lead to spatial isolation of inputs to prevent overactivation of SAC dendrites. Metabotropic glutamate receptors may control the dendritic excitability depending on network state (Otsu et al., 2014). Interestingly, the other cell types that may express mGluR2 in the retina are the rod amacrine cells (A17 or the distal dendrites of AII amacrine cells), which are notable for their varicosities which locally process inputs from rod bipolar cells and are spatially isolated (Oesch et al., 2011). While the role of mGluR2 inputs in the rod amacrine cells is not clear, this suggests that a similar mechanism by which levels of glutamate release mediate isolation of dendritic compartments may also operate in these cells.

6.2: Mechanism of cholinergic SAC-DSGC transmission

We found a significant latency difference between GABA release from null- and preferred-side pairs. This suggests that GABAergic transmission operates differently depending on the orientation of SAC-DSGC pairs, which is suggested by the absence of clear synaptic structures in preferred-side connections (Brigmann et al., 2011). It is possible that the difference in latency reflects the fact that preferred-side release of GABA comes from spillover from nearby synapses onto ganglion cells that prefer the opposite direction. Notably, the average difference between onset of cholinergic and GABAergic transmission in null-side pairs was small, which is not consistent with distinct mechanisms of transmission for null-side GABA and acetylcholine. The rapid transmission of acetylcholine is in contrast to synapses which are known to operate by volume transmission, which are necessarily characterized by longer latency to response onset (Ren et al., 2011) due to the greater distance. This may suggest that null-side cholinergic transmission occurs in classical synapses, which may also be found at SAC varicosities (Famiglietti et al., 2005). Interestingly, On DSGCs in rabbits show about 4 ms in delay between the GABAergic and cholinergic PSPs (Brombas et al., 2014), in contrast to the simultaneous transmission onto On-Off DSGCs (Lee et al., 2010). These data suggest that acetylcholine must diffuse a greater distance to activate nicotinic receptors on On DSGCs, at least in rabbits. Furthermore, the cholinergic post-synaptic component in rabbit On DSGCs can be modified bidirectionally by modulating acetylcholinesterase activity (Brombas et al., 2014). This is consistent with paracrine neurotransmission (Bennett et al., 2012), but it does not exclude wired transmission. Even in wired transmission, inhibitors of acetylcholinesterase could be expected to allow more spillover of acetylcholine between synaptic sites and exogenous acetylcholinesterase

may more rapidly break down acetylcholine within synapses. Most notably, these experiments do not exclude mixed wired and volume transmission, which may occur if nicotinic receptors on DSGCs are present at variable distances from SAC release sites (Bennett et al., 2012).

In support of a degree of wired nicotinic transmission, electron microscopy has shown that SAC vesicles, which are larger and rounder than typical amacrine cell GABAergic vesicles, are present adjacent to asymmetric synapses onto ganglion cells (Famiglietti, 2005). However, no studies have analyzed whether cholinergic PSCs are quantal, which would imply wired neurotransmission. In our paired recordings, there were few or no cholinergic PSCs in most conditions (data not shown), but further study of this question is required. One outstanding question is whether there is anisotropy in the mechanism of acetylcholine release: if there are direct cholinergic synapses, are these formed in the same sites as GABAergic synapses, making them more common between null-side SAC-DSGC pairs? If not, is there a difference in the location of cholinergic inputs relative to the DSGC soma between null- and preferred-side connections, as there is for GABAergic inputs (Morrie and Feller, 2015)? These questions will require analysis of EPSC kinetics during paired recordings in which neurotransmitter release is made asynchronous using strontium (Morrie and Feller, 2015). Additionally, a large number of SAC-DSGC paired recordings combined with detailed two-photon images of dendritic overlap could be used to determine if there are differences in the relationship of dendritic overlap and cholinergic transmission between the null- and preferred-side pairs. Finally, high-resolution imaging and immunoelectron microscopy may be used to localize VGAT and VAChT in order to determine if co-release occurs at the level of individual varicosities.

6.3: Facilitation of cholinergic transmission

Our data show that cholinergic transmission is potentiated by tonic (~10-second) DSGC depolarization during repeated SAC stimulation. Preliminary experiments suggest that repeated stimulation in the absence of DSGC depolarization does not lead to potentiation. In our experiments, GABAergic transmission was measured while depolarizing the DSGC to the reversal potential of excitatory currents (0 mV); therefore, we did not test GABAergic transmission in the absence of DSGC depolarization. Future experiments in pharmacological blockade of nicotinic receptors and DSGC voltage clamp at a polarized potential are necessary to determine if GABAergic transmission is also potentiated.

Analysis of paired recordings following bath application of gabazine shows that this cholinergic potentiation requires the effect of GABAA receptors. However, postsynaptic depolarization-induced potentiation does not require SAC expression of either the a2 subunit of GABAA receptors or VGAT. This suggests that GABA released by non-starburst amacrine cells onto another cell type, possibly DSGCs, is required for potentiation. However, a role of SACs has not been completely ruled out: some GABAergic transmission still occurs in SACs that lack VGAT, and SACs may express GABAA receptors that do not contain the a2 subunit. Furthermore, the role of GABAA receptors in transmission is unclear. It may be part of circuit mechanism acutely triggered by DSGC depolarization; alternatively, and perhaps more likely, the acute absence of GABAergic transmission depolarizes DSGCs, potentially occluding the experimental effect of electrophysiological depolarization of DSGCs. Future experiments are necessary to understand

the conditions governing potentiation, including the required degree of DSGC depolarization and the effect of pharmacological agents on this phenomenon.

Notably, the conditions under which we evoked potentiation of nicotinic transmission differ from those used to evoke paired-pulse facilitation of cholinergic transmission in rabbits (Lee et al., 2010) and paired-pulse depression of GABAergic transmission in mice (Morrie and Feller, 2015). In those studies, SACs were stimulated by two pulses with interstimulus intervals of 1-10 seconds and no dependence on DSGC depolarization was reported. The paired-pulse ratio is often used as a marker of presynaptic release properties, including quantal number and release probability (reviewed in Zucker and Regehr, 2002). However, postsynaptic mechanisms are thought to account for many forms of long-term plasticity (Granger and Nicoll, 2014). Our experiments on the potentiation of nicotinic transmission between SACs and DSGCs do not distinguish between presynaptic and postsynaptic mechanisms. It is not known how DSGC depolarization could modulate the properties of nicotinic receptors. The offset kinetics of nicotinic acetylcholine receptors have been shown to depend on membrane potential (Sheridan and Lester, 1975), but it is not clear if a 6-10-second depolarization in the absence of channel activity could result in a sustained effect on channel function. If this potentiation is primarily post-synaptic, local application of nicotine onto DSGC dendrites would be expected to cause a response that is also potentiated by transient DSGC depolarization.

Endocannabinoids are a potential candidate for a presynaptic potentiation mechanism, because they are involved in retrograde transmission and modulation of neurotransmitter release

elsewhere in the nervous system (Castillo et al., 2012). The retina widely expresses markers of endocannabinoid transmission (Bouchard et al., 2016), including fatty acid amide hydrolase, the enzyme that breaks down the endocannabinoid anandamide and is expressed on SAC dendrites (Yazulla et al., 1999). Electron microscopy studies have intermittently visualized vesicles in the ganglion cells postsynaptic to SAC release sites, which are likely to be DSGCs (Famiglietti, 2005). Non-vesicular retrograde transmitters, such as nitric oxide, are also released by retinal cells (Eldred and Blute, 2005) and are also potential candidates. The effects of these retrograde transmitters would be to enhance release of acetylcholine from SAC terminals, perhaps by modulating voltage-gated calcium channels. This effect, like that of mGluR2 signaling and blockade of N-type calcium channels (Lee et al., 2010), could be selective for acetylcholine release over GABA release because acetylcholine release requires higher calcium concentration (Lee et al., 2010). GABA release may be saturated at the lower baseline calcium concentration and therefore not be affected by increased calcium influx due to a secondary messenger cascade.

What might be the functional consequence of cholinergic potentiation mediated by DSGC depolarization? If the effect operates at smaller time scales than those tested in this study and can be evoked by high firing rate in DSGCs, it may form a crucial positive-feedback effect between SACs and DSGCs to enhance excitation during preferred-direction motion. Homosynaptic potentiation, which might occur if retrograde transmission is spatially restricted and triggered by dendritic spikes (Rancz and Häusser, 2006), could augment acetylcholine release from preferred-side SACs during preferred-direction motion. Alternatively, if retrograde transmission is not spatially restricted, depolarization of a DSGC in response to a moving edge of light increment

may enhance acetylcholine release onto the DSGC in response to a subsequent moving edge of light decrement. In this way, retrograde neurotransmission may be a mechanism of motion facilitation due to crosstalk between the On and Off pathways, which otherwise independently compute direction selectivity in DSGCs (Kittila and Massey, 1995).

6.4: Conservation of the direction selectivity circuit across species

Despite differences in the features of the retina between mammals, SACs and SAC morphology is remarkably conserved. In carnivores and primates, the arborization of SACs is similar to that in mice but less extensive, with a somewhat lower tiling factor: around 20 in cats (Famiglietti, 1987; Schmidt et al., 1987; Vardi et al., 1989) and around 10 in macaques (Rodieck, 1989; Rodieck and Marshak, 1992). Primates, including humans, have cholinergic retinal neurons with grossly similar dendritic morphology and stratification (Mariani, 1990; Rodieck, 1989), albeit with single primary dendrites and reduced branching. A recent study has identified primate retinal ganglion cells that may be homologues of mouse DSGCs (Rousso et al., 2016), but because they are rare, they are unlikely to be encountered during physiology experiments. Ongoing experiments using genetic labeling of potentially direction-selective primate ganglion cells may soon determine the extent of primate retinal direction selectivity. Nevertheless, even if primate DSGCs exist, it is not known whether SACs function in direction selectivity, since cell-type homology does not necessarily indicate functional similarity. If SACs indeed play a role in direction selectivity across species, it will be interesting to examine the effect of differences in dendritic arborization, such as the reduced tiling factor and the convergence of multiple SAC sectors onto a single primary dendrite. A role for SACs in human direction selectivity is

plausible because patients with mutations of a structural protein specific to SACs called frmd7 (4.1 protein, ezrin, radixin, and moesin domain containing 7) develop congenital nystagmus (Choi et al., 2015). A similar eye movement phenotype was found in frmd7-knockout mice, in which release of GABA by SACs is non-directional and DSGCs are no longer directionally tuned (Yonehara et al., 2015).

6.5: Conclusion

The retina is a special case in which spatial activation of a neuron corresponds to stimulation in visual space, imparting functional relevance to physiological studies of dendritic isolation and excitability. Nevertheless, there is increasing evidence from across the nervous system that meaningful computations are performed within individual dendritic branches and that electrotonic interactions between dendritic branches are tightly controlled and regulated. It is likely that many functional implications of regulated dendritic isolation will be revealed by growing understanding of subcellular connectivity in the brain and the information contained in the inputs to a particular dendrite. It is also likely that even minor defects in the intrinsic properties of dendrites will result in neurological disorders (Kulkarni and Firestein, 2012). Therefore, it is crucial to study mechanisms of dendritic compartmentalization across the nervous system in the context of circuit function, modulation or adaptation, and dysfunction.

References

Abbas, S. Y., Hamade, K. C., Yang, E. J., Nawy, S., Smith, R. G., and Pettit, D. L. (2013). Directional summation in non-direction selective retinal ganglion cells. PLoS Comput Biol. 9, e1002969.

Adrover, M. F., Shin, J. H., and Alvarez, V. A. (2014). Glutamate and dopamine transmission from midbrain dopamine neurons share similar release properties but are differentially affected by cocaine. J Neurosci. 34, 3183-3192.

Agnati, L.F., Zoli, M., Stromberg, I., and Fuxe, K. (1995). Intercellular communication in the brain: wiring versus volume transmission. Neuroscience. 69, 711-726.

Ahnert-Hilger, G., and Jahn, R. (2011). CLC-3 spices up GABAergic synaptic vesicles. Nat Neurosci. 14, 405-407.

Amthor, F.R., and Grzywacz, N.M. (1991). Nonlinearity of the inhibition underlying retinal directional selectivity. Vis. Neurosci. 6, 197–206.

Amthor, F. R., Grzywacz, N. M., and Merwine, D. K. (1996). Extra-receptive-field motion facilitation in on-off directionally selective ganglion cells of the rabbit retina. Vis Neurosci. 13, 303-309.

Apostolides, P. F., and Trussell., L. O. (2013). Rapid, activity-independent turnover of vesicular transmitter content at a mixed glycine/GABA synapse. J Neurosci. 33, 4768-4781.

Ascoli, G. A., Gasparini, S., Medinilla, V., and Migliore, M. (2010). Local control of postinhibitory rebound spiking in CA1 pyramidal neuron dendrites. J Neurosci. 30, 6434-6442.

Attwell, D., Barbour, B., and Szatkowski, M. (1993). Nonvesicular release of neurotransmitter. Neuron 11, 401-407.

Barlow, H. B., and Hill, R. M. (1963). Selective sensitivity to direction of movement in ganglion cells of the rabbit retina. Science. 139, 412-414.

Barlow, H. B., and Levick, W. R. (1965). The mechanism of directionally selective units in rabbit's retina. J Physiol. 178, 477-504.

Barth, A. M., Vizi, E. S., Zelles, T., and Lendvai, B. (2008). Alpha2-adrenergic receptors modify dendritic spike generation via HCN channels in the prefrontal cortex. J Neurophysiol. 99, 394-401.

Beltran, J. Q., and Gutierrez, R. (2012). Co-release of glutamate and GABA from single, identified mossy fibre giant boutons. J Physiol. 590, 4789-4800.

Bennett, C., Arroyo, S., Berns, D., and Hestrin, S. (2012). Mechanisms generating dual-component nicotinic EPSCs in cortical interneurons. J Neurosci. 32, 17287-17296.

Bischofberger, J., and Schild, D. (1996). Glutamate and N-acetylaspartylglutamate block HVA calcium currents in frog olfactory bulb interneurons via an mGluR2/3-like receptor. J. Neurophysiol. 76, 2089–2092.

Bittner, K.C., Grienberger, C., Vaidya, S.P., Milstein, A.D., Macklin, J.J., Suh, J., Tonegawa, S., and Magee, J.C. (2015). Conjunctive input processing drives feature selectivity in hippocampal CA1 neurons. Nat. Neurosci. 18, 1133–1142.

Bloomfield, S. A. (1992). Relationship between receptive and dendritic field size of amacrine cells in the rabbit retina. J Neurophysiol. 68, 711-725.

Borghuis, B.G., Marvin, J.S., Looger, L.L., and Demb, J.B. (2013). Two-Photon Imaging of Nonlinear Glutamate Release Dynamics at Bipolar Cell Synapses in the Mouse Retina. J. Neurosci. 33, 10972–10985.

Borst, A., and Helmstaedter, M. (2015). Common circuit design in fly and mammalian motion vision. Nat Neurosci. 18, 1067-1076.

Bouchard, J. F., Casanova, C., Cécyre, B., and Redmond, W. J. (2016). Expression and function of the endocannabinoid system in the retina and the visual brain. Neural plast. 2016, 9247057.

Bowling, D. B. (1980). Light responses of ganglion cells in the turtle of the retina. J Physiol. 299, 173-196.

Brainard, D.H. (1997). The Psychophysics Toolbox. Spat. Vis. 10, 433–436.

Branco, T., Clark, B. A., and Häusser, M. (2010). Dendritic discrimination of temporal input sequences in cortical neurons. Science 329, 1671-1675.

Branco, T., and Häusser, M. (2009). The selfish spike: local and global resets of dendritic excitability. Neuron 61, 815-817.

Branco, T., and Häusser, M. (2010). The single dendritic branch as a fundamental functional unit in the nervous system. Curr. Opin. Neurobiol. 20, 494–502.

Branco, T., and Häusser, M. (2011). Synaptic integration gradients in single cortical pyramidal cell dendrites. Neuron 69, 885-892.

Brandstätter, J.H., Koulen, P., and Wässle, H. (1998). Diversity of glutamate receptors in the mammalian retina. Vision Res. 38, 1385–1397.

Brecha, N., Johnson, D., Peichl, L., and Wässle, H. (1988). Cholinergic amacrine cells of the rabbit retina contain glutamate decarboxylase and gamma-aminobutyrate immunoreactivity. Proc. Natl. Acad. Sci. U. S. A. 85, 6187–6191.

Briggman, K.L., Helmstaedter, M., and Denk, W. (2011). Wiring specificity in the direction-selectivity circuit of the retina. Nature 471, 183–188.

Brombas, A., Katila-de Croft, S., Cooper-Williams, E. J., and Williams, S. R. (2017). Dendro-dendritic cholinergic excitation controls dendritic spike initiation in retinal ganglion cells. Nat Commun. 8, 15683.

Cai, W., and Pourcho, R.G. (1999). Localization of metabotropic glutamate receptors mGluR1alpha and mGluR2/3 in the cat retina. J. Comp. Neurol. 407, 427–437.

Cajal S. (1893). La rétine des vertébrés. Cellule 9, 121–255.

Caldwell, J. H., Daw, N. W., and Wyatt, H. J. (1978). Effects of picrotoxin and strychnine on rabbit retinal ganglion cells: lateral interactions for cells with more complex receptive fields. J Physiol. 276, 277-298.

Carandini, M., and Ferster, D. (2000). Membrane potential and firing rate in cat primary visual cortex. J. Neurosci. 20, 470–484.

Castillo, P. E., Younts, T. J., Chávez, A. E., and Hashimotodani, Y. (2012). Endocannabinoid signaling and synaptic function. Neuron 76, 70-81.

Chen, M., Lee, S., Park, S. J., Looger, L. L., and Zhou, Z. J. (2014). Receptive field properties of bipolar cell axon terminals in direction-selective sublaminas of the mouse retina. J Neurophysiol. 112, 1950-1962.

Chen, Q., Pei, Z., Koren, D., and Wei, W. (2016). Stimulus-dependent recruitment of lateral inhibition underlies retinal direction selectivity. Elife 5.

Chen, T.-W., Wardill, T.J., Sun, Y., Pulver, S.R., Renninger, S.L., Baohan, A., Schreiter, E.R., Kerr, R.A., Orger, M.B., Jayaraman, V., et al. (2013). Ultrasensitive fluorescent proteins for imaging neuronal activity. Nature 499, 295–300.

Choi, J. H., Shin, J. H., Seo, J. H., Jung, J. H., and Choi, K. D. (2015). A start codon mutation of the FRMD7 gene in two Korean families with idiopathic infantile nystagmus. Sci Rep. 5, 13003.

Cleland, B. G., and Levick, W. R. (1974). Properties of rarely encountered types of ganglion cells in the cat's retina and an overall classification. J Physiol. 240, 457-492.

Cohen, E.D. (2001). Voltage-gated calcium and sodium currents of starburst amacrine cells in the rabbit retina. Vis. Neurosci. 18, 799–809.

Cohen, E. D., and Miller, R. F. (1995). Quinoxalines block the mechanism of direction-selectivity in ganglion cells of the rabbit retina. Proc Natl Acad Sci USA. 92, 1127-1131.

Cruz-Martín, A., El-Danaf, R. N., Osakada, F., Sriram, B., Dhande, O. S., Nguyen, P. L., Callaway, E. M., Ghosh, A., and Huberman, A. D. (2014). A dedicated circuit links direction-selective retinal ganglion cells to the primary visual cortex. Nature 507, 358-361.

Dacheux, R. F., Chimento, M. F., and Amthor, F. R. (2003). Synaptic input to the on-off directionally selective ganglion cells in the rabbit retina. J Comp Neurol. 456, 267-278.

Demarque, M., Represa, A., Becq, H., Khalilov, I., Ben-Ari, Y., and Aniksztejn, L. (2002) Neuron 36, 1051-1061.

Demb, J. B., and Singer, J. H. (2015). Functional circuitry of the retina. Annu Rev Vis Sci. 24, 263-289.

Dhande, O. S., Estevez, M. E., Quattrochi, L. E., El-Danaf, R. N., Nguyen, P. L., Berson, D. M., and Huberman, A. D. (2013). Genetic dissection of retinal inputs to brainstem nuclei controlling image stabilization. J Neurosci. 33, 17797-17813.

Dhande, O. S., Stafford, B. K., Lim, J. A., and Huberman, A. D. (2015). Contributions of retinal ganglion cells to subcortical visual processing and behaviors. Annu Rev Vis Sci. 1, 291-328.

Ding, H., Smith, R.G., Poleg-Polsky, A., Diamond, J.S., and Briggman, K.L. (2016). Species-specific wiring for direction selectivity in the mammalian retina. Nature 535, 105–110.

Eldred, W. D., and Blute, T. A. (2005). Imaging of nitric oxide in the retina. Vision Res. 45, 3469-3486.

El Mestikawy, S., Wallén-Mackenzie, A., Fortin, G. M., Descarries, L., and Trudeau, L. E. (2011). From glutamate co-release to vesicular synergy: vesicular glutamate transporters. Nat Rev Neurosci. 12, 204-216.

Endo, T., Tarusawa, E., Notomi, T., Kaneda, K., Hirabayashi, M., Shigemoto, R., and Isa, T. (2008). Dendritic Ih ensures high-fidelity dendritic spike responses of motion-sensitive neurons in rat superior colliculus. J Neurophysiol. 99, 2066-2076.

Euler, T., Detwiler, P.B., and Denk, W. (2002). Directionally selective calcium signals in dendrites of starburst amacrine cells. Nature 418, 845–852.

Euler, T., Hausselt, S.E., Margolis, D.J., Breuninger, T., Castell, X., Detwiler, P.B., and Denk, W. (2009). Eyecup scope--optical recordings of light stimulus-evoked fluorescence signals in the retina. Pflugers Arch. 457, 1393–1414.

Famiglietti, E. V. (1985). Starburst amacrine cells: morphological constancy and systematic variation in the anisotropic field of rabbit retinal neurons. J Neurosci. 5, 562-577.

Famiglietti, E. V. (1987). Starburst amacrine cells in cat retina are associated with bistratified, presumed direction-selective, ganglion cells. Brain Res. 413, 404-408.

Famiglietti, E. V. (1991). Synaptic organization of starburst amacrine cells in rabbit retina: analysis of serial thin sections by electron microscopy and graphic reconstruction. J. Comp. Neurol. 309, 40–70.

Famiglietti, E. V. (2005). Synaptic organization of complex ganglion cells in rabbit retina: type and arrangement of inputs to directionally selective and local-edge-detector cells. J Comp Neurol. 484, 357-391.

Fattorini, G., Antonucci, F., Menna, E., Matteoli, M., and Conti, F. (2015) Co-expression of VGLUT1 and VGAT sustains glutamate and GABA co-release and is regulated by activity in cortical neurons. J Cell Sci. 128, 1669-1673.

Fransen, J.W., and Borghuis, B.G. (2017). Temporally Diverse Excitation Generates Direction-Selective Responses in ON- and OFF-Type Retinal Starburst Amacrine Cells. Cell Rep. 18, 1356–1365.

Fried, S.I., Münch, T.A., and Werblin, F.S. (2002). Mechanisms and circuitry underlying directional selectivity in the retina. Nature 420, 411–414.

Gasparini, S., Migliore, M., and Magee, J. C. (2004). On the initiation and propagation of dendritic spikes in CA1 pyramidal neurons. J Neurosci. 24, 11046-11056.

Gras, C., Amilhon, B., Lepicard, E. M., Poirel, O., Vinatier, J., Herbin, M., Dumas, S., Tzavara, E. T., Wade, M. R., Nomikos, G. G., et al. (2008). The vesicular glutamate transporter VGLUT3 synergizes striatal acetylcholine tone. Nat Neurosci. 11, 292-300.

Gavrikov, K.E., Dmitriev, A. V, Keyser, K.T., and Mangel, S.C. (2003). Cation--chloride cotransporters mediate neural computation in the retina. Proc. Natl. Acad. Sci. U. S. A. 100, 16047–16052.

Gollisch, T., and Meister, M. (2010). Eye smarter than scientists believed: neural computations in circuits of the retina. Neuron 65, 150-164.

Granger, A. J., Wallace, M. L., and Sabatini, B. L. (2017). Multi-transmitter neurons in the mammalian central nervous system. Curr Opin Neurobiol. 45, 85-91.

Greene, M. J., Kim, J. S., Seung, H. S.; EyeWirers. (2016). Analogous convergence of sustained and transient inputs in parallel on and off pathways for retinal motion computation. Cell Rep. 14, 1892-1900.

Grzywacz, N.M., and Amthor, F.R. (2007). Robust directional computation in on-off directionally selective ganglion cells of rabbit retina. Vis. Neurosci. 24, 647–661.

Grzywacz, N. M., Amthor, F. R., and Merwine, D. K. (1998a). Necessity of acetylcholine for retinal directionally selective responses to drifting gratings in rabbit. J Physiol. 512, 575-581.

Grzywacz, N. M., Merwine, D. K., and Amthor, F. R. (1998b). Complementary roles of two excitatory pathways in retinal directional selectivity. Vis Neurosci. 15, 1119-1127.

Hamlet, W.R., and Lu, Y. (2016). Intrinsic plasticity induced by group II metabotropic glutamate receptors via enhancement of high-threshold KV currents in sound localizing neurons. Neuroscience 324, 177–190.

Harnett, M.T., Xu, N.-L., Magee, J.C., and Williams, S.R. (2013). Potassium Channels Control the Interaction between Active Dendritic Integration Compartments in Layer 5 Cortical Pyramidal Neurons. Neuron 79, 516–529.

Hausselt, S.E., Euler, T., Detwiler, P.B., and Denk, W. (2007). A dendrite-autonomous mechanism for direction selectivity in retinal starburst amacrine cells. PLoS Biol. 5, e185.

Herzog, E., Gilchrist, J., Gras, C., Muzerelle, A., Ravassard, P., Giros, B., Gaspar, P., and El Mestikawy, S. (2004). Localization of VGLUT3, the vesicular glutamate transporter type 3, in the rat brain. Neuroscience 123, 983-1002.

Hillier, D., Fiscella, M., Drinnenberg, A., Trenholm, S., Rompani, S. B., Raicz, Z., Katona, G., Juettner, J., Hierlemann, A., Rozsa, B., and Roska, B. (2017). Causal evidence for retina-dependent and -independent visual motion computations in mouse cortex. Nat Neurosci. 20, 960-968.

Hoffmann, K. P., and Stone, J. (1985). Retinal input to the nucleus of the optic tract of the cat assessed by antidromic activation of ganglion cells. Exp Brain Res. 59, 395-403.

Hoggarth, A., McLaughlin, A. J., Ronellenfitch, K., Trenholm, S., Vasandani, R., Sethuramanujam, S., Schwab, D., Briggman, K. L., and Awatramani, G. B. (2015). Specific wiring of distinct amacrine cells in the directionally selective retinal circuit permits independent coding of direction and size. Neuron 86, 276-291.

Hua, S. Y., Raciborska, D. A., Trimble, W. S., and Charlton, M. P. (1998). Different VAMP/synaptobrevin complexes for spontaneous and evoked transmitter release at the crayfish neuromuscular junction. J Neurophysiol. 80, 3233-3246.

Hubel, D. H., and Wiesel, T. N. (1959). Receptive fields of single neurones in the cat's striate cortex. J Physiol. 148, 574-591.

Huberman, A. D., Wei, W., Elstrott, J., Stafford, B. K., Feller, M. B., and Barres, B. A. (2009). Genetic identification of an on-off direction-selective retinal ganglion cell subtype reveals a layer-specific subcortical map of posterior motion. Neuron 62, 327-334.

Ikeda, S.R., Lovinger, D.M., McCool, B.A., and Lewis, D.L. (1995). Heterologous expression of metabotropic glutamate receptors in adult rat sympathetic neurons: Subtype-specific coupling to ion channels. Neuron 14, 1029–1038.

Jadi, M., Polsky, A., Schiller, J., and Mel, B. W. (2012). Location-dependent effects of inhibition on local spiking in pyramidal neuron dendrites. PLoS Comput Biol. 8, e1002550.

Jahr, C. E., and Nicoll, R. A. (1982). Noradrenergic modulation of dendrodendritic inhibition in the olfactory bulb. Nature 297, 227-229.

Jarsky, T., Roxin, A., Kath, W.L., and Spruston, N. (2005). Conditional dendritic spike propagation following distal synaptic activation of hippocampal CA1 pyramidal neurons. Nat. Neurosci. 8, 1667–1676.

Jensen, R. J. (1995). Receptive-field properties of displaced starburst amacrine cells change following axotomy-induced degeneration of ganglion cells. Vis Neurosci. 12, 177-184.

Jensen, R.J. (2006). Activation of group II metabotropic glutamate receptors reduces directional selectivity in retinal ganglion cells. Brain Res. 1122, 86–92.

Jeon, C. J., Kong, J. H., Strettoi, E., Rockhill, R., Stasheff, S. F., and Masland, R. H. (2002). Pattern of synaptic excitation and inhibition upon direction-selective retinal ganglion cells. J Comp Neurol, 449, 195-205.

Jeong, S. A., Kwon, O. J., Lee, J. Y., Kim, T. J., and Jeon, C. J. (2006). Synaptic pattern of AMPA receptor subtypes upon direction-selective retinal ganglion cells. Neurosci Res. 56, 427-434.

Jonas, P., Bischofberger, J., and Sandkühler, J. (1998). Corelease of two fast neurotransmitters at a central synapse. Science 281, 419-424.

Jones, S. M., and Palmer, M. J. (2009). Activation of the tonic GABAC receptor current in retinal bipolar cell terminals by nonvesicular GABA release. J Neurophysiol. 102, 691-699.

Johnston, D., Hoffman, D.A., Magee, J.C., and Colbert, C.M. (1997). K+ channel regulation of signal propagation in dendrites of hippocampal pyramidal neurons. Nature 387, 869–875.

Juge, N., Muroyama, A., Hiasa, M., Omote, H., and Moriyama, Y. (2009). Vesicular inhibitory amino acid transporter is a Cl-/gamma- aminobutyrate Co-transporter. J Biol Chem. 284, 35073-35078.

Karnani, M. M., Jackson, J., Ayzenshtat, I., Tucciarone, J., Manoocheri, K., Snider, W. G., and Yuste, R. (2016). Cooperative subnetworks of molecularly similar interneurons in mouse neocortex. Neuron 90, 86-100.

Kay, J. N., De la Huerta, I., Kim, I. J., Zhang, Y., Yamagata, M., Chu, M. W., Mesiter, M., and Sanes, J. R. (2011). Retinal ganglion cells with distinct directional preferences differ in molecular identity, structure, and central projections. J Neurosci. 31, 7753-7762.

Keeley, P. W., Whitney, I. E., Raven, M. A., and Reese, B. E. (2007). Dendritic spread and functional coverage of starburst amacrine cells. J Comp Neurol. 505, 539-546.

Kim, J.S., Greene, M.J., Zlateski, A., Lee, K., Richardson, M., Turaga, S.C., Purcaro, M., Balkam, M., Robinson, A., Behabadi, B.F., et al. (2014). Space-time wiring specificity supports direction selectivity in the retina. Nature 509, 331–336.

Kim, S., Guzman, S. J., Hu, H., and Jonas, P. (2012). Active dendrites support efficient initiation of dendritic spikes in hippocampal CA3 pyramidal neurons. Nat Neurosci. 15, 600-606.

Kim, H. J., and Jeon, C. J. (2014). Synaptic pattern of nicotinic acetylcholine receptor a7 and b2 subunits on the direction-selective retinal ganglion cells in the postnatal mouse retina. Exp Eye Res. 122, 54-64.

Kingston, A.E., Ornstein, P.L., Wright, R.A., Johnson, B.G., Mayne, N.G., Burnett, J.P., Belagaje, R., Wu, S., and Schoepp, D.D. (1998). LY341495 is a nanomolar potent and selective antagonist of group II metabotropic glutamate receptors. Neuropharmacology 37, 1–12.

Kittila, C. A., and Massey, S. C. (1995). Effect of ON pathway blockade on directional selectivity in the rabbit retina. J Neurophysiol. 72, 703-712.

Kittila, C. A., and Massey, S. C. (1997). Pharmacology of directionally selective ganglion cells in the rabbit retina. J Neurophysiol. 77, 675-689.

Knoflach, F., and Kemp, J.A. (1998). Metabotropic glutamate group II receptors activate a G protein-coupled inwardly rectifying K+ current in neurones of the rat cerebellum. J. Physiol. 509, 347–354.

Koch, C., Poggio, T., and Toree, V. (1982). Retinal ganglion cells: a functional interpretation of dendritic morphology. Philos Trans R Soc Lond B Biol Sci. 298, 227-263.

Koren, D, Grove, J. C. R., and Wei, W. (2017). Cross-compartmental modulation of dendritic signals for retinal direction selectivity. Neuron 59, In Press.

Korenbrot, J. I. (2012). Speed, sensitivity, and stability of the light response in rod and cone photoreceptors: facts and models. Prog Retin Eye Res. 31, 442-466.

Kosaka, T., Tauchi, M., and Dahl, J.L. (1988). Cholinergic neurons containing GABA-like and/or glutamic acid decarboxylase-like immunoreactivities in various brain regions of the rat. Exp. Brain Res. 70, 605–617.

Koulen, P., Malitschek, B., Kuhn, R., Wässle, H., and Brandstätter, J.H. (1996). Group II and group III metabotropic glutamate receptors in the rat retina: distributions and developmental expression patterns. Eur. J. Neurosci. 8, 2177–2187.

Kulkarni, V. A., and Firestein, B. L. (2012). The dendritic tree and brain disorders. Mol Cell Neurosci. 50, 10-20.

Kupferschmidt, D.A., and Lovinger, D.M. (2015). Inhibition of presynaptic calcium transients in cortical inputs to the dorsolateral striatum by metabotropic $GABA_B$ and mGlu2/3 receptors. J. Physiol. 593, 2295–2310.

Kwon, O. J., Kim, M. S., Kim, T. J., and Jeon, C. J. (2007). Identification of synaptic pattern of kainate glutamate receptor subtypes on direction-selective retinal ganglion cells. Neurosci Res. 58, 255-264.

Larkum, M.E., Zhu, J.J., and Sakmann, B. (2001). Dendritic mechanisms underlying the coupling of the dendritic with the axonal action potential initiation zone of adult rat layer 5 pyramidal neurons. J. Physiol. 533, 447–466.

Laurent, G. (1993). A dendritic gain control mechanism in axonless neurons of the locust, Schistocerca americana. J Physiol. 470, 45-54.

Lee, J. S., Kim, H. J., Ahn, C. H., and Jeon, C. J. (2017). Expression of nicotinic acetylcholine receptor a4 and b2 subunits on direction-selective retinal ganglion cells in the rabbit. Acta Histochem Cytochem. 50, 29-37.

Lee, S., Chen, L., Chen, M., Ye, M., Seal, R. P., and Zhou, Z. J. (2014) An unconventional glutamatergic circuit in the retina formed by vGluT3 amacrine cells. Neuron 84, 708-715.

Lee, S., and Zhou, Z.J. (2006). The synaptic mechanism of direction selectivity in distal processes of starburst amacrine cells. Neuron 51, 787–799.

Lee, S., Kim, K., and Zhou, Z.J. (2010). Role of ACh-GABA cotransmission in detecting image motion and motion direction. Neuron 68, 1159–1172.

Lee, S., Zhang, Y., Chen, M., and Zhou, Z. J. (2016). Segregated glycine-glutamate co-transmission from vGluT3 amacrine cells to contrast-suppressed and contrast-enhanced retinal circuits. Neuron 90, 27-34.

Leung, L. S., and Peloquin, P. (2006). GABA(B) receptors inhibit backpropagating dendritic spikes in hippocampal CA1 pyramidal cells in vivo. Hippocampus 16, 388-407.

Li, W. C., Soffe, S. R., and Roberts, A. (2004). Glutamate and acetylcholine corelease at developing synapses. Proc Natl Acad Sci. 101, 15488-15493.

Lipin, M.Y., Taylor, W.R., and Smith, R.G. (2015). Inhibitory input to the direction-selective ganglion cell is saturated at low contrast. J. Neurophysiol. 114, 927–941.

Lledo, P. M., and Lagier, S. (2006). Adjusting neurophysiological computations in the adult olfactory bulb. Semin Cell Dev Biol. 17, 443-453.

Llinás, R., Nicholson, C., and Precht, W. (1969). Preferred centripetal conduction of dendritic spikes in alligator Purkinje cells. Science 163, 184-187.

Losonczy, A., and Magee, J. C. (2006). Integrative properties of radial oblique dendrites in hippocampal CA1 pyramidal neurons. Neuron 50, 291-307.

Makara, J.K., Losonczy, A., Wen, Q., and Magee, J.C. (2009). Experience-dependent compartmentalized dendritic plasticity in rat hippocampal CA1 pyramidal neurons. Nat. Neurosci. 12, 1485–1487.

Manita, S., Miyakawa, H., Kitamura, K., and Murayama, M. (2017). Dendritic spikes in sensory perception. Front Cell Neurosci. 11 doi: 10.3389/fncel.2017.00029.

Mariani, A. P. (1990). Amacrine cells of the rhesus monkey retina. J Comp Neurol. 301, 382-400.

Marshel, J. H., Kaye, A. P., Nauhaus, I., and Callaway, E. M. (2012). Anterior-posterior direction opponency in the superficial mouse lateral geniculate nucleus. Neuron 76, 713-720.

Maturana, H. R., and Frenk, S. (1963). Directional movement and horizontal edge detectors in the pidgeon retina. Science 142, 977-979.

Mehaffey, W. H., Doiron, B., Maler, L., and Turner, R. W. (2005). Deterministic multiplicative gain control with active dendrites. J Neurosci. 25, 9968-9977.

Meye, F. J., Soiza-Reilly, M., Smit, T., Diana, M. A., Schwarz, M. K., and Mameli, M. (2016). Shifted pallidal co-release of GABA and glutamate in habenula drives cocaine withdrawal and relapse. Nat Neurosci. 19, 1019-1024.

Miller, J. P., Rall, W., and Rinzel, J. (1985). Synaptic amplification by active membrane in dendritic spines. Brain Res. 325, 325-330.

Miller, R.F., and Bloomfield, S.A. (1983). Electroanatomy of a unique amacrine cell in the rabbit retina. Proc. Natl. Acad. Sci. U. S. A. 80, 3069–3073.

Morrie, R. D., and Feller, M. B. (2015). An asymmetric increase in inhibitory synapse number underlies the development of a direction selective circuit in the retina. J Neurosci 35, 9281-9286.

Münster-Wandowski, A., Zander, J-F., Richter, K., and Ahnert-Hilger, G. (2016). Co-existence of functionally different vesicular neurotransmitter transporters. Front Synaptic Neurosci. 8 doi: 10.3389/fnsyn.2016.00004.

Nabekura J., Katsurabayashi, S., Kakazu, Y., Shibati, S., Matsubara, A., Jinno, S., Mizoguchi, Y., Sasaki, A., and Ishibashi, H. (2004). Developmental switch from GABA to glycine release in single central synaptic terminals. Nat Neurosci. 7, 17-23.

Neal, M. J., and Cunningham, J. R. (1995). Baclofen enhancement of acetylcholine release from amacrine cells in the rabbit retina by reduction of glycinergic inhibition. J Physiol. 482, 363-372.

Nishimaru, H., Restrepo, C. E., Ryge, J., Yanagawa, Y., and Kiehn, O. (2005). Mammalian motor neurons corelease glutamate and acetylcholine at central synapses. Proc Natl Acad Sci USA. 102, 5245-5249.

Norton, A. L., Spekreijse, H., Wagner, H. G., and Wolbarsht, M. L. (1970). Responses to directional stimuli in retinal preganglionic units. J Physiol. 206, 93-107.

O'Brien, J. A., and Berger, A. J. (1999). Cotransmission of GABA and glycine to brain stem motoneurons. J Neurophysiol. 92, 1638-1641.

O'Malley, D.M., and Masland, R.H. (1989). Co-release of acetylcholine and gamma-aminobutyric acid by a retinal neuron. Proc. Natl. Acad. Sci. U. S. A. 86, 3414–3418.

Oesch, N., Euler, T., and Taylor, W. R. (2005). Direction-selective dendritic action potentials in rabbit retina. Neuron 47, 739-750.

Oesch, N. W., Kothmann, W. W., and Diamond, J. S. (2011). Illuminating synapses and circuitry in the retina. Curr Opin Neurobiol. 21, 238-244.

Oesch, N.W., and Taylor, W.R. (2010). Tetrodotoxin-resistant sodium channels contribute to directional responses in starburst amacrine cells. PLoS One 5, e12447.

Otsu, Y., Marcaggi, P., Feltz, A., Isope, P., Kollo, M., Nusser, Z., Mathieu, B., Kano, M., Tsujita, M., Sakimura, K., et al. (2014). Activity-dependent gating of calcium spikes by A-type K+ channels controls climbing fiber signaling in Purkinje cell dendrites. Neuron 84, 137–151.

Oyster, C. W. (1968). The analysis of image motion by the rabbit retina. J Physiol. 199, 613-635.

Oyster, C. W., and Barlow, H. B. (1967). Direction-selective units in rabbit retina: distribution of preferred directions. Science 155, 841-842.

Oyster, C. W., Simpson, J. I., Takahashi, E. S., and Soodak, R. E. (1980). Retinal ganglion cells projecting to the rabbit accessory optic system. J Comp Neurol. 190, 49-61.

Ozaita, A., Petit-Jacques, J., Völgyi, B., Ho, C.S., Joho, R.H., Bloomfield, S.A., and Rudy, B. (2004). A unique role for Kv3 voltage-gated potassium channels in starburst amacrine cell signaling in mouse retina. J. Neurosci. 24, 7335–7343.

Park, S. J., Borghuis, B. G., Rahmani, P., Zeng, Q., Kim, I. J., and Demb, J. B. (2015). Function and circuitry of VIP+ interneurons in the mouse retina. J Neurosci. 35, 10685-10700.

Pei, Z., Chen, Q., Koren, D., Giammarinaro, B., Acaron Ledesma, H., and Wei, W. (2015). Conditional Knock-Out of Vesicular GABA Transporter Gene from Starburst Amacrine Cells Reveals the Contributions of Multiple Synaptic Mechanisms Underlying Direction Selectivity in the Retina. J. Neurosci. 35, 13219–13232.

Percival, K. A., Venkataramani, S., Smith, R. G., and Taylor, R. W. (2017). Directional excitatory input to direction-selective ganglion cells in rabbit retina. J Comp Neurol. doi: 10.1002/cne.24207.

Perkel, D. H., and Perkel, D. J. (1985). Dendritic spines: role of active membrane in modulating synaptic efficacy. Brain Res. 325, 331-335.

Peters, B. N., and Masland, R. H. (1996). Responses to light of starburst amacrine cell. J Neurophysiol. 75, 469-480.

Piscopo, D. M., El-Danaf, R. N., Huberman, A. D., and Niell, C. M. (2013). Diverse visual features encoded in mouse lateral geniculate nucleus. J Neurosci. 33, 4642-4656.

Poleg-Polsky, A., and Diamond, J. S. (2016a). NMDA receptors multiplicatively scale visual signals and enhance directional motion discrimination in retinal ganglion cells. Neuron 89, 1277-1290.

Poleg-Polsky, A., and Diamond, J. S. (2016b). Retinal circuitry balances contrast tuning of excitation and inhibition to enable reliable computation of dendritic selectivity. J Neurosci. 36, 5861-5876.

Rahman, J., Latal, A. T., Besser, S., Hirrlinger, J., and Hülsmann, S. (2013). Mixed miniature postsynaptic currents resulting from co-release of glycine and GABA recorded from glycinergic neurons in the neonatal respiratory network. Eur J Neurosci. 37, 1229-1241.

Rall, W. (1959). Branching dendritic trees and motoneuron membrane resistivity. Exp Neurol. 1, 491-527.

Rall, W. (1964). Theoretical significance of dendritic trees for neuronal input-output relations. Neural Theory and Modeling, ed. Reiss, R., 73-97. Stanford Univ. Press: Stanford, CA.

Rall, W., and Shepherd, G. M. (1968). Theoretical reconstruction of field potentials and dendrodendritic synaptic interactions in olfactory bulb. J Neurophysiol. 31, 884-915.

Rancz, E. A., and Häusser, M. (2006). Dendritic calcium spikes are tunable triggers of cannabinoid release and short-term plasticity in cerebellar Purkinje neurons. J Neurosci. 26, 5428-5437.

Ren, J., Qin, C., Hu, F., Tan, J., Qiu, L., Zhao, S., Feng, G., and Luo, M. (2011). Habenula "cholinergic" neurons co-release glutamate and acetylcholine and activate postsynaptic neurons via transmission modes. Neuron 69, 445-452.

Remy, S., Csicsvari, J., and Beck, H. (2009). Activity-dependent control of neuronal output by local and global dendritic spike attenuation. Neuron 61, 906-916.

Riazanski, V., Deriy, L. V., Shevchenko, P. D., Le, B., Gomez, E. A., and Nelson, D. J. (2011). Presynaptic CLC-3 determines quantal size of inhibitory transmission in the hippocampus. Nat Neurosci. 14, 487-494.

Rivlin-Etzion, M., Zhou, K., Wei, W., Elstrott, J., Nguyen, P.L., Barres, B.A., Huberman, A. D., and Feller, M. B. (2011). Transgenic mice reveal unexpected diversity of on-off direction-selective retinal ganglion cell subtypes and brain structures involved in motion processing. J Neurosci 31, 8760-8769.

Rodieck, R. W. (1989). Starburst amacrine cells of the primate retina. J Comp Neurol. 385, 18-37.

Rodieck, R. W., and Marshak, D. W. (1992). Spatial density and distribution of choline acetyltransferase immunoreactive cells in human, macaque, and baboon retinas. J Comp Neurol. 321, 46-64.

Rousso, D. L., Qiao, M., Kagan, R. D., Yamagata, M., Palmiter, R. D., and Sanes, J. R. (2016). Two pairs of ON and OFF retinal ganglion cells are defined by intersectional patterns of transcription factor expression. Cell Rep. 15, 1930-1944.

Russier, M., Kopysova, I. L., Ankri, N., Ferrand, N., and Debanne, D. (2002). GABA and glycine co-release optimized functional inhibition in rat brainstem motoneurons in vitro. J Physiol. 541, 123-137.

Sabbah, S., Gemmer, J. A., Bhatia-Lin, A., Manoff, G., Castro, G., Siegel, J. K., Jeffery, N., and Berson, D. M. (2017). A retinal code for motion along the gravitational and body axes. Nature 546, 492-497.

Saugstad, J.A., Segerson, T.P., and Westbrook, G.L. (1996). Metabotropic glutamate receptors activate G-protein-coupled inwardly rectifying potassium channels in Xenopus oocytes. J. Neurosci. 16, 5979–5985.

Schachter, M. J., Oesch, M., Smith, R. G., and Taylor, W. R. (2010). Dendritic spikes amplify the synaptic signal to enhance detection of motion in a simulation of the direction-selective ganglion cell. PLoS Comput Biol. 6, pii: e1000899.

Schmidt, M., Humphrey, M. F., and Wässle, H. (1987). Action and localization of acetylcholine in the cat retina. J Neurophysiol. 58, 997-1015.

Schmidt-Hieber, C., Toleikyte, G., Aitchison, L., Roth, A., Clark, B. A., Branco, T., and Haüsser, M. (2017). Active dendritic integration as a mechanism for robust and precise grid cell firing. Nat Neurosci. doi: 10.1038/nn.4582.

Schoepp, D.D., Johnson, B.G., Wright, R.A., Salhoff, C.R., Mayne, N.G., Wu, S., Cockerman, S.L., Burnett, J.P., Belegaje, R., Bleakman, D., et al. (1997). LY354740 is a potent and highly selective group II metabotropic glutamate receptor agonist in cells expressing human glutamate receptors. Neuropharmacology 36, 1–11.

Schoppa, N. E., and Urban, N. N. (2003). Dendritic processing within olfactory bulb circuits. Trends Neurosci. 26, 501-506.

Seal, R. P., and Edwards, R. H. (2006). Functional implications of neurotransmitter co-release: glutamate and GABA share the load. Curr Opin Pharmacol. 6, 114-119.

Seebahn, A., Rose, M., and Enz, R. (2008). RanBPM is expressed in synaptic layers of the mammalian retina and binds to metabotropic glutamate receptors. FEBS Lett. 582, 2453–2457.

Segev, I., Friedman, A., White, E. L., and Gutnick, M. J. (1995). Electrical consequences of spine dimensions in a model of cortical spiny stellate cell completely reconstructed from serial thin sections. J Comp Neurol. 2, 117-130.

Sethuramanujam, S., McLaughlin, A. J., deRosenroll, G., Hoggarth, A., Schwab, D. J., and Awatramani, G. B. (2016). A central role for mixed acetylcholine/GABA transmission in direction coding in the retina. Neuron 90, 1243-1256.

Sethuramanujam, S., and Slaughter, M. M. (2015). Properties of a glutamatergic synapse controlling information output from retinal bipolar cells. PLoS One. 10, e0129133.

Shabel, S. J., Proulx, C. D., Piriz, J., and Malinow, R. (2014). Mood regulation. GABA/glutamate co-release controls habenula output and is modified by antidepressant treatment. Science 345, 1494-1498.

Shepherd, G. M., Brayton, R. K., Miller, J. P., Segev, I., Rinzel, J., and Rall, W. (1985). Signal enhancement in distal cortical dendrites by means of interactions between active dendritic spines. Proc Natl Acad Sci USA. 82, 2192-2195.

Sheridan, R. E., and Lester, H. A. (1975). Relaxation measurements on the acetylcholine receptor. Proc Natl Acad Sci USA. 72, 3496-3500.

Shi, X., Barchini, J., Ledesma, H. A., Koren, D., Jin, Y., Liu, X., Wei, W., and Cang, J. (2017). Retinal origin of direction selectivity in the superior colliculus. Nat Neurosci. 20, 550-558.

Shin, J., Kim, J., and Song, K. (2012). Effects of tetanus toxin on spontaneous and evoked transmitter release at inhibitory and excitatory synapses in rat SDCN neurons. Toxicon. 59, 385-392.

Sivyer, B., van Wyk, M., Vaney, D. I., and Taylor, W. R. (2010). Synaptic inputs and timing underlying the velocity tuning of direction-selective ganglion cells in rabbit retina. J Physiol. 588, 3243-5352.

Sivyer, B., and WIlliams, S. R. (2013). Direction selectivity is computed by active dendritic integration in retinal ganglion cells. Nat Neurosci. 16, 1848-1856.

Slaughter, M. M., and Pan, Z. H. (1992). The physiology of GABAB receptors in the vertebrate retina. Prog Brain Res. 90, 47-60.

Smith, S. L., Smith, I. T., Branco, T., and Haüsser, M. (2013). Dendritic spikes enhance stimulus selectivity in cortical neurons in vivo. Nature 503, 115-120.

Stincic, T., Smith, R.G., and Taylor, W.R. (2016). Time course of EPSCs in ON-type starburst amacrine cells is independent of dendritic location. J. Physiol. 594, 5685–5694.

Sugita, Y., Miura, K., Araki, F., Furukawa, T., and Kawano, K. (2013). Contributions of retinal direction-selective ganglion cells to optokinetic responses in mice. Eur J Neurosci. 38, 2823-2831.

Sun, L. O., Brady, C. M., Cahill, H., Al-Khindi, T., Sakuta, H., Dhande, O. S., Noda, M., Huberman, A. D., Nathans, J., and Kolodkin, A. L. (2015). Functional assembly of accessory optic system circuitry critical for compensatory eye movements. Neuron 86, 971-984.

Sun, Q., Srinivas, K. V., Sotayo, A., and Siegelbaum, S. A. (2014). Dendritic Na+ spikes enable cortical input to drive action potential output from hippocampal CA2 pyramidal neurons. Elife 3, 10.7554/eLife.04551.

Suresh, V., Çiftçioğlu, U. M., Wang, X., Lala, B. M., Ding, K. R., Smith, W. A., Sommer, F. T., and Hirsch, J. A. (2016). Synaptic contributions to receptive field structure and response properties in the rodent lateral geniculate nucleus of the thalamus. J Neurosci. 36, 10949-10963.

Syková, E., and Chvátal., A. (2000). Glial cells and volume transmission in the CNS. Neurochem Int. 36, 397-409.

Taniguchi, M., Yokoi, M., Shinohara, Y., Okutani, F., Murata, Y., Nakanishi, S., and Kaba, H. (2013). Regulation of synaptic currents by mGluR2 at reciprocal synapses in the mouse accessory olfactory bulb. Eur. J. Neurosci. 37, 351–358.

Tasic, B., Menon, V., Nguyen, T. N., Kim, T. K., Jarsky, T., Yao, Z., Levi, B., Gray, L. T., Sorensen, S. A., Dolbeare, T., et al. (2016). Adult mouse cortical cell taxonomy revealed by single cell transcriptomics. Nat Neurosci 19, 335-346.

Taylor, W.R., and Vaney, D.I. (2002). Diverse synaptic mechanisms generate direction selectivity in the rabbit retina. J. Neurosci. 22, 7712–7720.

Taylor, W. R., and Wässle, H. (1995). Receptive field properties of starburst cholinergic amacrine cells in the rabbit retina. Eur J Neurosci. 7, 2308-2321.

Trisch, N. X., Ding, J. B., and Sabatini, B. L. (2012). Dopaminergic neurons inhibit striatal output through non-canonical release of GABA. Nature 490, 262-266.

Trudeau, L. E. (2004). Glutamate co-transmission as an emerging concept in monoamine neuron function. J Psyciatry Neurosci. 29, 296-310.

Tsubokawa, H., and Ross, W. N. (1997). Muscarinic modulation of spike backpropagation in the apical dendrites of hippocampal CA1 pyramidal neurons. J Neurosci. 17, 5782-5791.

Tukker, J.J., Taylor, W.R., and Smith, R.G. (2004). Direction selectivity in a model of the starburst amacrine cell. Vis. Neurosci. 21, 611–625.

van Wyk, M., Wässle, H., and Taylor, W.R. (2009). Receptive field properties of ON- and OFF-ganglion cells in the mouse retina. Vis. Neurosci. 26, 297–308.

Vaney, D. I., Sivyer, B., and Taylor, W. R. (2012). Direction selectivity in the retina: symmetry and asymmetry in structure and function. Nat Rev Neurosci. 13, 194-208.

Vaney, D.I., and Young, H.M. (1988). GABA-like immunoreactivity in cholinergic amacrine cells of the rabbit retina. Brain Res. 438, 369–373.

Vardi, N., Masarachia, P. J., and Sterling, P. (1989). Structure of the starburst amacrine network in the cat retina and its association with alpha ganglion cells. J Comp Neurol. 288, 601-611.

Velte, T.J., and Miller, R.F. (1997). Spiking and nonspiking models of starburst amacrine cells in the rabbit retina. Vis. Neurosci. 14, 1073–1088.

Verderio, C., Coco, S., Bacci, A., Rossetto, O., De Camili, P., Montecucco, C., and Matteoli, M. (1999). Tetanus toxin blocks the exocytosis of synaptic vesicles clustered at synapses but not of synaptic vesicles in isolated axons. J Neurosci 19, 6723-6732.

Vlasits, A.L., Morrie, R.D., Tran-Van-Minh, A., Bleckert, A., Gainer, C.F., DiGregorio, D.A., and Feller, M.B. (2016). A Role for Synaptic Input Distribution in a Dendritic Computation of Motion Direction in the Retina. Neuron 89, 1317–1330.

Wei, W., Elstrott, J. J., and Feller, M. B. (2010). Two-photon targeted recording of GFP-expressing neurons for light responses and live-cell imaging in the mouse retina. Nat Protoc. 5, 1347-1352.

Wei, W., Hamby, A.M., Zhou, K., and Feller, M.B. (2011). Development of asymmetric inhibition underlying direction selectivity in the retina. Nature 469, 402–406.

Wei, W., and Feller, M.B. (2011). Organization and development of direction-selective circuits in the retina. Trends Neurosci. 34, 638-645.

Williams, S. R., and Stuart, G. J. (2003). Voltage- and site-dependent control of the somatic impact of dendritic IPSPs. J Neurosci. 23, 7358-7368.

Wu, L. J., Li, Y., and Xu, T. L. (2002). Co-release and interaction of two inhibitory co-transmitters in rat sacral dorsal commissural neurons. Neuroreport 13, 977-981.

Wu, Y., Wang, W., Díez-Sampedro, A., and Richerson, G. B. (2007). Nonvesicular inhibitory neurotransmission via reversal of the GABA transporter GAT-1. Neuron 56, 851-865.

Yang, G., and Masland, R. H. (1994). Receptive fields and dendritic structure of directionally selective retinal ganglion cells. J Neurosci. 14, 5267-5280.

Yang, H., and Kunes, S. (2004). Nonvesicular release of acetylcholine is required for axon targeting in the Drosophila visual system. Proc Natl Acad Sci USA. 101, 15213-15218.

Yazulla, S., and Studholme, K. M. (1995). Volume transmission of dopamine may modulate light-adaptive plasticity of horizontal cell dendrites in the recovery phase following dopamine depletion in goldfish retina. Vis Neurosci. 12, 827-836.

Yazulla, S., Studholme, K. M., McIntosh, H. H., and Deutsch, D. G. (1999). Immunocytochemical localization of cannabinoid CB1 receptor and fatty acid amide hydrolase in rat retina. J Comp Neurol. 415, 80-90.

Yonehara, K., Farrow, K., Ghanem, A., Hillier, D., Balint, K., Teixeira, M., Jüttner, J., Noda, M., Neve, R. L., Conzelmann, K. K., and Roska, B. (2013). The first stage of cardinal direction selectivity is localized to the dendrites of retinal ganglion cells. Neuron 79, 1078-1085.

Yoo, J. H., Zell, V., Gutierrez-Reed, N., Wu, J., Ressler, R., Shenasa, M. A., Johnson, A. B., Fife, K. H., Faget, L., and Hnasko, T. S. (2016). Ventral tegmental area glutamate neurons co-release GABA and promote positive reinforcement. Nat Commun. 15, 13697.

Yoshida, K., Fiscella, M., Drinnenberg, A., Esposti, F., Trenholm, S., Krol, K., Franke, F., Scherf, B. G., Kusnyerik, A., Müller, J., et al. (2016). Congenital nystagmus gene FRMD7 is necessary for establishing a neuronal circuit asymmetry for direction selectivity. Neuron 89, 177-193.

Yoshida, K., Watanabe, D., Ishikane, H., Tachibana, M., Pastan, I., and Nakanishi, S. (2001). A key role of starburst amacrine cells in originating retinal directional selectivity and optokinetic eye movement. Neuron 30, 771-780.

Zhang, S., Qi, J., Li, X., Wang, H. L., Britt, J. P., Hoffman, A. F., Bonci, A., Lupica, C. R., and Morales, M. (2015). Dopaminergic and glutamatergic microdomains in a subset of rodent mesoaccumbens axons. Nat Neurosci. 18, 386-392.

Zhou, Z. J., and Fain, G. L. (1995). Neurotransmitter receptors of starburst amacrine cells in rabbit retinal slices. J Neurosci. 15, 5334-5345.

Zhou, Z. J., and Lee, S. (2008). Synaptic physiology of direction selectivity in the retina. J Physiol 586, 4371-4376.

Zucker, C. L., Nilson, J. E., Ehinger, B., and Grzywacz, N. M. (2005). Compartmental localization of gamma-aminobutyric acid type B receptors in the cholinergic circuitry of the rabbit retina. J Comp Neurol. 493, 448-459.

Zucker, R. S., and Regehr, W. G. (2002). Short-term synaptic plasticity. Annu Rev Physiol. 64, 355-405.